DAMPING CONTROLLER DESIGNS TO SUPPRESS INTER-AREA OSCILLATIONS IN POWER SYSTEMS BY USING NOVEL EIGENSTRUCTURE-BASED INDEXES

KE DEPING

Ph. D

The Hong Kong Polytechnic University

2012

The Hong Kong Polytechnic University

Department of Electrical Engineering

DAMPING CONTROLLER DESIGNS TO SUPPRESS INTER-AREA OSCILLATIONS IN POWER SYSTEMS BY USING NOVEL EIGENSTRUCTURE-BASED INDEXES

KE DEPING

A thesis submitted in partial fulfillment of the requirements

for the Degree of Doctor of Philosophy

September 2011

CERTIFICATE OF ORIGINALITY

I hereby declare that this thesis is my own work and that, to the best of my knowledge and belief, it reproduces no material previously published or written or material which has been accepted for the award of any other degree or diploma, except where due acknowledgement has been made in the text.

_____(Signed)

_____KE Deping_____(Name of student)

Abstract

The low frequency power oscillation of inter-area modes inherently induced by interconnections of local electric networks aiming at transmission of power between different areas, over long distances, to realize stable power supply, as well as to balance the uneven distribution of primary energy sources (such as coal and renewable energy), has resulted in severe threats to safety of operations of power systems. Normally, use of damping controllers such as power system stabilizers (PSSs) and supplementary damping controllers (SDCs) for flexible AC transmission system (FACTS) devices is the most cost-effective means to alleviate the problem of inter-area oscillations, though design of them for modern power systems is never a trivial work. Therefore, on the basis of the foundation laid by the excellent pioneering research works already done, this thesis strives to make further contribution to the knowledge about design of damping controllers for suppression of inter-area oscillations.

So far, limited attention has been paid to closed loop system eigenvectors in design of damping controllers as most existing designs focus only on eigenvalues. In fact, it is readily accepted that appropriate design of eigenstructure (both eigenvalues and eigenvectors) can obtain more satisfactory control effects than assignment of only eigenvalues. This thesis harnesses the eigenstructure of closed loop systems by exploring its integral and structural relationship with time domain responses. Accordingly, a novel way of constructing the eigenstructure-based index, which is equivalent to the corresponding quadratic cost function

defined in time domain in terms of measuring the system dynamics objective, is proposed. Specifically, unlike the cost function, this index is not associated with the initial state of the system. Moreover, calculation of the index is independent of structures adopted by controllers. Thus, by formation of eigenstructure-based indexes for different measurement intentions, various optimization-based methods which use these indexes as objective functions can be formulated to tune the structurally constrained damping controllers for expected control effects.

Firstly, a tuning scheme is proposed to coordinate wide-area signals based PSSs and SDCs for FACTS devices to mitigate inter-area oscillations with optimal control efforts under multiple operating conditions. This involves minimizing of an eigenstructure-based index which measures the dynamic performance of inter-area oscillations and control efforts together. Here, PSSs and SDCs are simple controllers with structural constraints, for consideration their applications in practice. Besides, SDCs and PSSs are simultaneously tuned by another proposed two-stage optimization method named IAMO-PS where an inter-area mode oriented pole placement strategy is implemented for damping of inter-area oscillations in the first stage while control efforts measured by eigenstructure-based indexes are coordinated under the constraints of such pole placement in the second stage.

Subsequently, it is emphasized in this thesis that wind turbines employing doubly fed induction generators (DFIGs) have to sacrifice their dynamic performance as they are controlled to suppress inter-area oscillations. Thereby, a dual-channel SDC is proposed and tuned to drive the DFIG to offer the required damping to inter-area modes by using the method of IAMO-PS with optimizing of weighted control efforts of active and reactive power modulation, measured by

eigenstructure-based indexes. Consequently, the DFIG dynamics are apparently improved because of their tight relationship with the optimized power outputs.

The effectiveness of the proposed eigenstructure-based indexes and the associated tuning methods are validated in the classic two-area systems and New England and New York interconnected systems.

Acknowledgement

Foremost, I would like to express my deep and sincere gratitude to my chief supervisor Dr. C. Y. Chung for the continuous support to my PhD study and research. His wide knowledge and logical way of thinking have been of significant value for me, and his perseverance and achievements in research works on power systems have always encouraged me. My sincere thanks also go to my two co-supervisors Professor K. P. Wong and Professor Xue Yusheng who have generously helped me during my studies in Hong Kong.

I have spent three really memorable and substantial years with the team of Computational Intelligence Applications Research Laboratory (CIARLab). The favorable research environment created by all team members has benefited me so much. I heartily appreciate them all. Also, I would like to convey my special thanks to the Department of Electrical Engineering and the Research Office for all the help and assistance provided during my PhD study.

My genuine thanks and love are due to my dear parents who have borne the burden of unconditionally supporting me in chasing dreams.

Last but not the least, I would like to thank everyone who directly or indirectly offered his or her help while working on this thesis.

Table of Contents

VIII

Lists of Figures, Tables and Abbreviations

List of Figures

List of Tables

List of Abbreviations

AVR	Auto voltage regulator
DE	Differential evolution
DFIG	Doubly fed induction generator
FSIG	Fixed speed induction generator
FACTS	Flexible alternating current transmission system
GSC	Grid side converter
GEP	The generator, exciter and power system
HSV	Hankel singular value
HVDC	High voltage direct current
IDTC	Induced damping torque coefficient
IPFC	Interline power flow controller
LMI	Linear matrix inequalities
MIMO	Multi-input multi-output
NLP	Nonlinear programming problem
PLL	Phase locked loop
PM	Active power modulation
PSS	Power system stabilizer
PV	Power and voltage
QM	Reactive power modulation
RSC	Rotor side converter
SDC	Supplementary damping controller
SISO	Single-input single-output

SMIB	Single machine infinite bus
SQP	Sequential quadratic programming
SSSC	Static synchronous series compensator
STATCOM	Static synchronous compensator
SVC	Static var compensator
TCSC	Thyristor controlled series compensator
UPFC	Unified power flow controller
VC	Voltage control
WTG	Wind turbine generator

Chapter 1

Introduction

1.1 Research Background

In the modern society, people's lives as well as economic development in general have become increasingly dependent on electricity. Few are likely to have forgotten the failure of the electricity supply system in large portions of Midwest and Northeast regions of United States and Ontario, Canada on 14 August 2003, resulting in loss of US$ 10 billion to American businesses, and about 50 million persons being affected by the large scale blackout [1, 2]. Therefore, more and more strict requirements have been imposed on operations of power systems to ensure power supply with security, reliability and quality.

Power system stability is the key issue in ensuring secure and uninterrupted power supply. The IEEE/CIGRE Joint Task Force Report [3] has defined power system stability as *the ability of an electric power system, for a given initial operating condition, to regain a state of operating equilibrium after being subjected to a physical disturbance, with all system variables bounded so that practically the entire system remains intact.* Nevertheless, among various categories of stability problems in power systems, power angle oscillatory instability (electromechanical oscillation) caused by insufficient damping torque has become a serious problem in power systems because of the rapid growth of

power demand, as well as wide usage of high gain and fast acting automatic voltage regulators (AVR) which can largely eliminate the insufficient synchronizing torque [4]. The nature of electromechanical oscillations can be classified into the following types [5, 6]:

(1) Intraplant mode oscillations: generators in the same power plant swing against each other at frequencies of 2.0 to 3.0 Hz, which is dependent on unit ratings and the reactance connecting them.

(2) Local plant mode oscillations: one generator oscillates against the rest of the system at 1.0 to 2.0 Hz.

(3) Inter-area mode oscillations: two or more large coherent groups of generators swing against each other at low frequency (1 Hz or less).

(4) Control mode oscillations: these are related to generating units and other controls such as poorly tuned exciters and governors.

(5) Torsional mode oscillations: these modes are with frequencies in the range of 10-46 Hz, associated with a turbine generator shaft system.

Obviously, compared to the other four types of oscillations, inter-area mode oscillation is more complex due to its association with a large number of components with highly nonlinear dynamic behaviors which distributes in the power grid covering hundreds and thousands of miles [7, 8]. Generally, when a power source is far away from a load center in terms of the electric distance (or say, the two areas are weakly electrically coupled), transmitting an amount of power between the two areas may give rise to inter-area oscillation. Moreover, frequency of inter-area oscillations decreases to quite a low value as the number of synchronous generators increases, to produce more power to meet the rising demand which actually augments the equivalent inertia of each area. A more

serious factor is that the planned power transmission between interconnected areas may be forbidden because the damping of inter-area oscillation can deteriorate significantly when the transmitted power increases. The Western Electricity Co-ordination Council (WECC) has a long history of lightly damped inter-area oscillations at 0.33 Hz and 0.7 Hz which greatly influenced its planning, design and operations strategy [6, 9]. Inter-area oscillations among the four provincial power grids occurred several times and were a significant problem in the operation of the China Southern Power Grid, a long-distance bulk power transmission system with AC/DC hybrid interconnections [10-12]. A major concern in the Brazilian power system project for interconnection of North-Northeast and South-Southeast subsystems in 1999 was a poorly damped low frequency (0.17-0.25 Hz) inter-area mode [13, 14]. [15] and [16] reported a 0.2 Hz poorly damped power oscillation existing between Greece and the rest of UCTE (Union for the Co-ordination of Transmission of Electricity) networks which had posed threats to further interconnection of Turkey and UCTE networks.

Although building more transmission circuits to strengthen power networks can substantially alleviate the inter-area oscillation problem, the associated huge capital investment implies that this is doomed to be an impractical approach. The most cost-effective method for damping electromechanical oscillations is installation of power system stabilizers (PSS) which can produce an electrical torque (called damping torque) proportional to rotor speed change so as to suppress the oscillation by only adding a supplementary exciting signal to the excitation system [17]. PSSs have been widely employed in power systems all over the world and have played an indispensable role in enhancing stability [18,

19]. Originally, PSSs were designed to provide damping to local oscillatory modes, to address destabilization caused by high gain, fast acting AVRs. Therefore, their designs were based on a simple equivalent dynamic model, i.e. a single-machine-infinite-bus (SMIB) system, to achieve robust performance with relatively higher gains [20-22]. However, design of PSSs for inter-area oscillations requires more proper representation of the entire interconnected system, and their performance may be more sensitive to change of operating conditions and network configuration [5, 8].

The mechanism of the PSSs is that the generators act to amplify their power so that they can damp the electromechanical oscillations [4]. The high power electronic equipments such as high voltage direct current (HVDC) links and flexible alternating current transmission system (FACTS) devices have been deployed in power systems with primary functions like power flow control or voltage control [23-27]. Moreover, they are also able to enact the role of power amplifier during the transient dynamics because of their fast power switching capabilities. Thus, once installed, an auxiliary function of these devices, to increase damping of electromechanical oscillations, can be implemented with the help of a supplementary damping controller (SDC) which modulates their power outputs. Unlike synchronous generators, power electronic devices with primary controls are rarely involved in electromechanical oscillations because they do not contain any rotating mechanical parts. They initiatively engage in damping control via SDCs which control them to induce additional damping torques on generator shafts [28].

FACTS devices of different types [29, 30] have been utilized for damping control, for example, Static Var Compensator (SVC) [31], Thyristor Controlled

4

Series Compensator (TCSC) [32], STATic synchronous COMpensator (STATCOM) [33], Static Synchronous Series Compensator (SSSC) [34], Unified Power Flow Controller (UPFC) [35], and Interline Power Flow Controller (IPFC) [36]. Though these devices can be employed to effectively damp power oscillations, it has been figured out that the series-connected devices (TCSC, SSSC and IPFC) may be generally more efficient than the shunt-connected devices (SVC and STATCOM), in terms of damping effects per installed MVar [37]. This can be heuristically accepted as shunt-connected devices perform only reactive power modulation while series-connected devices can be modeled as equivalent to shunt-connected devices which are able to inject both active and reactive power to grids. It is known that power angle oscillations directly result from imbalance of active power in the system, which indicates that the active power modulation should be more efficient and direct than the reactive power modulation, in damping of oscillations.

Stimulated by the need for reducing carbon emissions and addressing global warming, wind power generation has grown considerably all over the world during the past few years [38]. Massive wind power penetration also poses great challenges to operation and control of power systems [39]. However, at early stages, wind turbine generators (WTGs) have relatively small capacities and tend to employ squirrel cage induction generators because of their simple structures and low investment. The generator is directly connected to the grid and is normally referred to as fixed speed induction generator (FSIG) since its rotor slip changes slightly as the operating power level changes. Apparently, unlike conventional synchronous generators, FSIGs are unable to contribute to network support and operation, due to lack of control capability. Actually, as generated

power increases, they consume more reactive power and thus it is generally necessary to provide power factor correction capacitors at each wind turbine. What is more, FSIG cannot capture the maximum wind power at various wind speeds via rotor speed adjustment. As the size of individual wind turbines and total wind power penetration increase, these issues are becoming more important and complex and the corresponding technologies are naturally switching from fixed to variable speeds [40]. Among various variable speed WTG technologies, doubly fed induction generator (DFIG) based WTG is considered state-of-the-art. The torque-slip characteristic of DFIG can be changed by injecting magnitude and angle controllable voltage with slip frequency from a back-to-back voltage-source converter to the wound rotor so that it can operate at different rotor speeds to capture maximum wind power [41]. Furthermore, through implementation of proper control on the rotor side converter (RSC) to adjust active and reactive power outputs, DFIG is also capable of active participation in network frequency and voltage control [42, 43].

An important aspect of DFIG contributing to network support is enhancement of network damping via a SDC loop [44]. It has been recognized that DFIGs can act similar to FACTS devices to provide additional damping to inter-area oscillations since both employ power electronic devices to realize flexible output power control [45-47]. However, unlike the shunt-connected FACTS devices, although the DFIG is connected in shunt with the network, it can perform both active and reactive power modulations. Normally, when employed for damping control, the dynamics of FACTS devices can be ignored or simply represented because time constants of power electronic devices and associated control systems are much smaller than time constants of electromechanical oscillations

[48-50]. Nevertheless, it is noted that power outputs of DFIG are coupled with its rotor slip, a state variable regarding the mechanical dynamics. Therefore, though the DFIG does not participate in electromechanical oscillations since no power angle is defined, its shaft dynamics inevitably impact power modulation. This situation is especially noticeable when the WTG uses a relatively "soft" (low stiffness) shaft which leads to the torsional mode falling into the frequency range of electromechanical oscillations [51, 52]. So, it is generally necessary to model DFIG dynamics which may interact electromechanical dynamics, when used for damping control. In this context, greater consideration of the dynamics of DFIGs is warranted during designing of damping controllers.

1.2 Incentives of Thesis

It has to be admitted that currently numerous approaches are available for the design of PSSs and SDCs for damping inter-area oscillations [4, 6, 53-55]. However, there is still significant room for exploring novel control methods. According to linear system theories, eigenvalues of the system state matrix contain the information of damping and frequencies of oscillations in time domain [56]. Hence, positioning closed loop eigenvalues at locations with adequate damping (or damping ratio) in the complex plane is the common objective of many damping controller design methods [57-61]. Undoubtedly, such a way of pole placement for damping of electromechanical oscillations is feasible and effective. However, it has been recognized that assigning only eigenvalues does not utilize all available degrees of freedom for a MIMO system [62]. Left and right eigenvectors are coupled with time domain responses as well, which indicates that proper design may further improve system dynamics. The

7

left eigenvector determines the extent to which the corresponding mode is excited, while the right eigenvector decides energy distribution of the mode among all states. Actually, several state and output feedback algorithms making use of available degrees of control freedom with eigenstructures (both eigenvalues and eigenvectors) assignment have been proposed, one example being aerospace applications related to flight control stabilization [63]. In addition to assignment of eigenvalues, the partial right eigenvectors are appropriately assigned in power system controller designs so that the presence of critical mode in certain state variables is minimized [64, 65]. Moreover, the possible adverse excitation of critical modes themselves is explicitly minimized in coordinated design of PSS and active damping controller for the DFIG by additionally assigning partial left eigenvectors [52].

As is known to all, time domain responses are the most direct representations to assess system dynamic performance. However, it should be mentioned that eigenstructure assignment techniques deal with eigenvalues, left and right eigenvectors partially and separately, whereas time domain responses are integrally and structurally dependent on them. Partial assignation of eigenvectors is unable to consider effects on other eigenvectors. Furthermore, interactions between assignments of left and right eigenvectors, as well as between assignments of eigenvalues and eigenvectors are also considerable issues during the design process [52]. Therefore, theoretically speaking, it is never easy to achieve competitive improvements in system dynamics by additionally assigning the eigenvectors, compared to assignment of only eigenvalues.

The difficulties of using eigenstructure assignment to enhance system dynamics can be attributed to the fact that the integral structural relationship

between the time domain responses and the eigenstructure is not explicitly considered. This relationship was first explored in tuning of PSSs by Kahaldi (1993) and a time domain modal performance measure, an analytical function of eigenstructure, initial state and studied time span, was defined [66]. By minimizing this performance measure, PSSs' parameters were optimized. Similar works were conducted by Simo in 1996 for the design of flexible controllers based on the improved modal performance measure which additionally takes into account damping ratios [67]. It is noted that with any given initial state, the modal performance measure evaluated over the studied time span can be analytically calculated and no numerical integration is required. Thus, optimizations based on this measure are much faster than those employing time domain indexes evaluated from nonlinear numerical integrations [68, 69]. However, both types of optimizations suffer the drawback that optimization results are influenced by the initial state as well as the selected time span. This is undesirable because the initial state (post-fault states) depend only on the intrinsic characteristics of the system and the disturbance events are undermined. An appropriate initial state has to be carefully selected by the designer in advance so as to assure the final solution is consistently feasible for maximum possible other initial states. Obviously, this may be a laborious process. Thus, in order to cure this weakness, [70] defined a selective modal performance index by artificially setting test inputs and observation outputs in the closed loop system and performing unit impulse response tests on all input-output pairs. Although this index can be analytically computed, irrespective of the initial state, it is definitely impacted by selection of inputs and outputs. Moreover, a pre-set time horizon is also required for calculation of this index.

To make use of the closed loop system eigenstructure for improving system dynamics, [66, 67, 70] attempted to analytically create linkages between the time domain performance indexes and the eigenstructure, though they suffer several defects, as mentioned above. This thesis continues along this direction but with full consideration of these defects. The above analysis naturally leads to derivation of a performance index which relies only on eigenstructure and has no relationship with initial state and time span. Moreover, this eigenstructure-based index should entirely preserve the structural relationship between eigenstructure and time domain responses. Therefore, the fundamental contribution of this thesis is to derive such an index. Definitely, there are some predictable benefits of derivation of the index. First, it is easily inferred that calculation of the index is independent of control structures because it uses eigenstructure of the closed loop system. Thus, one significance of the index is that it can be applied for solution of structurally constrained control problems [67, 70]. Furthermore, for development of the optimization techniques, a number of (deterministic or stochastic) methods are available which can solve constrained nonlinear optimization problems [71-73]. This truly provides opportunities for this research work to develop optimization based damping controller design methods which employ the eigenstructure-based indexes as objective functions. These methods can combine the merits of the indexes and generic optimization based methods. Hence, some design specifications like structural constraints and robustness, as well as optimization and coordination of control efforts, should be considered.

It is not difficult to validate the eigenstructure-based performance indexes and the corresponding controller tuning methods by applying them to coordinated design of PSSs and SDCs for FACTS devices. However, the thesis

also tries to exploit their potential to challenge some special issues in designing SDCs for DFIGs. As easily observed in [44, 46, 74], use of DFIGs with SDCs to damp inter-area oscillations sacrifices their dynamic performance, compared to cases with no SDCs. Thus, intuitively, when providing necessary damping to inter-area oscillations, dynamics of DFIGs can also be optimal. The DFIG contributes to damping control by injecting modulated active and reactive power to grid, which inherently impacts its dynamics. For instance, the active power modulation may interact with the torsional dynamics whereas the reactive power modulation obviously influences the stator voltage dynamics [51]. Consequently, seeking optimized DFIG active and reactive power outputs during the transient appears natural. Moreover, although additional damping can be supplied to inter-area oscillations by active or reactive power modulation, flexible coordination of the two means does not appear to have been addressed by any researchers. Thus, these issues are specifically addressed in this thesis with the help of the eigenstructure-based indexes which are expected to be capable of measuring the performance of active or reactive power output dynamics.

1.3 Thesis Layout

The remainder of the thesis is organized as follows.

Chapter 2 introduces some essential details regarding small signal stability analysis and control, which serves as the foundation for the work reported in this thesis. The eigen-analysis and the damping torque analysis are investigated, and their relationship is explained. Moreover, various methods for model reduction are reviewed. In addition, the damping control structure is thoroughly

investigated, and the structurally constrained controllers used throughout the thesis are specifically emphasized.

Chapter 3 proposes an eigenstructure-based index to measure the dynamic performance of the system as well as control efforts. This index can be utilized for solving structurally constrained control problems. Thus, a tuning scheme based on this index is proposed for coordinating PSSs and SDCs for FACTS devices to damp inter-area oscillations of systems and to optimize their control efforts under multiple operating conditions. Here, both PSSs and SDCs are designed as structurally constrained controllers.

Chapter 4 proposes an inter-area mode oriented pole-shifting method (named: IAMO-PS) that coordinates control efforts to tune power oscillation damping controllers. IAMO-PS is indeed a two-stage optimization problem in which a specific pole placement strategy suitable for control of inter-area modes is implemented in the first stage while still being subjected to constraints of pole placement in the second stage; control efforts of different controllers measured by an eigenstructure-based index are flexibly coordinated.

Chapter 5 proposes designs of controllers for DFIG-based WTGs to demonstrate the capability of DFIG to suppress inter-area oscillations. In addition to the primary power and voltage (PV) controllers, a SDC is proposed for the DFIG to adequately harness its damping function. Furthermore, the design scheme employs differential evolution (DE) algorithms to simultaneously optimize parameters of PV controllers and SDCs.

Chapter 6 proposes a dual-channel SDC for DFIG-based WTG to optimally coordinate its active and reactive power modulation for suppression of inter-area oscillations. The IAMO-PS is employed to tune the SDC for providing expected

damping to inter-area modes with optimizing of weighted sum of control efforts of active and reactive power modulation. Consequently, since the dynamics of DFIG are directly coupled with power outputs as optimized and coordinated active and reactive power outputs lead to significant improvements in DFIG dynamics when it is controlled for initiative damping function.

Chapter 7 concludes the thesis. Some prospective extensions as well as the possible direction for future research are also presented.

1.4 List of Publications

Journal paper published:

1. D. P. Ke, C. Y. Chung, and Y. Xue, "An eigenstructure-based performance index and its application to control design for damping inter-area oscillations in power systems," *IEEE Transactions on Power Systems*, vol. 26, no. 4, pp. 1-10, Nov. 2011.

2. D. P. Ke and C. Y. Chung, "An inter-area mode oriented pole-shifting method with coordination of control efforts for robust tuning of power oscillation damping controllers," *IEEE Transactions on Power Systems*, vol. 27, 2012. Article in press.

Conference paper presented:

3. D. P. Ke, C. Y. Chung, and Y. Xue, "Controller design for DFIG-based wind power generation to damp inter-area oscillation," in 5th *International Conference on Critical Infrastructure* (*CRIS*), Beijing, 2010.

Journal paper under preparation:

4. D. P. Ke and C. Y. Chung, "Optimal coordination of active and reactive power modulation of DFIG-based wind turbine generators to damp inter-area oscillations in power systems"

Chapter 2

Essentials for Small Signal Stability Analysis and Control

2.1 Eigen-Analysis of Dynamic Systems

Real power systems are highly nonlinear and non-stationary systems whose dynamics should be generically represented by a parameter dependent differential-algebraic-discrete model [75]. But, for electromechanical oscillation studies, the major concerned dynamics with frequencies range from less than 1 Hz to 3 Hz can be well preserved in the reduced nonlinear differential and algebraic equations as follows [5]:

$$\dot{\mathbf{x}} = \mathbf{F}(\mathbf{x}, \mathbf{g}, \mathbf{u}) \tag{2.1}$$

$$\mathbf{0} = \mathbf{G}(\mathbf{x}, \mathbf{g}, \mathbf{u}) \tag{2.2}$$

$$\mathbf{y} = \mathbf{H}(\mathbf{x}, \mathbf{g}, \mathbf{u}) \tag{2.3}$$

where $\mathbf{F}$ is the vector of differential equations depicting electromechanical dynamics of equipments such as generators, excitation systems and governors; $\mathbf{G}$ is the vector comprising static network equations as well as algebraic equations of the dynamic equipments, for example, the stator voltage equations of generators; $\mathbf{H}$ is the vector of output equations; and $\mathbf{x}$, $\mathbf{g}$, $\mathbf{u}$ and $\mathbf{y}$ are vectors of state variable, algebraic variable, input and output, respectively. In small signal

15

stability analysis, (2.1)-(2.3) are linearized around an operating point ($\mathbf{x}_0$, $\mathbf{g}_0$, $\mathbf{u}_0$, $\mathbf{y}_0$), and then algebraic variables are eliminated to obtain a standard state-space representation as follows:

$$\Delta\dot{\mathbf{x}} = \mathbf{A}\Delta\mathbf{x} + \mathbf{B}\Delta\mathbf{u} \tag{2.4}$$

$$\Delta\mathbf{y} = \mathbf{C}\Delta\mathbf{x} + \mathbf{D}\Delta\mathbf{u} \tag{2.5}$$

where $\Delta\mathbf{x}=\mathbf{x}-\mathbf{x}_0$, $\Delta\mathbf{y}=\mathbf{y}-\mathbf{y}_0$, and $\Delta\mathbf{u}=\mathbf{u}-\mathbf{u}_0$ denote increments from the operating point; $\mathbf{A}$, $\mathbf{B}$, $\mathbf{C}$ and $\mathbf{D}$ are the state matrix, input matrix, output matrix and feedforward matrix, respectively. The symbol 'Δ' will be omitted in the following text for the sake of statement simplicity. Moreover, since there is in general not any feedforward path directly connecting inputs and outputs, (2.4) and (2.5) can be rewritten with $\mathbf{D}=\mathbf{0}$ as follows:

$$\dot{\mathbf{x}} = \mathbf{A}\mathbf{x} + \mathbf{B}\mathbf{u} \tag{2.6}$$

$$\mathbf{y} = \mathbf{C}\mathbf{x} \tag{2.7}$$

The small signal stability of the system (2.1)-(2.3) can be judged depending on eigenvalues of $\mathbf{A}$ of the above linear system: the original system is asymptotically stable when all eigenvalues have negative real parts, whereas it will be unstable if at least one eigenvalue has a positive real part. However, when some eigenvalues have real parts equal to zero, it will be futile to use (2.6)-(2.7) to depict the manifold of (2.1)-(2.3) around the equilibrium point and the high-order approximation is normally necessary [76]. Moreover, the ith eigenvalue λ_i, the ith right eigenvector $\mathbf{v}_i$ and the ith left eigenvector $\mathbf{w}_i$ of $\mathbf{A}$ satisfy the following relationship:

$$\mathbf{A}\mathbf{v}_i = \lambda_i\mathbf{v}_i \qquad i = 1, 2, ..., n_o \tag{2.8}$$

$$\mathbf{w}_i\mathbf{A} = \lambda_i\mathbf{w}_i \tag{2.9}$$

16

where n_o is the dimension of the open loop system. v_i is normalized so that $\| v_i \|_2 = 1$. Furthermore, the eigenvectors are related to each other as follows:

$$w_i v_j = \begin{cases} 1 & i=j \\ 0 & i \neq j \end{cases} \tag{2.10}$$

Or, (2.10) can be expressed in terms of matrices as follows:

$$\mathbf{WV} = \mathbf{VW} = \mathbf{I} \tag{2.11}$$

where $\mathbf{I}$ is a n_o-dimensional identity matrix; $\mathbf{W}$ and $\mathbf{V}$ are the left and right eigenvector matrices defined as follows:

$$\mathbf{W} = \left[w_1^{\mathrm{T}}, w_2^{\mathrm{T}}, ..., w_{n_o}^{\mathrm{T}} \right]^{\mathrm{T}} \tag{2.12}$$

$$\mathbf{V} = \left[v_1, v_2, ..., v_{n_o} \right] \tag{2.13}$$

Physically, the kth element v_{ki} of v_i measures the activity of the kth state variable x_k in the ith mode and the kth element w_{ik} of w_i weights the contribution of this activity to the mode. Thus, the net measurement of the relative participation of x_k in the ith mode which is termed participation factor is defined as follows:

$$\mathrm{p}_{ki} = v_{ki} w_{ik} \tag{2.14}$$

Moreover, it is easily to verify the following equations:

$$\sum_{k=1}^{n_o} \mathrm{p}_{ki} = 1 \quad \text{or} \quad \sum_{i=1}^{n_o} \mathrm{p}_{ki} = 1 \tag{2.15}$$

Therefore, the nature of a mode can be identified according to the participation factors [77]. For example, electromechanical modes are much more significantly participated by state variables regarding the power angle and the rotor speed of synchronous generators, than by other non-mechanical state variables. Moreover, in general an inter-area mode is evenly participated by a large number of generators, while a local mode is only participated by several generators.

Another merit of participation factor is that it can be utilized to choose PSS site. In principle, as a generator markedly participates in an electromechanical mode, it should be an ideal location to site PSS to damp the mode. Nevertheless, it is noted that participation factors are only based on the state matrix. The effectiveness of the selected control loops in controlling targeted modes should be exactly evaluated based on indexes which are calculated from eigenvectors as well as input and output matrices.

By applying similar transformation $\mathbf{x}=\mathbf{V}\mathbf{z}$ to (2.6)-(2.7), the dynamic equations in a decoupled form can be obtained as follows:

$$\begin{bmatrix} \dot{z}_1 \\ \dot{z}_2 \\ \vdots \\ \dot{z}_{n_o} \end{bmatrix} = \begin{bmatrix} \lambda_1 & & & \\ & \lambda_2 & & \\ & & \ddots & \\ & & & \lambda_{n_o} \end{bmatrix} \begin{bmatrix} z_1 \\ z_2 \\ \vdots \\ z_{n_o} \end{bmatrix} + \begin{bmatrix} w_1 b_1 & w_1 b_2 & \cdots & w_1 b_{n_b} \\ w_2 b_1 & w_2 b_2 & \cdots & w_2 b_{n_b} \\ \vdots & \vdots & & \vdots \\ w_{n_o} b_1 & w_{n_o} b_2 & \cdots & w_{n_o} b_{n_b} \end{bmatrix} \begin{bmatrix} u_1 \\ u_2 \\ \vdots \\ u_{n_b} \end{bmatrix} \qquad (2.16)$$

$$\begin{bmatrix} y_1 \\ y_2 \\ \vdots \\ y_{n_c} \end{bmatrix} = \begin{bmatrix} c_1 v_1 & c_1 v_2 & \cdots & c_1 v_{n_o} \\ c_2 v_1 & c_2 v_2 & \cdots & c_2 v_{n_o} \\ \vdots & \vdots & & \vdots \\ c_{n_c} v_1 & c_{n_c} v_2 & \cdots & c_{n_c} v_{n_o} \end{bmatrix} \begin{bmatrix} z_1 \\ z_2 \\ \vdots \\ z_{n_o} \end{bmatrix} \qquad (2.17)$$

where $\mathbf{z} = \begin{bmatrix} z_1, z_2, ..., z_{n_o} \end{bmatrix}^{\mathrm{T}}$ represents the state vector in the modal space; n_b and n_c are the number of inputs and outputs, respectively; u_k denotes the kth input and b_k the kth column vector of $\mathbf{B}$ corresponding to this input; and y_j denotes the jth output and c_j the jth row vector of $\mathbf{C}$ corresponding to this output. Apparently, from (2.16)-(2.17) it is known that the index $w_i b_k$ measures the controllability of u_k in the ith mode while the index $c_j v_i$ reflects the observability of the ith mode in y_j. The geometric approach used in [78] and [79] to represent controllability and observability for control loop selections is derived from these two indexes.

Hence, the net effectiveness of control of the ith mode by using u_k and y_j to form the feedback control loop can be jointly indicated by the following index:

$$\mathrm{R}^{i}_{kj} = c_j v_i w_i b_k \tag{2.18}$$

where R^{i}_{kj} is also known as modal residue that can be calculated as follows:

$$\mathrm{R}^{i}_{kj} = \lim_{s \to \lambda_i} \left[(s - \lambda_i) \mathrm{G}_{kj}(s) \right] \tag{2.19}$$

where $\mathrm{G}_{kj}(\cdot)$ denotes the transfer function between u_k and y_j.

The significance of the residue is that it successfully connects the modal controllability and observability to the eigenvalue sensitivity [80]. As illustrated in Fig. 2.1, the sensitivity of the ith eigenvalue (mode) with respect to K_{kj} can be computed when K_{kj} is initially equal to zero (open loop), as follows:

$$\frac{\partial \lambda_i}{\partial K_{kj}} = \mathrm{R}^{i}_{kj} H_{kj}(\lambda_i) \tag{2.20}$$

where K_{kj} is the gain of the feedback controller and $H_{kj}(\cdot)$ denotes the phase compensation blocks. Thus, the first order prediction of the closed loop eigenvalue λ'_i can be calculated as follows:

$$\lambda'_i = \lambda_i + K_{kj} \mathrm{R}^{i}_{kj} H_{kj}(\lambda_i) \tag{2.21}$$

If $H_{kj}(\lambda_i)$ exactly compensates the phase angle of R^{i}_{kj} to -180º, increasing K_{kj} will purely enhance the damping of λ_i in the sense of linear prediction. In such case, obviously larger magnitude of R^{i}_{kj} implies that the control loop from y_j to u_k will be more efficient in increasing the damping of λ_i. According to (2.18), this actually fits to the general conclusion that the control loop with higher controllability and observability to a mode will be more suitable for controlling the mode.
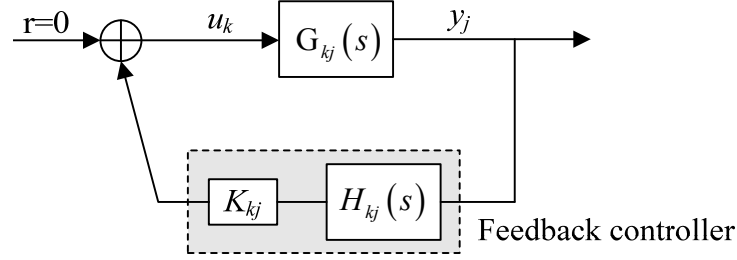
Fig. 2.1. SISO feedback control system

2.2 Damping Torque Analysis

A SMIB system is originally employed for understanding the essences of damping of power system electromechanical oscillations [17]. The block diagram of the linearized model of such system is shown in Fig. 2.2 where δ and ω are power angle and rotor speed, respectively, of the generator; H is the inertia constant; D_0 is the mechanical damping coefficient; T'_{d0} is the d-axis open-circuit transient time constant; T_m is the mechanical torque; EXC(s) is the transfer function of the excitation system; and K_1 to K_6 are constant coefficients associated with parameters of the external network and generation system. Process of deducing K_1 to K_6 can refer to that in [5]. Firstly, it is assumed that a controller of proportional gain K_D is able to directly produce an additional torque on the shaft of the generator, as shown in Fig. 2.2(a). This hypothetic controller uses the rotor speed as control input, and thus the produced torque can be calculated as follows:

$$T_D = K_D \omega \tag{2.22}$$

In the complex frequency domain, T_D is clearly in phase with ω and well known as the damping torque. If the initial value of K_D is zero (open loop), the residue of the control loop from T_D to ω with respect to the only electromechanical mode λ_e can be derived based on (2.18), as follows [28]:

20

$$R^e = -\frac{p_{\omega e}}{2H} \tag{2.23}$$

where $p_{\omega e}$ is the participation factor of ω with respect to λ_e. Thus, according to (2.21), the linear prediction of the closed loop electromechanical λ_e' can be calculated as follows:

$$\lambda_e' = \lambda_e - K_D \frac{p_{\omega e}}{2H} \tag{2.24}$$

Because the electromechanical mode is almost exclusively participated by δ and ω, $p_{\omega e}$ is very close to a real value [53]. Consequently, augment of K_D will just increase the damping of λ_e. This also accounts for that introduction of additional damping torque to the generator shaft can help to suppress its oscillation.
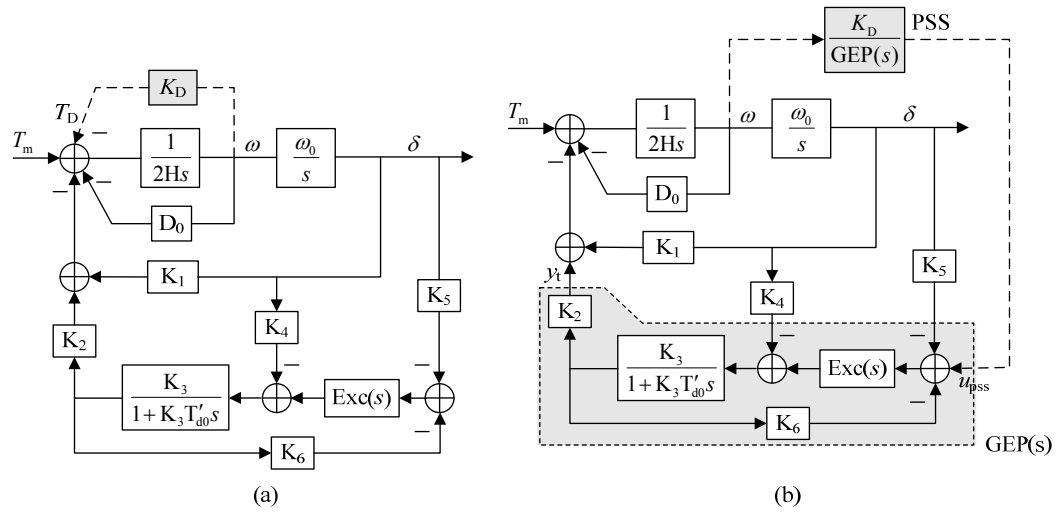
Fig. 2.2. Detailed block diagram of a SMIB system

Although forming a hypothetic control loop from T_D to ω can assist to consolidate the mathematical foundation of the damping torque concept based on residue analysis, it is apparently impossible to employ it in the damping control design. The practical situation is shown in Fig. 2.2(b) where the PSS produces the output directly added to the voltage reference input, rather than the generator shaft. In this diagram, GEP(s) denotes the transfer function from u_{pss} to y_t,

assuming that the generator inertia constant is infinite [20]. Moreover, according to Mason's gain formula [81], Fig. 2.2(b) is equivalent to Fig. 2.2(a) in terms of the closed loop eigenvalues. This indicates that the PSS can operate to introduce an additional damping torque on the generator shaft as done in Fig. 2.2(a), as long as the phase of the PSS can exactly counteract that of GEP($\cdot$) at the frequency λ_e. Such phase compensation technique is well known as the GEP method and has been intensively investigated for the PSS design in multimachine power systems [82, 83]. Apart from the PSS, the damping torque induced by the SDC installed in FACT device is deduced in [28] through proper manipulation of the transfer function, and the induced damping torque coefficients (IDTCs) are thus defined. Based on the relationship between the residue and the damping torque as discussed above, the pole shifting due to the SDC can be linearly predicted by using the IDTCs [53, 84]. Therefore, relying on such linear prediction of the pole shifting, Reference [85] uses a linear programming method to tune the PSSs and SDCs in a coordinate manner.

2.3 Model Reduction for Damping Control Design

The order of a power system model is often quite high, and in reality it easily reaches several thousands. Direct use of this model for control design may encounter numerical problems and/or cost an unacceptable computational time. Moreover, because modern control design methods such as optimal control or H_∞, produce controllers of order at least equal to the order of the plant, the resulted controllers will be very complex if these methods are implemented based on a full system model [6]. Thus, it is necessary to simplify original high-order system model to ease the design procedure and to avoid complexity in final controllers.

This simplification is known as model reduction and requires that the reduced model should be a good approximation of the original model.

Given the n_o-dimensional open loop system (2.6)-(2.7) which can be expressed by the transfer function $\mathbf{G}(s)=\mathbf{C}(s\mathbf{I}-\mathbf{A})^{-1}\mathbf{B}$, the model reduction procedure is to derive a low-order approximation $\mathbf{G}_r(s)$ of order n_r ($n_r \ll n_o$) such that the infinite norm of their error $\|\mathbf{G}-\mathbf{G}_r\|_\infty$ which denotes the peak gain of the error transfer function across frequency is sufficiently small. Among various methods for model reduction, the Schur balanced truncation method is a commonly used one which can ensure a definite bound on the H_∞ of the error as follows [86]:

$$\left\|\mathbf{G}(s)-\mathbf{G}_r(s)\right\|_\infty \leq \sum_{i=n_r+1}^{n_o} \sigma_i \tag{2.25}$$

where σ_i is termed the ith Hankel singular value (HSV) of $\mathbf{G}(s)$ and defined as the square root of the ith largest eigenvalue of the Hermite matrix $\mathbf{PQ}$ which are the solutions of the following Lyapunov equations:

$$\mathbf{PA}^T + \mathbf{AP} + \mathbf{BB}^T = \mathbf{0} \tag{2.26}$$

$$\mathbf{QA} + \mathbf{A}^T\mathbf{Q} + \mathbf{C}^T\mathbf{C} = \mathbf{0} \tag{2.27}$$

where $\mathbf{P}$ and $\mathbf{Q}$ are known as the controllability and observability grammians, respectively. Moreover, the largest singular value σ_1 is defined as the Hankel norm of the system, that is $\|\mathbf{G}\|_H = \sigma_1$. In the balanced truncation method, the original system is transformed to a balanced realization through a series of similarity transformation such that $\mathbf{P}$ and $\mathbf{Q}$ are equal and diagonal. The entries in the diagonal of $\mathbf{P}$ or $\mathbf{Q}$ are thus the HSVs of $\mathbf{G}(s)$. The most useful aspect of such realization is that it relates each transformed state to a HSV which indicates to what extends this state influences the frequency response of $\mathbf{G}(s)$. For example, if

$\sigma_i \gg \sigma_{i+k}$, the effect of state x_i in input-output behavior will be considerable greater than that of x_{i+k}. In such case, each state is as equally controllable as it is observable and HSV can be viewed as an index which guides to what extend a system model can be reduced. Therefore, according to the HSV, the states in the balanced realization are partitioned into two groups: one group includes states which show significance in the input-output behaviors and the rest least significant states with poor controllability and observability form another group. The truncation is then applied to obtain the reduced model by ignoring the least significant states.

In the approach of optimal Hankel norm approximation, the reduced low-order model is derived by solving an optimization problem where the Hankel norm of the error transfer function $\|\mathbf{G} - \mathbf{G_r}\|_H$ is minimized [87]. Nevertheless, it is noted that the conventional calculation of the controllability and obervability grammians, and thus the HSVs of a quite high-order model on the basis of a state-space representation is quite computationally expensive, sometimes even prohibitive [88]. Thus, Reference [89] has proposed a sparse low-rank Cholesky factorization-alternating direction implicit method based on descriptors of power system models to computes approximations to the grammians. The method exploits the sparsity of the descriptor systems and thus is applicable to large scale systems while keeping memory and CPU requirements at modest levels. Moreover, model reduction of large scale power systems is performed in [90] by using a Krylov subspaces based moment matching method which presents less computational effort and less storage requirements than the grammian-based methods although the ability of global approximation in the frequency domain of the former is inferior to that of the latter. Furthermore, the modal truncation

method numerically computes the dominant poles and zeros of the system and preserves them in the reduced model [91, 92]. As the method avoids the prohibitive effort in calculation of HSVs of the full order system, it is suitable for cope with large scale interconnected power system problems although it requires reliably and correctly determining the dominant poles and zeros.

All above mentioned methods directly manipulate the linearized models of systems. Another important class of attempts for model reduction is to use the identification techniques on the basis of the time domain responses of the systems which are obtained from either the numerical simulation programs or actual measurements. The Prony method is a representative one which in essence fits weighted sum of exponential terms to given signals [93, 94]. Reference [95] fits a low-order state-space model to system impulse response based on the singular value decomposition of the Hankel matrix associated with the impulse response. This method is further improved in [96] for the better numerical characteristics. Moreover, the genetic algorithm is employed in [97] to combine with the standard Prony algorithm to overcome its insufficiency in identifying transfer function zeros of the reduced model.

2.4 Power System Damping Control Structures

Commonly, in the case of using a SISO or MIMO controller employing local signals to control a plant, *control structure* can be viewed as the *model structure* of the controller. However, in the context of power system damping control, especially for inter-area modes, multiple components (generators or FACTS devices) which are distributed in networks should be controlled simultaneously and coordinatedly. Thus, the concept of control structure should be necessarily

extended to cover the meaning of *control architecture*, i.e. how the damping controllers are configured.

2.4.1 Damping Control Architectures

Generally, four types of architectures having been proposed for damping control are shown in Fig. 2.3 [98]:

(1) Decentralized control: each controller receives local feedback signals and sends produced control outputs to the controlled object in situ. Although this architecture is easily implemented, it may be ineffective to damp inter-area oscillations because local signals often lack of good observability of some significant inter-area modes [85, 99].

(2) Quasi-decentralized control: its difference from the decentralized control is that the remote signals are additionally fed-back to the local controller as control input (sometimes local signal is unnecessary). Its advantage is that the local controller can perceive the global system dynamics from the remote signals which make it act more effectively to suppress inter-area oscillations. Furthermore, this architecture could well preserve the simplicity of the decentralize control though inducing remote signals may decrease its reliability [32, 100].

(3) Centralized control: a centralized control can be conceptually regarded as a MIMO controller which is actually placed in a control center that is responsible for collecting remote feedback signals and transmitting control outputs to the remote controlled objects. Obviously, powerful modern control tools can be applied to synthesize this controller. However, it suffers the complexity of using a control center as well as risk of loss of communication links [101].

26

(4) Hierarchical or multilevel control: two or more control levels are constructed, for example, C_1 and C_2 form level one while C_3 is level two. Controllers in one level receive control signals from controllers in a level above. Although a control center is still required, this structure can maintain a minimum performance in the event of loss of communication links with the help of the controllers in lower level [98, 102, 103].
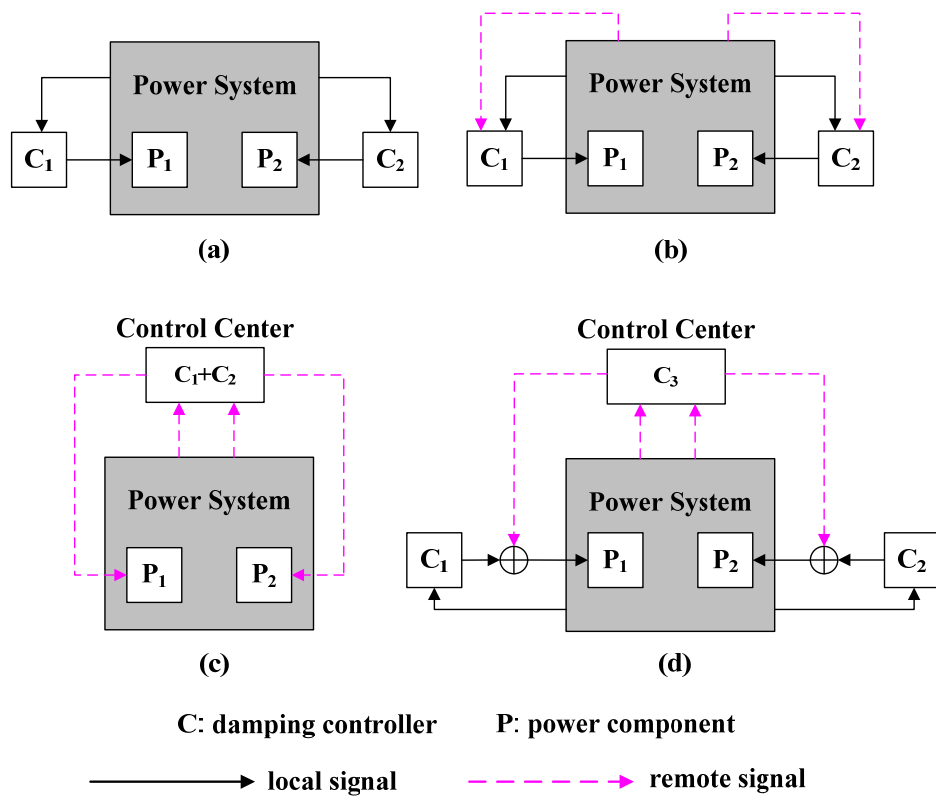
Fig. 2.3. Damping control architectures: (a) decentralized control; (b) quasi-decentralized control; (c) centralized control; (d) hierarchical control

2.4.2   Model Structures of PSS and SDC

In order to conveniently discuss the control architecture in Fig. 2.3, the model structures of C_1, C_2 and C_3 are ignored. However, they are actually the function parts in the whole control system. In this subsection, the commonly used model structures of PSS and SDC are introduced.

27

During the developing history of PSS, several standard structures have been proposed for field application. In 1992, IEEE Std-421.5 recommended Type PSS1A and PSS2A [18]. Type PSS2B, PSS3B and PSS4B were suggested in 1996 [19]. Most recently, a novel multi-band PSS was proposed and later included in the revised IEEE Std-421.5 as Type PSS4B [104]. The most commonly used PSS structure—Type PSS1A is shown in Fig. 2.4. Such conventional structure comprises a gain, phase compensation blocks, a washout filter and output limits [5]. The washout block is a high-pass filter to eliminate the steady state output of the PSS so that it does not impact the steady state of system. The value of T_w is selected to present a band-pass effect to the input signal containing local and inter-area modes. The output of the PSS is limited properly otherwise it might prevent the action of AVR which functions to induce sufficient synchronizing torque for the first swing stability. Originally, when only local signals are available for control, shaft speed and terminal frequency are among the commonly used input signals. Although shaft speed is the most direct variable to observe electromechanical oscillation, application of it as control input to the PSS in thermal units should carefully consider the effects on torsional oscillations. A torsional filter is normally required in the stabilizing path to attenuate the torsional components. This filter, however, has a destabilizing effect on the 'exciter mode', thus imposing a maximum limit on the allowable stabilizer gain which may limit the overall effectiveness of the stabilizer in damping rotor oscillations. Since the sensitivity of the terminal frequency to rotor oscillations increases as the electrical connection strength of external transmission system becomes weaker, the frequency based PSS may give more contributions in damping inter-area mode oscillations than the speed

based PSS. Nevertheless, as in the case of speed based PSS, care has to be taken to remove torsional modes when frequency based PSS is used in steam turbine unit. The problem of deteriorating torsional modes is not serious when dual-input PSS (PSS2A and PSS2B) employs shaft speed and electrical power to derive the equivalent speed signal as control input which does not contain torsional modes because the torsional components are inherently attenuated in the integral of electrical power. So far, although no authoritative document addresses the issue of structure standardization, effective and simple structures imitating those of the PSSs have been successfully utilized in many literatures for the SDC design, for example, a classic low-order phase lead-lag compensator [28, 85, 99, 105].
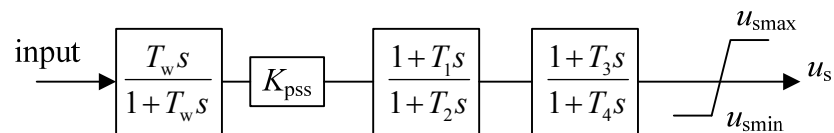
Fig. 2.4. Block diagram of Type PSS1A

2.4.3 Structurally Constrained Controllers

It is not surprised that power engineers favor to use simple control structures which they are familiar to. This is readily accepted as on the one hand a familiar control structure can enhance their confidence for practical application, and on the other hand the implementation as well as maintenance in the future of a controller with a simple structure will be relatively easy [106]. Therefore, besides the expected control effects, they usually impose *structural constraints* on the control architecture as well as model structures of the damping controllers. A normal way to fulfill control design with structural constraints is to give control structures in advance with some tunable parameters by the designers based on analysis of characteristics of the controlled objects as well as consideration of

their preferences, and then tune these parameters with the adopted design methods to achieve certain control effects. It is not difficult to note that a large category of damping controllers reported in existing literatures is synthesized in such way, and thus these controllers can be termed *structurally constrained controllers* [34, 66, 85, 98, 99, 106-109].

No matter what structure a PSS or SDC is used, there are commonly some key parameters which can significantly impact electromechanical oscillations, for example, K, T_1, T_2, T_3, and T_4 in Fig. 2.4. Tuning these critical parameters play central role in damping the power oscillations. Although power engineers can design control structure according to their experiences and preferences, it is obviously not straightforward to obtain optimal parameters to fulfill the expected performance. In fact, many modern control methods are yet unable to flexibly tune the structurally constrained controllers, for example, the linear matrix inequalities (LMI) and the H_∞ robust control, because they normally produce MIMO controllers whose transfer function matrices have non-zero elements in all positions while the transfer function matrices of the structurally constrained MIMO controllers are often in specific forms, such as the diagonal form in the decentralized or quasi-decentralized control [32, 61, 110, 111]. Moreover, as mentioned in Section 2.3, these methods produce controllers whose order is at least as large as the open-loop system [112]. Thus, together with some other requirements on the control design such as robustness in multiple operating conditions and optimization of control efforts, the structural constraints indeed pose great challenges on the design of damping controllers for the inter-area oscillations.

2.5 Summary

In this chapter, the fundamentals for the small signal stability analysis and control have been introduced. The eigen-analysis is prone to address the small signal stability problem from a mathematical viewpoint, while the damping torque analysis gives a more physical picture depicting the essence of power system damping. These two naturally distinctive methods have been successfully unified by the residue analysis. Since the model reduction is an indispensable step in the design of damping controllers for a practical large power system, various model reduction techniques have been reviewed. Moreover, the damping control structures have been discussed. It has been pointed out that the design methods should be capable of dealing with the structurally constrained controllers to obtain the desired control effects.

Chapter 3

Application of Eigenstructure-Based Performance Index to Control Design for Damping Inter-Area Oscillations in Power Systems

3.1 Introduction

Generally, it is expected that as damping controllers (PSSs and SDCs) work in a coordinated manner to provide adequate additional damping to inter-area oscillations, their control efforts should be optimal [113, 114]. Moreover these controllers should be robust for different operating conditions or network configurations [105, 106]. Besides, structural constraints are usually imposed on damping controllers: they must use dynamic output feedback control schemes because it is difficult to implement state feedback control in power systems; they should be low order and with a simple structure familiar to engineers so that implementation and the subsequent tuning are easy [98, 105, 106]. Moreover, although a decentralized implementation scheme using only local signals as inputs is more practical for damping controllers, they can be configured for quasi-decentralized implementation when wide area signals are employed as inputs to enhance their effectiveness in damping inter-area oscillations [98].

However time delays that occur because of use of wide area signals should be considered in the design.

Several methods have been proposed for the design of damping controllers. Approaches based on robust control theories and LMI have been applied for damping controller design to deal with uncertainties of operating conditions [6, 32, 105, 113, 115]. However they cannot be applied for design of structurally constrained controllers. In [105], for designing structurally constrained SDCs for coordinated functioning, the LMI based regional pole placement problem is converted into the iteratively solved bilinear matrix inequalities (BMI) problem. Nevertheless, this method assumes that input matrices of state space equations of the controllers are known. Methods that directly optimize eigenvalues of the closed loop system can readily be applied to structurally constrained controllers while considering multiple operating conditions [70, 99, 106, 116, 117]. However, system dynamics in time domain are not only related to eigenvalues, but also associated with eigenvectors [52]. Moreover, control effort cannot be explicitly optimized in these methods. Therefore, one salient merit of optimal control [98, 114] is that the control process, together with the system dynamics objective, can be explicitly considered in the cost function. Unfortunately standard optimal control cannot be applied to structurally constrained controllers although it can perform well for state feedback controllers [6]. The method applied in [98], [107] and [118] tries to solve this problem by assuming that poles of synthesized controllers are known. However, this assumption is only applicable for some certain control structures and the method cannot take multiple operating conditions into consideration.

In this chapter an eigenstructure-based performance index is proposed to measure the system dynamic performance as well as the control efforts. Computation of this index does not rely on the control structures because it is only related to the eigenstructure of the closed loop system and the design parameters. Minimizing this index can improve system dynamics and optimize the control efforts. Therefore, by utilizing this index to construct objective functions, structurally constrained controllers can be designed for optimization of control. Based on this idea, a tuning method is proposed for coordination of structurally constrained PSSs and SDCs as stated above, to damp inter-area oscillations as well as to optimize the control efforts under multiple operating conditions.

This chapter is organized as follows. Firstly, the eigenstructure-based performance index is introduced. Then, the closed loop power system model used to calculate the index is synthesized. Subsequently, the tuning scheme for coordination of PSSs and SDCs is introduced. Simulation results are reported at the final stage.

3.2 Eigenstructure-Based Performance Index

Irrespective of the structure adopted by damping controllers, the synthesized linear model of a closed loop power system around an operating point can generally be described as follows:

$$\dot{\mathbf{x}}_j = \mathbf{A}_j \mathbf{x}_j \qquad (3.1)$$

$$\mathbf{y}_o = \mathbf{E}_j \mathbf{x}_j \qquad (3.2)$$

$$\mathbf{u}_c = \mathbf{K}_j \mathbf{x}_j \qquad (3.3)$$

where $\mathbf{x}_j \in \mathfrak{R}^n$ and $\mathbf{A}_j \in \mathfrak{R}^{n \times n}$ are the state vector and state matrix, respectively, for the jth operating condition taken into consideration; $\mathbf{y}_o$ is the output vector representing system dynamics objective; $\mathbf{u}_c$ is the output vector of damping controllers; and $\mathbf{E}_j$ and $\mathbf{K}_j$ are output matrices. The system dimension may vary in different operating conditions. Nevertheless, the deduction shown afterward is irrespective of the variation of system dimension which thus is denoted by n for the sake of statement simplicity.

For the jth operating condition, a quadratic performance measurement (cost function) is defined as:

$$\text{cost}_j = \int_0^\infty \left[\mathbf{y}_o^H \mathbf{Q}_j \mathbf{y}_o + \mathbf{u}_c^H \mathbf{R}_j \mathbf{u}_c \right] dt \quad \mathbf{x}_j(0) = \mathbf{x}_{j0} \tag{3.4}$$

where $\mathbf{Q}_j \in \mathfrak{R}^{n_Q \times n_Q}$ and $\mathbf{R}_j \in \mathfrak{R}^{n_R \times n_R}$ are diagonal matrices with positive entries on their respective diagonals; H is the conjugate transpose operator; and $\mathbf{x}_{j0}$ is the initial value of $\mathbf{x}_j$. As variables denoting relative power angles of generators are often selected as components of $\mathbf{y}_o$, minimization of (3.4) will suppress power angle oscillations of the system and also optimize control efforts of damping controllers. Substituting (3.2) and (3.3) into (3.4), cost_j can be rewritten as:

$$\text{cost}_j = \int_0^\infty \mathbf{x}_j^H \mathbf{P}_j \mathbf{x}_j \, dt \tag{3.5}$$

where $\mathbf{P}_j$ is a Hermite matrix defined as:

$$\mathbf{P}_j = \mathbf{E}_j^H \mathbf{Q}_j \mathbf{E}_j + \mathbf{K}_j^H \mathbf{R}_j \mathbf{K}_j \tag{3.6}$$

In power system dynamic analysis, state matrix $\mathbf{A}_j$ can be similarly diagonalized [5, 119]. Thus the time domain solution of (3.1) can be derived as:

$$\mathbf{x}_j(t) = \mathbf{U}_j e^{\mathbf{\Lambda}_j t} \mathbf{V}_j \mathbf{x}_{j0} \quad t \geq 0 \tag{3.7}$$

where $\mathbf{U}_j$ and $\mathbf{V}_j$ are right and left eigenvector matrices, respectively, of $\mathbf{A}_j$; $\mathbf{\Lambda}_j$ is

a diagonal matrix defined as follows:

$$\mathbf{\Lambda}_j = \mathrm{diag}\left(\lambda_{1j}, \lambda_{2j}, ..., \lambda_{nj}\right) \tag{3.8}$$

where $\lambda_{1j}, \lambda_{2j}, ..., \lambda_{nj}$ are eigenvalues of $\mathbf{A}_j$.

If the system is stable, i.e. all eigenvalues of $\mathbf{A}_j$ are with negative real parts, then (3.5) can be calculated based on (3.7), as follows:

$$
\begin{aligned}
\mathrm{cost}_j &= \int_0^\infty \left[\mathbf{x}_{j0}^H \mathbf{V}_j^H e^{\mathbf{\Lambda}_j^H t} \mathbf{U}_j^H \mathbf{P}_j \mathbf{U}_j e^{\mathbf{\Lambda}_j t} \mathbf{V}_j \mathbf{x}_{j0} \right] \mathrm{d}t \\
&= \mathbf{x}_{j0}^H \mathbf{V}_j^H \left[\int_0^\infty \left(e^{\mathbf{\Lambda}_j^H t} \mathbf{U}_j^H \mathbf{P}_j \mathbf{U}_j e^{\mathbf{\Lambda}_j t} \right) \mathrm{d}t \right] \mathbf{V}_j \mathbf{x}_{j0} \\
&= \mathbf{x}_{j0}^H \mathbf{V}_j^H \left[\left(\mathbf{U}_j^H \mathbf{P}_j \mathbf{U}_j \right) \cdot \mathbf{L}_j \right] \mathbf{V}_j \mathbf{x}_{j0} \\
&= \mathbf{x}_{j0}^H \mathbf{M}_j \mathbf{x}_{j0}
\end{aligned}
\tag{3.9}
$$

where $\mathbf{M}_j$ is termed as cost matrix for the jth operating condition and is defined as follows:

$$\mathbf{M}_j = \mathbf{V}_j^H \left[\left(\mathbf{U}_j^H \mathbf{P}_j \mathbf{U}_j \right) \cdot \mathbf{L}_j \right] \mathbf{V}_j \tag{3.10}$$

Here $\cdot$ denotes dot production and $\mathbf{L}_j$ is a Hermite matrix with the following definition:

$$
\mathbf{L}_j = -\begin{bmatrix}
\dfrac{1}{\lambda_{1j}^* + \lambda_{1j}} & \dfrac{1}{\lambda_{1j}^* + \lambda_{2j}} & \cdots & \dfrac{1}{\lambda_{1j}^* + \lambda_{nj}} \\
\dfrac{1}{\lambda_{2j}^* + \lambda_{1j}} & \dfrac{1}{\lambda_{2j}^* + \lambda_{2j}} & \cdots & \dfrac{1}{\lambda_{2j}^* + \lambda_{nj}} \\
\vdots & \vdots & \vdots & \vdots \\
\dfrac{1}{\lambda_{nj}^* + \lambda_{1j}} & \dfrac{1}{\lambda_{nj}^* + \lambda_{2j}} & \cdots & \dfrac{1}{\lambda_{nj}^* + \lambda_{nj}}
\end{bmatrix}
\tag{3.11}
$$

where * is the conjugate operator. The core of deduction for obtaining (3.9) is presented in the Appendix.

It is seen from (3.4) that cost$_j$ is positive for any given $\mathbf{x}_{j0}$. Therefore, from (3.9) and (3.10), it is inferred that $\mathbf{M}_j$ is a positive definite matrix. Consequently (3.9) can be further decomposed as follows:

$$\mathbf{x}_{j0}^{\mathrm{H}}\mathbf{M}_j\mathbf{x}_{j0} = \sigma_{1j}\left|z_{1j}\right|^2 + \sigma_{2j}\left|z_{2j}\right|^2 + \cdots + \sigma_{nj}\left|z_{nj}\right|^2$$

$$\sigma_{1j} \geq \sigma_{2j} \geq \ldots \geq \sigma_{nj} > 0 \tag{3.12}$$

$$\left\|\mathbf{x}_{j0}\right\|_2^2 = \left|z_{1j}\right|^2 + \left|z_{2j}\right|^2 + \cdots + \left|z_{nj}\right|^2 \tag{3.13}$$

where $\sigma_{1j}, \sigma_{2j}, \ldots, \sigma_{nj}$ are eigenvalues of $\mathbf{M}_j$ and are real positive numbers; $z_{1j}, z_{2j}, \ldots, z_{nj}$ are the corresponding coordinates' values when projecting $\mathbf{x}_{j0}$ onto the orthogonal basis formed by the right eigenvectors of $\mathbf{M}_j$. It is noted that $\sigma_{1j}, \sigma_{2j}, \ldots, \sigma_{nj}$ are only related to the eigenstructure of the system ($\mathbf{U}_j$, $\mathbf{V}_j$ and $\mathbf{L}_j$) and design parameters ($\mathbf{E}_j$, $\mathbf{K}_j$, $\mathbf{Q}_j$ and $\mathbf{R}_j$) for the jth operating condition.

Actually, $\mathbf{x}_{j0}$ denotes the initial disturbed deviation from the operating point and it cannot be determined in the control design process [113], which means that $z_{1j}, z_{2j}, \ldots, z_{nj}$ are also undetermined. Therefore, though cost$_j$ is a direct time domain indicative of the dynamic performance of the system and has been utilized in the state feedback optimal control [114], it is generally ineffective to use cost$_j$ directly for designing the structurally constrained controllers because the undetermined $\mathbf{x}_{j0}$ can not be dealt with in such cases. Nevertheless, according to (3.12), a way to reduce cost$_j$ for the undetermined $\mathbf{x}_{j0}$ is to reduce $\sigma_{1j}, \sigma_{2j}, \ldots, \sigma_{nj}$, and vice versa. Therefore, a new performance index is proposed in this chapter as follows:

$$f_{pj} = \sum_{k=1}^{n} \sigma_{kj} \tag{3.14}$$

Obviously this index is independent of $\mathbf{x}_{j0}$, and it is equivalent to cost$_j$ in terms of measuring the performance of system dynamics as well as the control efforts. Furthermore, irrespective of control structures, derivation of this index can be just based on the synthesized closed loop system model.

It is clear that $f_{\text{p}j}$ is the function of parameters of damping controllers. The system dynamics as well as control efforts can be optimized by adjusting these parameters to minimize $f_{\text{p}j}$. However in order to calculate $f_{\text{p}j}$, the linear model of the closed loop system has to be constructed; this is introduced in the next section.

3.3 Modeling of the Closed Loop System

3.3.1 System Structure

The structure of the overall system in which PSSs and SDCs work in a coordinated manner to damp inter-area oscillations is illustrated in Fig. 3.1. Both PSSs and SDCs are assumed to be a classical phase lead-lag compensator. They are implemented in a quasi-decentralized manner, and wide-area signals are employed to enhance their effectiveness in damping inter-area oscillations. Possible time delays are approximately considered in the design. The modeling of each part in Fig. 3.1 and synthesis of the closed loop system model are presented in the following subsections.
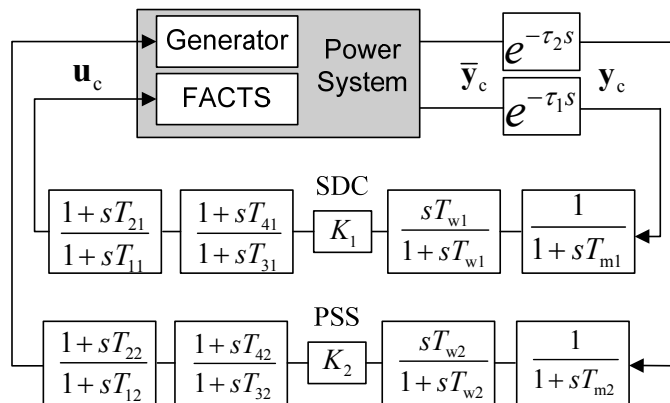
Fig. 3.1. Overall system structure

3.3.2 Reduced-Order Open Loop Power System Model

To reduce the time required for computation of f_{pj} and to accelerate the tuning process, the Schur balanced model truncation algorithm [86] is applied to obtain the following reduced-order open loop power system model:

$$\dot{\mathbf{x}}_{rj} = \mathbf{A}_{rj}\mathbf{x}_{rj} + \mathbf{B}_{rj}\mathbf{u}_c \tag{3.15}$$

$$\left[\overline{\mathbf{y}}_c, \mathbf{y}_o\right]^H = \left[\mathbf{C}_{rj}, \mathbf{E}_{rj}\right]^H \mathbf{x}_{rj} \tag{3.16}$$

where $\mathbf{x}_{rj} \in \Re^{n_r}$ and $\mathbf{A}_{rj} \in \Re^{n_r \times n_r}$ are the state vector and state matrix, respectively, of the reduced-order system for the jth operating condition; $\overline{\mathbf{y}}_c$ is the output vector for inputs of damping controllers; $\mathbf{B}_{rj}$ is the input matrix; $\mathbf{C}_{rj}$ and $\mathbf{E}_{rj}$ are output matrices.

3.3.3 Time Delay Approximation

Time delays are approximated by using the second order Pade formula [98]:

$$e^{-\tau s} \approx \frac{\tau^2 s - 6\tau s + 12}{\tau^2 s + 6\tau s + 12} \tag{3.17}$$

where τ is the time delay vector and right hand side of (3.17) will be calculated based on each of its elements separately. The state space equations describing the dynamics of time delays are obtained as follows:

$$\dot{\mathbf{x}}_\tau = \mathbf{A}_\tau \mathbf{x}_\tau + \mathbf{B}_\tau \overline{\mathbf{y}}_c \tag{3.18}$$

$$\mathbf{y}_c = \mathbf{C}_\tau \mathbf{x}_\tau + \mathbf{D}_\tau \overline{\mathbf{y}}_c \tag{3.19}$$

where $\mathbf{x}_\tau$ is the state vector of time delays; $\mathbf{y}_c$ is the input vector of damping controllers; $\mathbf{A}_\tau$, $\mathbf{B}_\tau$, $\mathbf{C}_\tau$ and $\mathbf{D}_\tau$ are state matrix, input matrix, output matrix and feed-forward matrix, respectively.

By incorporating (3.18) and (3.19) into (3.15) and (3.16), the following linear model is obtained:

39

$$\dot{\mathbf{x}}_{1j} = \mathbf{A}_{1j}\mathbf{x}_{1j} + \mathbf{B}_{1j}\mathbf{u}_{c} \tag{3.20}$$

$$\left[\mathbf{y}_{c}, \mathbf{y}_{o}\right]^{H} = \left[\mathbf{C}_{1j}, \mathbf{E}_{1j}\right]^{H} \mathbf{x}_{1j} \tag{3.21}$$

with the following matrix definition:

$$\mathbf{x}_{1j} = \begin{bmatrix} \mathbf{x}_{rj} \\ \mathbf{x}_{\tau} \end{bmatrix} \quad \mathbf{A}_{1j} = \begin{bmatrix} \mathbf{A}_{rj} & \mathbf{0} \\ \mathbf{B}_{\tau}\mathbf{C}_{rj} & \mathbf{A}_{\tau} \end{bmatrix} \quad \mathbf{B}_{1j} = \begin{bmatrix} \mathbf{B}_{rj} \\ \mathbf{0} \end{bmatrix}$$

$$\mathbf{C}_{1j} = \begin{bmatrix} \mathbf{D}_{\tau}\mathbf{C}_{rj} & \mathbf{C}_{\tau} \end{bmatrix} \quad \mathbf{E}_{1j} = \begin{bmatrix} \mathbf{E}_{rj} & \mathbf{0} \end{bmatrix}$$

3.3.4 Modeling of Controllers

Suppose there are n_c damping controllers (specifically in Fig. 3.1, n_c=2) and the ith controller has parameters T_{wi}, T_{mi}, K_i, T_{1i}, T_{2i}, T_{3i} and T_{4i}. These controllers can be modeled as:

$$\dot{\mathbf{x}}_{ci} = \mathbf{A}_{ci}\mathbf{x}_{ci} + \mathbf{B}_{ci}y_{ci} \tag{3.22}$$

$$u_{ci} = \mathbf{C}_{ci}\mathbf{x}_{ci} \qquad i = 1, 2, ..., n_c \tag{3.23}$$

where u_{ci} and y_{ci} are output and input, respectively, of the ith controller; $\mathbf{x}_{ci}$ is the state vector; and the following matrices are defined:

$$\mathbf{u}_{c} = \begin{bmatrix} u_{c1}, u_{c2}, ..., u_{cn_c} \end{bmatrix}^{H} \quad \mathbf{y}_{c} = \begin{bmatrix} y_{c1}, y_{c2}, ..., y_{cn_c} \end{bmatrix}^{H}$$

$$\mathbf{A}_{ci} = \begin{bmatrix} 0 & 1 & 0 & 0 \\ 0 & 0 & 1 & 0 \\ 0 & 0 & 0 & 1 \\ \dfrac{-1}{a_4} & \dfrac{-a_1}{a_4} & \dfrac{-a_2}{a_4} & \dfrac{-a_3}{a_4} \end{bmatrix} \quad \mathbf{B}_{ci} = \begin{bmatrix} 0 \\ 0 \\ 0 \\ \dfrac{-1}{a_4} \end{bmatrix}$$

$$\mathbf{C}_{ci} = \begin{bmatrix} 0 & K_i T_{wi} & K_i T_{wi}(T_{2i} + T_{4i}) & K_i T_{wi} T_{2i} T_{4i} \end{bmatrix}$$

$$a_1 = T_{1i} + T_{3i} + T_{mi} + T_{wi}$$

$$a_2 = T_{1i}T_{3i} + T_{mi}T_{wi} + T_{mi}T_{1i} + T_{mi}T_{3i} + T_{wi}T_{1i} + T_{wi}T_{3i}$$

$$a_3 = T_{1i}T_{3i}(T_{mi} + T_{wi}) + T_{mi}T_{wi}(T_{1i} + T_{3i})$$

$$a_4 = T_{1i}T_{3i}T_{mi}T_{wi}$$

Then state space equations of the synthesized controller are expressed as:

$$\dot{\mathbf{x}}_c = \mathbf{A}_c\mathbf{x}_c + \mathbf{B}_c\mathbf{y}_c \qquad (3.24)$$

$$\mathbf{u}_c = \mathbf{C}_c\mathbf{x}_c \qquad (3.25)$$

where

$$\mathbf{A}_c = \mathrm{diag}\left(\mathbf{A}_{c1}, \mathbf{A}_{c2}, ..., \mathbf{A}_{cn_c}\right) \qquad \mathbf{B}_c = \mathrm{diag}\left(\mathbf{B}_{c1}, \mathbf{B}_{c2}, ..., \mathbf{B}_{cn_c}\right)$$

$$\mathbf{C}_c = \mathrm{diag}\left(\mathbf{C}_{c1}, \mathbf{C}_{c2}, ..., \mathbf{C}_{cn_c}\right) \qquad \mathbf{x}_c = [\mathbf{x}_{c1}, \mathbf{x}_{c2}, ..., \mathbf{x}_{cn_c}]^{\mathrm{H}}$$

The linear model (3.1)-(3.3) can then be constructed by incorporating (3.24) and (3.25) into (3.20) and (3.21). The corresponding matrix relationships are obtained as follows:

$$\mathbf{x}_j = \begin{bmatrix} \mathbf{x}_{1j} \\ \mathbf{x}_c \end{bmatrix} \qquad \mathbf{A}_j = \begin{bmatrix} \mathbf{A}_{1j} & \mathbf{B}_{1j}\mathbf{C}_c \\ \mathbf{B}_c\mathbf{C}_{1j} & \mathbf{A}_c \end{bmatrix} \qquad \mathbf{E}_j = \begin{bmatrix} \mathbf{E}_{1j} & \mathbf{0} \end{bmatrix} \qquad \mathbf{K}_j = \begin{bmatrix} \mathbf{0} & \mathbf{C}_c \end{bmatrix}$$

Consequently the proposed index can be calculated from the synthesized linear model of the closed loop system. A tuning scheme based on this index is proposed in the next section to simultaneously adjust parameters of PSSs and SDCs to damp inter-area oscillations and to optimize their control efforts under multiple operating conditions.

3.4 Procedure of Controller Tuning

3.4.1 Tuning Problem Formulation

Choosing variables to form $\mathbf{y}_o$ should take into account two points: one is that inter-area modes should be sufficiently observed in $\mathbf{y}_o$ so that minimizing f_{pj} will result in suppression of inter-area oscillations; and another is that if the damping of a mode (i.e. a local mode) deteriorates dramatically after controller tuning due

41

to its poor visibility in $\mathbf{y}_o$, variables that significantly participate in this mode should be included in reconstruction of $\mathbf{y}_o$ so that it can be considered in controller tuning and thus appropriately damped.

To ensure robustness of the controllers, typical multiple operating conditions are considered in the design. In this chapter, parameters K_i, T_{1i}, T_{2i}, T_{3i} and T_{4i} of PSSs and SDCs are assumed to be adjustable, while filter constant T_{mi} and washout time constant T_{wi} are preset and remain fixed during the tuning process. Therefore, an optimization based tuning scheme for coordination of PSSs and SDCs is proposed as follows:

$$\min_{\mathbf{p}} \sum_{j=1}^{n_p} \alpha_j f_{pj} \tag{3.26}$$

$$\text{s.t.} \quad \xi_{kj} \geq \xi_c \qquad k = 1, 2, \ldots, n \quad j = 1, 2, \ldots, n_p \tag{3.27}$$

$$\mathbf{p}_{min} \leq \mathbf{p} \leq \mathbf{p}_{max} \tag{3.28}$$

where n_p is the number of operating conditions; α_j is the weight of the jth operating condition; ξ_{kj} is the damping ratio of λ_{kj}; ξ_c is a real positive number (2% in this chapter) to ensure some small signal stability margin while the objective of system damping control is achieved by minimization of (3.26); and $\mathbf{p}$ is the parameter vector with the following definition:

$$\mathbf{p} = \left[K_1, T_{11}, T_{21}, T_{31}, T_{41}, \ldots, K_{n_c}, T_{1n_c}, T_{2n_c}, T_{3n_c}, T_{4n_c} \right]^H$$

$\mathbf{p}_{min}$ and $\mathbf{p}_{max}$ are lower and upper limits, respectively, of $\mathbf{p}$; calculation of these limits is presented in the following.

Suppose there is a phase lead-lag block shown as follows:

$$\left(1 + sT_q\right) \big/ \left(1 + sT_h\right) \tag{3.29}$$

If the phase of this block reaches maximum (or minimum) of θ_c at frequency ω_c,

42

then time constants T_q and T_h can be determined by:

$$T_q = \left(\sqrt{1+\tan^2\theta_c} + \tan\theta_c\right)\Big/\omega_c \qquad (3.30)$$

$$T_h = \left(\sqrt{1+\tan^2\theta_c} - \tan\theta_c\right)\Big/\omega_c \qquad (3.31)$$

When the maximum and minimum compensated phases provided by the block and frequencies of inter-area modes are given, upper and lower limits of T_q and T_h can be calculated depending on (3.30) and (3.31), respectively. Upper and lower limits of the gain of the phase compensator can be calculated by residue analysis [105].

3.4.2   Solving the Optimization Problem

The optimization problem (3.26)-(3.28) is a standard constrained nonlinear programming problem (NLP) solved in this thesis by sequential quadratic programming (SQP), a highly effective and matured method for the NLP [71].

Initial values of controller parameters used as a starting point for the SQP are given by the conventional sequential tuning method, which is also employed for comparison with the proposed tuning scheme [99]. Firstly, the compensated phase supplied by a controller to an inter-area mode is derived by residue analysis in the nominal operating condition [6]. The gain of this controller is then increased gradually to enhance damping of the mode while considering the control effort of the controller as well as side effects on other modes. Each controller is tuned sequentially while the other already tuned controllers are online.

To depict the solving process more conveniently, (3.26)-(3.28) are expressed in a more general and compact form as follows:

$$\min_{\mathbf{p}} F(\mathbf{p}) \qquad (3.32)$$

$$\text{s.t. } \mathbf{h}(\mathbf{p}) \le 0 \tag{3.33}$$

(3.32)-(3.33) are solved by an iteration process based on the Lagrangian function, constructed as follows:

$$L(\mathbf{p}, \lambda_{\mathrm{h}}) = F(\mathbf{p}) + \lambda_{\mathrm{h}} \mathbf{h}(\mathbf{p}) \tag{3.34}$$

where λ_{h} is the Lagrangian multiplier vector for $\mathbf{h}(\mathbf{p})$. At the beginning of the lth iteration, the controller parameter vector $\mathbf{p}^l$ and the positive definite Hessian matrix $\mathbf{H}_l$ (which is initially an identity matrix and is updated iteratively to finally converge to the real Hessian matrix of the Lagrangian function) are available. Then, the following steps are executed [71]:

S.1) Formulate and solve the following convex quadratic programming (QP) subproblem:

$$\min_{\mathbf{s}^l} \nabla F(\mathbf{p}^l)^{\mathrm{T}} \mathbf{s}^l + 0.5(\mathbf{s}^l)^{\mathrm{T}} \mathbf{H}_l \mathbf{s}^l \tag{3.35}$$

$$\text{s.t. } \mathbf{h}(\mathbf{p}^l) + \nabla \mathbf{h}(\mathbf{p}^l)^{\mathrm{T}} \mathbf{s}^l \le 0 \tag{3.36}$$

where $\mathbf{s}^l$ is the search direction vector of parameters at the lth iteration; ∇ and T are Hamilton and transpose operators, respectively.

S.2) Based on $\mathbf{s}^l$, the controller parameter vector at the next iteration is calculated as follows:

$$\mathbf{p}^{l+1} = \mathbf{p}^l + \beta^l \mathbf{s}^l \tag{3.37}$$

where β^l is the optimal step length along the search direction $\mathbf{s}^l$ and it can be determined by minimizing the following merit function:

$$\min_{\beta^l} \left\{ F(\mathbf{p}^{l+1}) + \rho \max\left[\mathbf{0}, \mathbf{h}(\mathbf{p}^{l+1}) \right] \right\} \tag{3.38}$$

where $\boldsymbol{\rho}$ is the penalty parameter vector.

S.3) If the stopping criteria are satisfied, terminate the iteration process;

otherwise, go to next step.

S.4) The new Hessian matrix is obtained by using the quasi-Newton method, as follows:

$$\mathbf{H}_{l+1} = \mathbf{H}_l + \frac{\gamma_l \gamma_l^{\mathrm{T}}}{\gamma_l^{\mathrm{T}} \mathbf{d}_l} - \frac{\mathbf{H}_l \mathbf{d}_l \mathbf{d}_l^{\mathrm{T}} \mathbf{H}_l}{\mathbf{d}_l^{\mathrm{T}} \mathbf{H}_l \mathbf{d}_l} \qquad (3.39)$$

$$\mathbf{d}_l = \mathbf{p}^{l+1} - \mathbf{p}^l \qquad (3.40)$$

$$\gamma_l = \theta_l \mathbf{J}_l + (1 - \theta_l) \mathbf{H}_l \mathbf{d}_l \qquad (3.41)$$

$$\mathbf{J}_l = \nabla_{\mathrm{p}} L\left(\mathbf{p}^{l+1}, \lambda_{\mathrm{h}}^{l+1}\right) - \nabla_{\mathrm{p}} L\left(\mathbf{p}^l, \lambda_{\mathrm{h}}^l\right) \qquad (3.42)$$

$$\theta_l = \begin{cases} 1.0 & \text{if } \mathbf{d}_l^{\mathrm{T}} \mathbf{J}_l \geq 0.2 \mathbf{d}_l^{\mathrm{T}} \mathbf{H}_l \mathbf{d}_l \\ \dfrac{0.8 \mathbf{d}_l^{\mathrm{T}} \mathbf{H}_l \mathbf{d}_l}{\mathbf{d}_l^{\mathrm{T}} \mathbf{H}_l \mathbf{d}_l - \mathbf{d}_l^{\mathrm{T}} \mathbf{J}_l} & \text{otherwise} \end{cases} \qquad (3.43)$$

S.5) Set $l=l+1$ and go to the next iteration.

3.4.3 Selection of Design Parameters $\mathbf{Q}_j$, $\mathbf{R}_j$ and α_j

Firstly, the appropriate initial guesses for $\mathbf{Q}_j$, $\mathbf{R}_j$ and α_j are determined. From (3.6), (3.10) and (3.14), $f_{\mathrm{p}j}$ can be rewritten in an alternative expression, as follows:

$$f_{\mathrm{p}j} = \sum_{ii=1}^{n_{\mathrm{Q}}} \mathbf{Q}_j(ii, ii) \mathbf{CQ}_j(ii) + \sum_{kk=1}^{n_{\mathrm{R}}} \mathbf{R}_j(kk, kk) \mathbf{CR}_j(kk) \qquad (3.44)$$

where $\mathbf{Q}_j(ii,ii)$ and $\mathbf{R}_j(kk,kk)$ are iith and kkth diagonal entries of $\mathbf{Q}_j$ and $\mathbf{R}_j$, respectively; $\mathbf{CQ}_j$ is the n_{Q}-dimensional vector and its iith component $\mathbf{CQ}_j(ii)$ is computed from $f_{\mathrm{p}j}$ when setting $\mathbf{Q}_j(ii,ii)=1$, the rest of entries of $\mathbf{Q}_j$ are zeros and $\mathbf{R}_j=0$; $\mathbf{CR}_j$ is the n_{R}-dimensional vector and its kkth component $\mathbf{CR}_j(kk)$ is computed from $f_{\mathrm{p}j}$ when setting $\mathbf{R}_j(kk,kk)=1$, the rest of entries of $\mathbf{R}_j$ are zeros and $\mathbf{Q}_j=0$. Depending on the initial values of controller parameters, $\mathbf{CQ}_j$ and $\mathbf{CR}_j$ can be calculated. It is expected that all additive terms on the right hand side of (3.44)

can be weighted in the same order of magnitude in f_{pj} so that all components of $\mathbf{y}_o$ and $\mathbf{u}_c$ can be equivalently considered in optimization. Hence, the initial guesses for $\mathbf{Q}_j$ and $\mathbf{R}_j$ are determined by simply setting these additive terms equal. With these initial guesses, f_{pj} can be calculated. Thus, the initial guesses for α_j are derived by assuming that all additive terms in objective function (3.26) are equal as well.

Based on the initial guesses, a trial process is then performed to adjust $\mathbf{Q}_j$, $\mathbf{R}_j$ and α_j until acceptable controller tuning results for all operating conditions are derived [98]. The adjustment of design parameters is according to the following heuristic principles: enhancing corresponding entries of $\mathbf{Q}_j$ may increase damping of the system, while controller outputs would be significantly constrained by larger entries of $\mathbf{R}_j$; increasing α_j could give more control priority to the jth operating condition.

3.5 Case Studies

3.5.1 Four-Machine Two-Area System

The classic 4-machine 2-area system (Fig. 3.2) is employed to demonstrate the proposed performance index and its application in simultaneous tuning of PSSs and SDCs. The data of this system is given in the Appendix. A Statcom is installed at Bus 8 to maintain its voltage. The steady voltage at Bus 8 will rise to nearly 1.0 p.u. with reactive power support from the Statcom. The Statcom is modeled as a current injection I_q always kept in perpendicular with bus voltage so that there is only reactive power exchange between the grid and the Statcom (Fig. 3.3) [120]. The voltage regulator of the Statcom is an inert block, with $K_{st}=100$ and $T_{st}=0.005$. The unit of time constants used in this chapter is seconds,

unless otherwise specified. The loads are modeled as a combination of constant impedances (50%) and induction motors (50%). The 47-order open loop system, therefore, has 24 state variables of generators (power angle, angular speed, d-axis and q-axis transient voltages, and d-axis and q-axis sub-transient voltages), 16 state variables of excitation systems, 1 state variable of the Statcom and 6 state variables of induction motors (angular speed, and d-axis and q-axis voltages behind transient reactance).
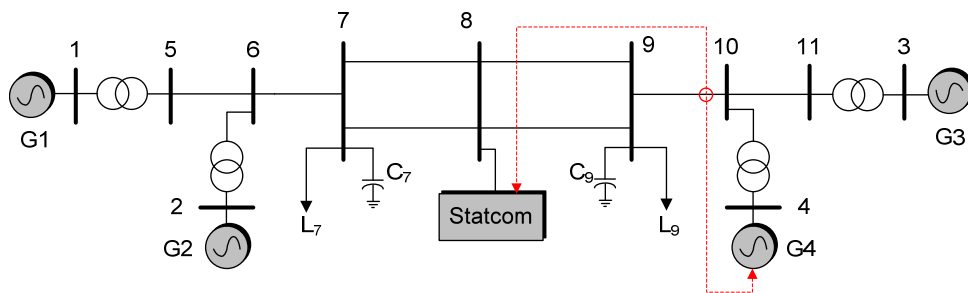
Fig. 3.2. Four-machine two-area system
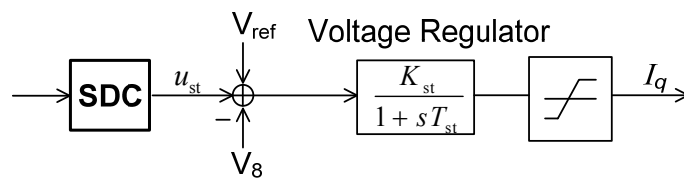
Fig. 3.3. Control structure of Statcom.

Operating conditions considered for this system are as in Table 3.1, where the first five are used for design while the last one is applied for validation of robustness of the controllers. The loads remain fixed for all operating condition. Two local modes in this system are well damped. However, an inter-area mode (-0.1069+4.0898i, in the nominal operating condition) residing between Area 1 and Area 2 is poorly damped. Hence a SDC is equipped in the Statcom, together with a PSS installed in Generator 4, to provide additional damping for inter-area

oscillation. PSS is installed in Generator 4 on the basis of analysis of participation factors.

Selection of wide-area feedback signals is based on residue analysis. Large residues of a system's input-output pair, with respect to a mode, indicate that this mode can be effectively controlled by the input-output pair using closed loop feedback control [6]. Accordingly, it is found that active power in line 10-9 is the most effective input signal for both PSS and SDC in damping inter-area oscillation and, therefore, it is chosen as the control input for these two controllers. The communication latency will be around 20ms for sending this signal to the remote SDC site through a dedicated fiber-optic communication channel [121, 122]. Moreover, since the time required for phasor measurement (about 3 60Hz-cycles or 50ms [121]) and signal processing is also considered, the total delay of 80ms in feedback signal for the SDC is used in this design. Furthermore, the time delay in feedback signal for the PSS is assumed to be zero. The filter time constant and the washout time constant are set to 0.01 and 10, respectively, for both controllers.

TABLE 3.1 OPERATING CONDITIONS FOR THE 4-MACHINE 2-AREA SYSTEM

Case	P_{g1}(MW)	P_{g2}(MW)	P_{g3}(MW)	P_{g4}(MW)	Line outage
1	700	700	716	700	no outage
2	400	1000	708	700	no outage
3	700	700	408	1000	no outage
4	700	700	727	700	8-9
5	700	700	727	700	7-8
6	800	700	836	500	no outage

Since the inter-area mode is mainly dominated by the relative motions of generators between the two areas, output vectors used to form the cost function are defined as follows:

$$\mathbf{y}_o = \begin{bmatrix} \delta_3 - \delta_1 & \delta_3 - \delta_2 & \delta_4 - \delta_1 & \delta_4 - \delta_2 \end{bmatrix}^H \tag{3.45}$$

$$\mathbf{u}_c = \begin{bmatrix} u_{st} & u_{pss} \end{bmatrix}^H \tag{3.46}$$

where δ_1, δ_2, δ_3 and δ_4 are power angles of Generators 1, 2, 3 and 4, respectively; and u_{st} and u_{pss} are outputs of the SDC and the PSS, respectively.

The open loop frequency response of output of the SDC to input of the SDC is illustrated in Fig. 3.4. A 15-order reduced model is obtained through model reduction of the original 47-order system and time delay is approximated by the Pade formula. Model reduction for each operating condition takes about 0.082s; all time consumption tests in this chapter are conducted in a desktop computer with 2.66GHz CPU and 2G RAM. It is clearly seen that the approximated model can be employed to accurately represent the full model within the frequency range of interest.
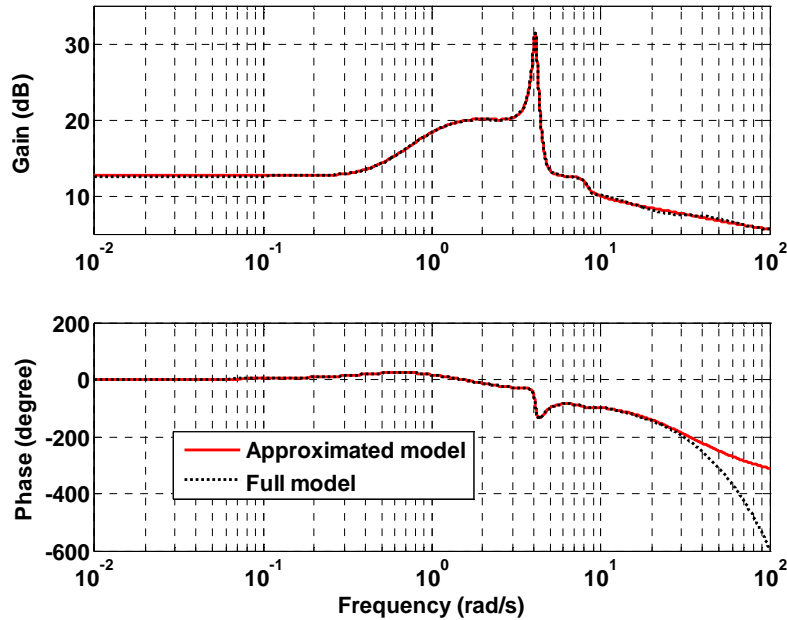
Fig. 3.4. Open loop frequency response of output of SDC to input of SDC

Lower and upper boundaries LB and UB of controller parameters are given in Table 3.2. Here parameters K_1, T_{11}, T_{21}, T_{31} and T_{41} are corresponding to the

49

SDC, while K_2, T_{12}, T_{22}, T_{32} and T_{42} are for the PSS. Initial as well as tuned values of these parameters are also shown in the table. The searching process for solution of (3.26)-(3.28) is illustrated in Fig. 3.5 and the time cost for finding this solution is about 1.74s. It is clearly seen that the SQP is quite efficient in solving the proposed controller tuning problem.

TABLE 3.2 CONTROLLER PARAMETERS

Parameter	LB	UB	Initial (Conventional)	Tuned
K_1	0.0000	0.0250	0.0050	0.0030
T_{11}	0.0655	0.9125	0.1426	0.1300
T_{21}	0.0655	0.9125	0.5224	0.7290
T_{31}	0.0655	0.9125	0.1426	0.1478
T_{41}	0.0655	0.9125	0.5224	0.7167
K_2	0.0000	0.2500	0.0500	0.0925
T_{12}	0.0655	0.9125	0.1973	0.2669
T_{22}	0.0655	0.9125	0.3447	0.5187
T_{32}	0.0655	0.9125	0.1973	0.1787
T_{42}	0.0655	0.9125	0.3447	0.2530
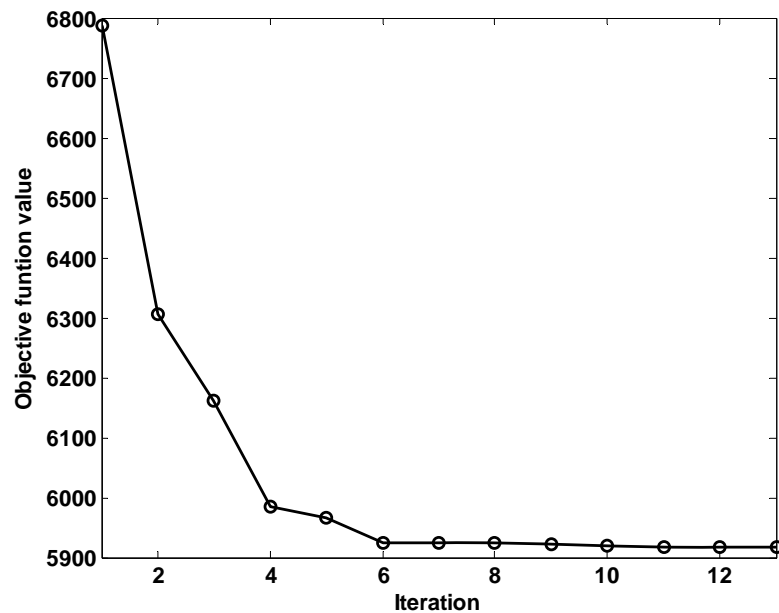
Fig. 3.5. Searching process of SQP

Eigenvalues of cost matrices are calculated when the PSS and the SDC are simultaneously tuned by the proposed method and are sequentially tuned by the

conventional method. The first four eigenvalues for each operating condition considered in the design are depicted in Fig. 3.6. The first is the dominant one; it is much larger than the remaining. It is clear that this eigenvalue is obviously reduced when the proposed controllers are installed, compared to when the system is equipped with sequentially tuned controllers. Moreover, from (3.14), it is known that f_{pj} is defined as the sum of eigenvalues of the cost matrix, which means the proposed controllers will result in smaller f_{pj} than that given by sequentially tuned controllers. Because f_{pj} is capable of indicating the system's dynamic performance, it is naturally inferred that simultaneously tuned controllers will lead to a better dynamic performance of the system than sequentially tuned controllers. This is verified by computation of the closed loop system eigenvalues and the time domain simulations shown in the following.
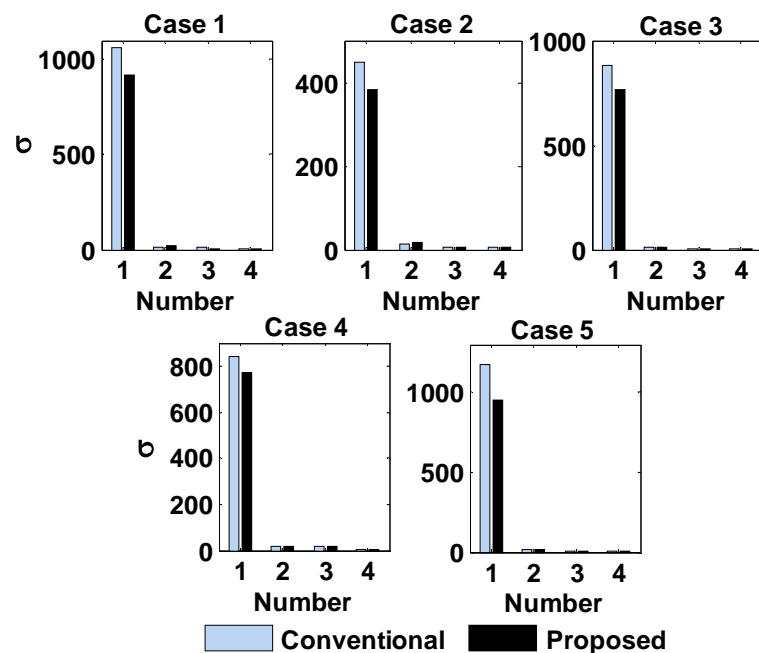
Fig. 3.6. Eigenvalues of cost matrices.

The inter-area mode eigenvalues of the closed loop system for all operating conditions are presented in Table 3.3. The comparison shows that the proposed

51

controllers truly provide more additional damping to the inter-area mode than sequentially tuned controllers not only for operating conditions used for design but also for the condition included in validation; damping of the inter-area mode is enhanced considerably by the proposed controllers.

Because inter-area oscillations are adequately observed in $\mathbf{y}_o$, f_{pj} can effectively measure the performance of these inter-area oscillation dynamics according to the inference drawn in Section 3.2. Minimization of f_{pj} suppresses inter-area oscillations and thus inevitably increases damping of the inter-area mode. Accordingly, though the proposed index is directly related to eigenvalues of the cost matrix, rather than the closed loop system, lowering it can actually enhance damping of closed loop system modes strongly associated with $\mathbf{y}_o$. This is verified as reduction of σ accords well with increase of damping of the inter-area mode shown above.

TABLE 3.3 EIGENVALUES OF INTER-AREA MODE

Case	No controller	Conventional	Proposed
1	-0.1069±4.0898i	-0.4180±4.2037i	-0.7213±4.3490i
2	-0.1147±4.0758i	-0.4263±4.1712i	-0.7231±4.3017i
3	-0.1293±4.0661i	-0.4417±4.1867i	-0.7580±4.3301i
4	-0.1883±3.2122i	-0.4632±3.2401i	-0.8086±3.3177i
5	-0.0009±3.6318i	-0.3860±3.8065i	-0.8046±3.9831i
6	-0.1328±3.9576i	-0.4784±4.1180i	-0.8374±4.2733i

A three phase short circuit fault occurs at Bus 6 when the system is in operating condition 5 and the fault is cleared 50ms later. The power angle oscillations between Generators 2 and 4 are shown in Fig. 3.7. It is seen that inter-area oscillation decay quite fast when the system is equipped with simultaneously tuned controllers, compared to the marginally stable system without controllers and the system with sequentially tuned controllers. Outputs of PSS and SDC are also optimized when they are coordinately designed by the

proposed method (Fig. 3.8). The limits for outputs of PSS and SDC are set to ± 0.10 and ± 0.05, respectively. Therefore, together with the above eigen-analysis, these results indicate that the proposed index is an effective measurement of performance of system dynamics as well as control efforts. Furthermore the proposed simultaneous tuning method based on this index for coordination of PSS and SDC can well damp inter-area oscillation under multiple operating conditions.
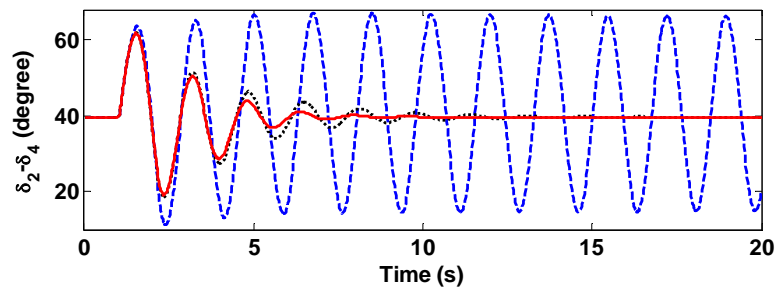
Fig. 3.7. Power angle oscillations (solid line: proposed; dot line: conventional; dash line: no controller).
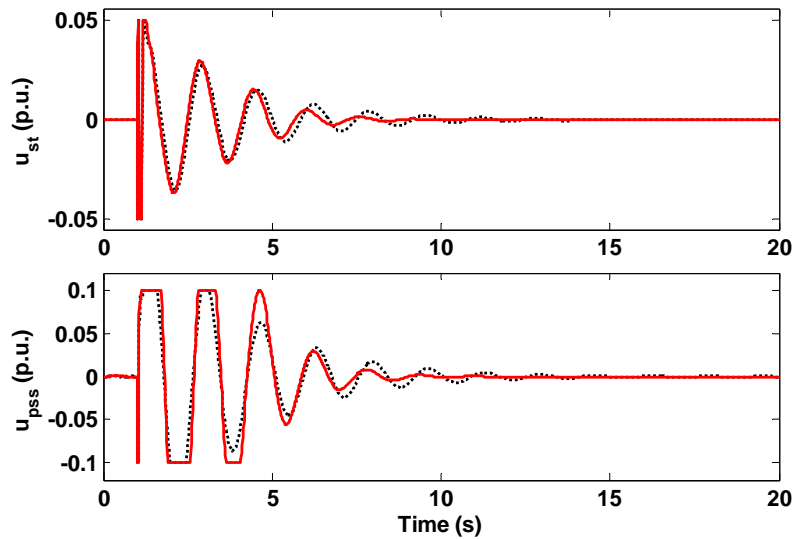
Fig. 3.8. Control signals (solid line: proposed; dot line: conventional).

3.5.2 New England and New York Interconnected System

The equivalent (16-machine 5-area) model of New England and New York interconnected networks (Fig. 3.9) is employed to demonstrate performance of the proposed controller design including multiple inter-area modes. This system is a modified version of [6]: the quite large mechanical damping coefficients in the original model have been removed from some generators and local PSSs are then installed in some generators to damp their local mode oscillations. A TCSC is installed in transmission line 50-18 to compensate 50% of its reactance in the steady state. The allowable TCSC dynamic compensation is from 10% to 90% of line reactance. The dynamic model of the TCSC is shown in Fig. 3.10 [32], where time constant T_{tc} is chosen to be 10ms. A combination of constant impedances (50%) and induction motors (50%) is employed to model the large loads and the remaining is modeled as constant impedance Thus, there are 96 state variables of generators (the same six-order model as in the first example), 64 state variables of excitation systems, 18 state variables of local PSSs, 1 state variable of TCSC, and 57 state variables of induction motors in this system. By changing network configurations and transmitting different levels of power from area A_1 to A_2, 9 typical operating conditions (Table 3.4) are considered in this study. The detailed data of this system is presented in the Appendix.

Eigen-analysis shows that for all operating conditions there are two quite poorly damped inter-area modes in this system: M_1 and M_2. M_1 with frequency at about 0.65Hz is dominated by the oscillation between generators in areas A_1 and A_2, while M_2 with frequency at about 0.32Hz depicts oscillations of generators in areas A_1 and A_2 with respect to generators in the rest of the system. The participation factors of all generators with respect to M_1 (-0.0292+4.4623i) and

M_2 (0.0402+2.3903i) in the operating condition of Case 1 are shown in Fig. 3.11.

Meanwhile, Fig. 3.12 depicts the modal shape of the two modes in such case.
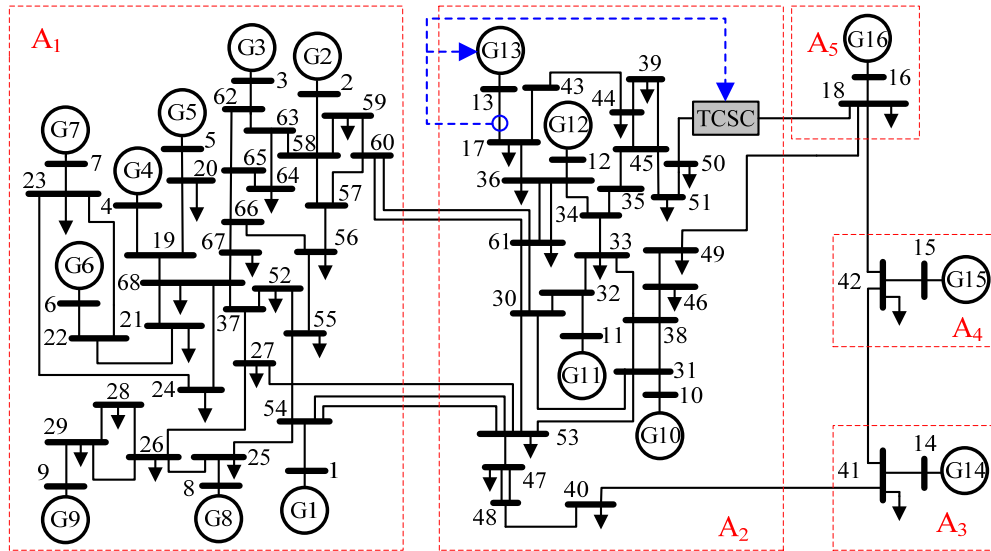
Fig. 3.9. New England and New York interconnected system.
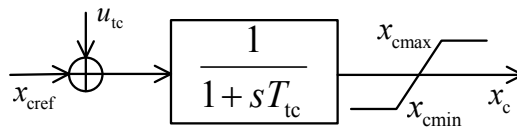
Fig. 3.10. Dynamic model of TCSC.

TABLE 3.4 OPERATING CONDITIONS FOR THE 16-MACHINE 5-AREA SYSTEM

Case	Tie-line flow(MW)	Line outage
1	715	no outage
2	715	53-54
3	714	60-61
4	715	27-53
5	914	no outage
6	102	no outage
7	524	no outage
8	524	60-61
9	914	53-54
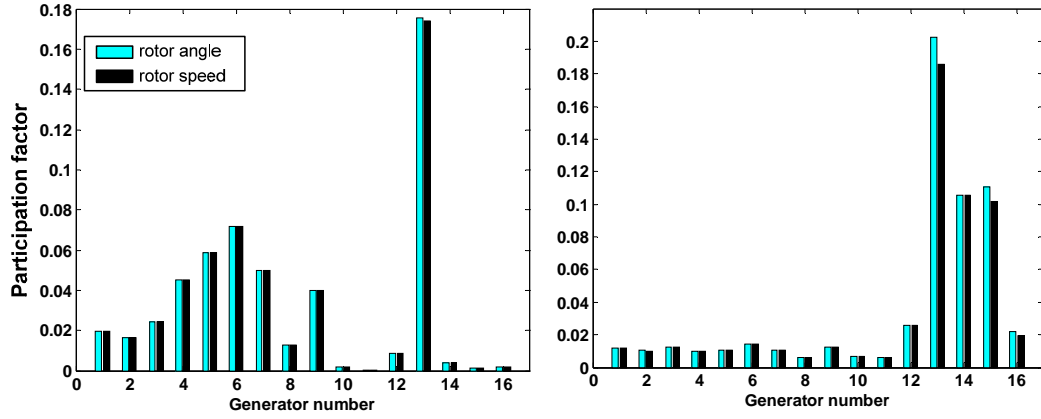
Fig. 3.11. Participation factors of generators (left plot: M_1; right plot: M_2).
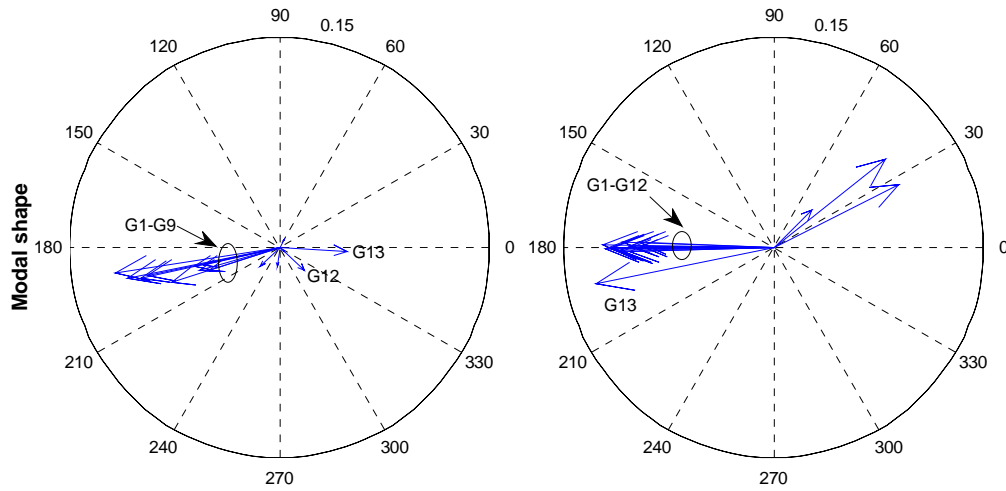
Fig. 3.12. Modal shapes (left plot: M_1; right plot: M_2).

To provide additional damping to the two inter-area modes, a SDC equipped in TCSC is designed. Meanwhile since Generator 13 greatly participates in both inter-area modes, a PSS is installed in Generator 13 to work in coordination with the SDC for damping control. Furthermore according to residue analysis, active power in transmission line 13-17 is selected as control input for both PSS and SDC. Time delay is assumed to be 80ms for transmitting the signal to the remote SDC. Participation factor analysis shows that Generators 13, 5 and 6 greatly participate in M_1, while Generators 14, 15 and 13 greatly participate in M_2. Therefore output vectors are formed as follows:

$$\mathbf{y}_o = \begin{bmatrix} \delta_5 - \delta_{13} & \delta_6 - \delta_{13} & \delta_{14} - \delta_{13} & \delta_{15} - \delta_{13} \end{bmatrix}^{\mathrm{H}} \tag{3.47}$$

$$\mathbf{u}_{c} = \begin{bmatrix} u_{tc} & u_{pss} \end{bmatrix}^{H} \tag{3.48}$$

where δ_5, δ_6, δ_{13}, δ_{14} and δ_{15} are power angles of Generators 5, 6, 13, 14 and 15, respectively; and u_{tc} and u_{pss} are outputs of SDC and PSS, respectively. The first six operating conditions in Table 3.4 are used for design, while the last three are applied for validation. It costs about 3.29s to reduce the 236-order open loop power system model to a 28-order reduced model which can lead to satisfactory results of controller tuning by the proposed method.

The lower and upper boundaries, the initial values, and the tuned values of controller parameters are shown in Table 3.5. Here parameters K_1, T_{11}, T_{21}, T_{31} and T_{41} are for the SDC, while K_2, T_{12}, T_{22}, T_{32} and T_{42} are for the PSS. Specifically, it takes about 15 iterations and 6.18s for the SQP method to converge. It is found that the controller parameter searching process for this much higher order system is still as efficient as that in the first example, although the time cost (3.29s) for model reduction in this system is relatively larger, compared to that (0.082s) in the first small system. This means that the proposed tuning scheme can be applied to large scale power systems due to the efficient reduced-order model based controller parameter searching process.

TABLE 3.5 CONTROLLER PARAMETERS

Parameter	LB	UB	Initial (Conventional)	Tuned
K_1	0.0000	0.0050	0.0035	0.0018
T_{11}	0.0600	0.8364	0.3546	0.1206
T_{21}	0.0600	0.8364	0.3058	0.1985
T_{31}	0.0600	0.8364	0.3546	0.1206
T_{41}	0.0600	0.8364	0.3058	0.0891
K_2	0.0000	0.2000	0.0600	0.0754
T_{12}	0.1121	1.5316	0.9892	0.6517
T_{22}	0.1121	1.5316	0.3823	0.1121
T_{32}	0.1121	1.5316	0.9892	0.6517
T_{42}	0.1121	1.5316	0.3823	0.1121

Eigenvalues of cost matrices for the first six operating conditions are illustrated in Fig. 3.13. It is obvious that they are reduced by optimization. According to the verification shown in the first example, the proposed controllers perform better than the sequentially tuned controllers. This is indeed confirmed again by facts shown in Table 3.6, that the proposed controllers provide more damping to both inter-area modes than the sequentially tuned controllers. The two inter-area modes are sufficiently damped for all operating conditions when the proposed controllers are installed.
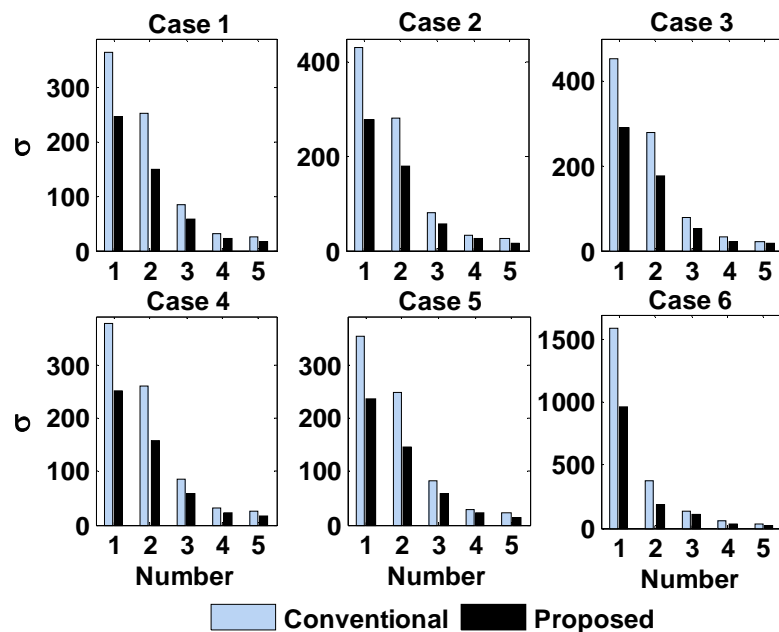
Fig. 3.13. Eigenvalues of cost matrices.

A three phase short circuit fault occurs at Bus 60 when the system is in operating condition 1. The fault is cleared 100ms later by tripping one of tie-lines between Bus 60 and 61. Oscillations of relative power angles and active power in key tie-lines are depicted in Fig. 3.14 and Fig. 3.15, respectively. The compensation percentage provided by the TCSC and the output of the PSS during the dynamics are illustrated in Fig. 3.16. It is clear that simultaneously

tuned controllers outperform sequentially tuned controllers, and the two inter-area oscillations are well damped by coordinately tuned PSS and SDC with optimum control outputs.

TABLE 3.6 EIGENVALUES OF INTER-AREA MODE

Case	No controller	Conventional	Proposed
1	$0.0402\pm2.3903i$	$-0.2214\pm2.4280i$	$-0.5475\pm2.6984i$
	$-0.0292\pm4.4623i$	$-0.2658\pm4.3266i$	$-0.4815\pm4.5881i$
2	$0.0305\pm2.3679i$	$-0.2194\pm2.4065i$	$-0.5448\pm2.6645i$
	$-0.0140\pm4.2788i$	$-0.2712\pm4.1621i$	$-0.5388\pm4.4882i$
3	$0.0314\pm2.3843i$	$-0.2201\pm2.4253i$	$-0.5381\pm2.6876i$
	$-0.0215\pm4.2542i$	$-0.2752\pm4.1453i$	$-0.5472\pm4.4854i$
4	$0.0382\pm2.3851i$	$-0.2211\pm2.4231i$	$-0.5473\pm2.6909i$
	$-0.0251\pm4.4164i$	$-0.2655\pm4.2856i$	$-0.4907\pm4.5602i$
5	$0.0347\pm2.3858i$	$-0.2197\pm2.4299i$	$-0.5503\pm2.6927i$
	$-0.0475\pm4.4422i$	$-0.2626\pm4.3256i$	$-0.4780\pm4.5725i$
6	$0.0590\pm2.3993i$	$-0.2266\pm2.4171i$	$-0.5439\pm2.7116i$
	$0.0270\pm4.5007i$	$-0.2723\pm4.3125i$	$-0.4953\pm4.6165i$
7	$0.0458\pm2.3940i$	$-0.2231\pm2.4255i$	$-0.5456\pm2.7033i$
	$-0.0116\pm4.4784i$	$-0.2683\pm4.3252i$	$-0.4855\pm4.6000i$
8	$0.0368\pm2.3893i$	$-0.2216\pm2.4239i$	$-0.5357\pm2.6929i$
	$-0.0029\pm4.2799i$	$-0.2746\pm4.1519i$	$-0.5372\pm4.5028i$
9	$0.0254\pm2.3627i$	$-0.2176\pm2.4074i$	$-0.5479\pm2.6569i$
	$-0.0325\pm4.2549i$	$-0.2697\pm4.1578i$	$-0.5470\pm4.4673i$
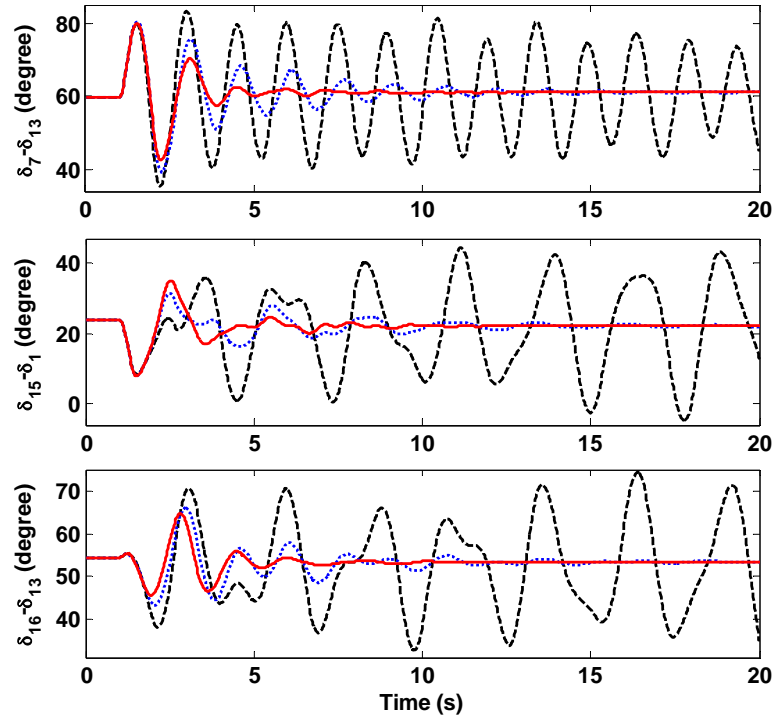
Fig. 3.14. Power angle oscillations (solid line: proposed; dot line: conventional; dash line: no controller).
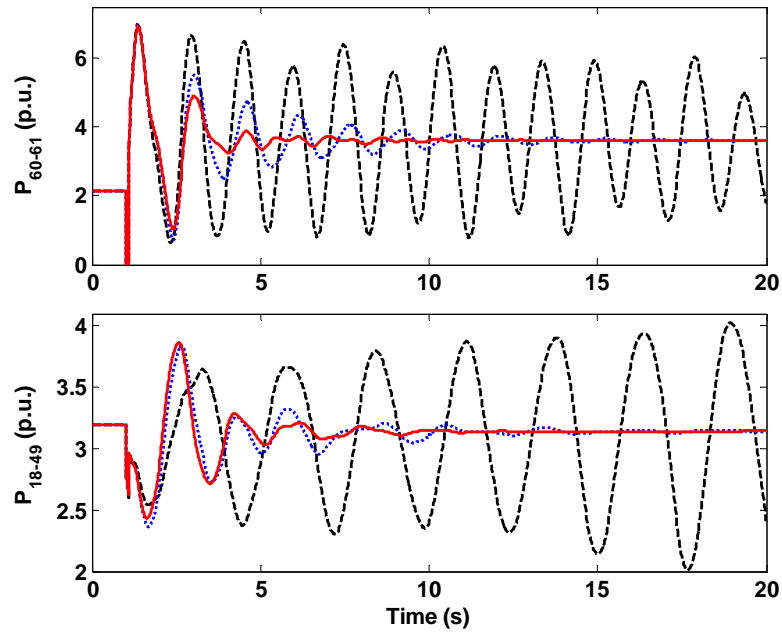
Fig. 3.15. Oscillations of active power in key tie-lines (solid line: proposed; dot line: conventional; dash line: no controller).
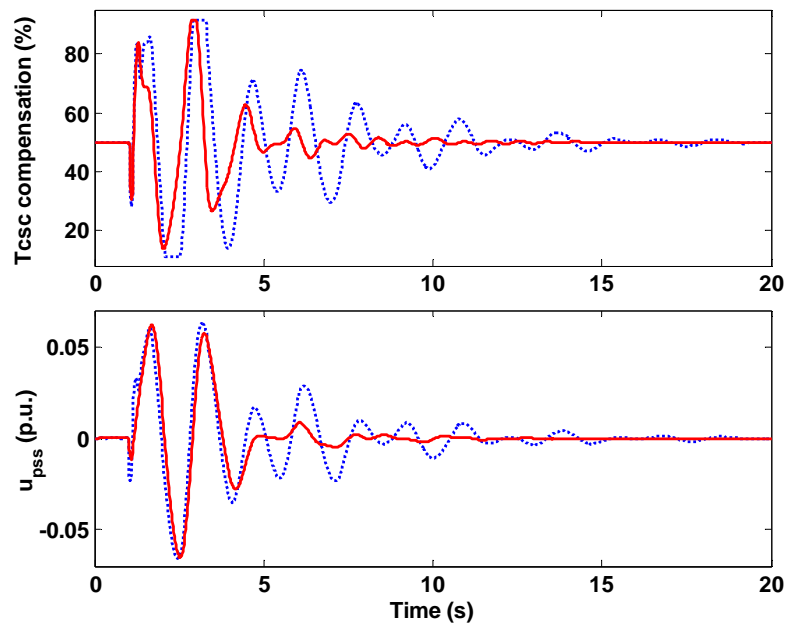
Fig. 3.16. Dynamics of controllers (solid line: proposed; dot line: conventional).

3.6 Summary

A novel eigenstructure-based performance index is proposed to solve structurally constrained control problems. This index can measure performance of system dynamics as well as control efforts. Calculation of this index has no

bearing on control structures; it is based only on eigenstructure of the closed loop system and the design parameters. This index has been applied to a proposed optimization based tuning scheme used for coordination of structurally constrained PSSs and SDCs to damp inter-area oscillations and to optimize their control efforts under multiple operating conditions. Applications of the proposed control design method on a 4-machine 2-area system and the New England and New York interconnected system have been demonstrated. Results show that the proposed index is an effective way of measuring system's dynamic performance and reducing this index can improve the system dynamics. Structurally constrained PSSs and SDCs simultaneously tuned by the proposed method can effectively damp inter-area oscillations and their control efforts are also optimized.

Chapter 4

An Inter-Area Mode Oriented Pole-Shifting Method with Coordination of Control Efforts for Tuning Power Oscillation Damping Controllers

4.1 Introduction

Reference [123] has pointed out that using PSS to damp electromechanical oscillations is generally at the expense of the generator's terminal voltage profile during the transient. Moreover, when FACTS devices are installed on the key corridors of grids, they show significant potential for damping inter-area oscillations by using their available capacities [124]. Hence, with an additional aim of reducing side effects of the PSS, the FACTS device, equipped with a SDC, is expected to assist damping control. To achieve this objective, an effective index that is able to accurately measure the control effort of the damping controller used needs to be designed. Then the adopted tuning method has to possess capability of coordinating control efforts of different damping controllers. However, this will proceed only under the premise that inter-area oscillations are satisfactorily damped when the tuning method is applied to the controllers.

Many damping controller design methods ensure the dynamic performance of the closed loop system by driving all poles to a so-called LMI region specifically

62

defined in the complex plane [6, 113, 125]. The LMI region can be shaped into various forms for which the extended Lyapunov Theorem is applicable [126]. For example, a conic region has been used in [32] and [127] for H_∞ control, while the mixed H_∞/H_2 synthesis used in [128] has employed a trapezoidal region. Though use of the LMI region, where all poles should locate, to damp inter-area oscillations has been reported in literature [32, 105, 127, 128], no reports addressing impacts of other modes on control of the inter-area modes have been found.

Generally, in damping control of inter-area oscillations, the aim is to push inter-area modes, not all modes, to the specific region. It is reasonable to expect that the pole placement can guarantee that major available control capacities are used for control of inter-area modes; little adverse effect is caused on other modes by the controllers. Although some other specific pole placements have been implemented for designing damping controllers by properly defining objective and constraint functions consisting of closed loop poles in some mathematical programming based methods [85, 109, 129], they are not capable of measuring and coordinating control efforts of different controllers. Two simple heuristic indices have been used in [130] for optimization of control efforts: one is defined as the sum of weighted magnitudes of the controller at some specific frequencies, and another is simply the sum of numerator coefficients of the transfer function. Nevertheless, in order to conduct incremental optimization based on linear predictions of eigenvalues, coefficients of the controller transfer function denominator should be given in advance and they should remain fixed during the optimization. An effective eigenstructure based index has been proposed in Chapter 3 to measure system dynamic

performances as well as control efforts. However, since no pole placement has been used, it achieves acceptable damping control of inter-area oscillations and coordination of control efforts through proper selection of weights of objective function which is obviously an onerous work. Moreover, frequency drift of the inter-area mode has not been explicitly limited.

In this chapter, firstly, impacts of other modes on control of inter-area modes are studied via a proposed pole-shifting method (named: SCCS-PS) which tunes the controllers by moving all poles to a sequentially compressed conic section. Motivated by this study, therefore, an inter-area mode oriented pole-shifting method (named: IAMO-PS) is proposed, which can not only achieve a specific pole placement suitable for controlling inter-area oscillations, but also provide the mechanism to distribute control burden among different controllers since an effective index is employed for measuring the control effort. The SQP method is used to solve optimization of both methods, and a two-stage optimization procedure is proposed for IAMO-PS to ensure that a feasible starting point that enables its convergence can be readily derived, which thus can greatly facilitate its practical application.

This chapter is organized as follows. Firstly, SCCS-PS and IAMO-PS are introduced. Then, the system used for demonstrating both methods is given. Finally, simulation results are discussed.

4.2 Impacts of Other Modes on Control of Inter-Area Modes with Use of a Conic Section

Before introduction of SCCS-PS, the closed loop system model should be obtained. Firstly, a reduced-order model which can accurately approximate the

input-output relationship of the high-dimensional full model within the frequency range of interest is commonly employed for design [6]. Wide-area signals are used to enhance the effectiveness of the controllers in damping inter-area oscillations and the corresponding time-delays involved in the signals are then approximately considered by the second order Pade formula [98]. Further-more, the control structure of each individual controller (PSS or SDC) is a classic phase lead-lag compensator. Finally, when the reduced-order open loop power system model (including time-delays) and the controller models are available, they are used to synthesize the closed loop system model as follows:

$$\dot{\mathbf{x}} = \mathbf{A}\mathbf{x} \tag{4.1}$$

$$\mathbf{u} = \mathbf{E}\mathbf{x} \tag{4.2}$$

where $\mathbf{x} \in \Re^{\mathrm{n}}$ is the state vector; $\mathbf{A}$ and $\mathbf{E}$ are the state matrix and the output matrix, respectively; and $\mathbf{u}$ is the output vector with the following definition:

$$\mathbf{u} = \left[u_1, u_2, ..., u_k, ..., u_{\mathrm{m}}\right]^{\mathrm{T}} \tag{4.3}$$

where u_k is the output of the kth controller and m denotes the number of controllers. Among all eigenvalues of $\mathbf{A}$: λ_1, λ_2… λ_{n}, there are some weakly damped inter-area modes. A pole-shifting method used for tuning the controllers, as well as providing insight into influences on control of inter-area modes caused by other modes when a conic section is employed for pole placement, is proposed in the following.

4.2.1 Pole Shifting via Sequentially Compressing Conic Section (SCCS-PS)

When all closed loop poles have shifted into a conic section (there will be one or more poles on its border), as the shadowed area shown in Fig. 4.1(a), it gives the system some small signal stability margin in terms of damping ratio ξ_{m}. However, no systematic method has been found so far to compute the maximum

ξ_m (minimum conic section) with respect to tunable parameters of damping controllers. Thus, an optimization based approach is proposed, as follows:

$$\min_{\mathbf{x}_p} \; -\xi_m \qquad\qquad (4.4a)$$

$$\text{s.t.} \quad \xi_m - \xi_l \le 0 \qquad\qquad l = 1, 2, ..., \text{n} \qquad\qquad (4.4b)$$

$$\mathbf{x}_{p\,\text{min}} \le \mathbf{x}_p \le \mathbf{x}_{p\,\text{max}} \qquad\qquad (4.4c)$$

where ξ_l is the damping ratio of the lth eigenvalue λ_l; $\mathbf{x}_{p\text{max}}$ and $\mathbf{x}_{p\text{min}}$ are the upper and lower boundaries, respectively, of the variable vector $\mathbf{x}_p$, defined as:

$$\mathbf{x}_p = \begin{bmatrix} \mathbf{p} & \xi_m \end{bmatrix}^{\text{T}} \qquad\qquad (4.4d)$$

where $\mathbf{p}$ is the tunable controller parameter vector.

(a) SCCS-PS   (b) IAMO-PS
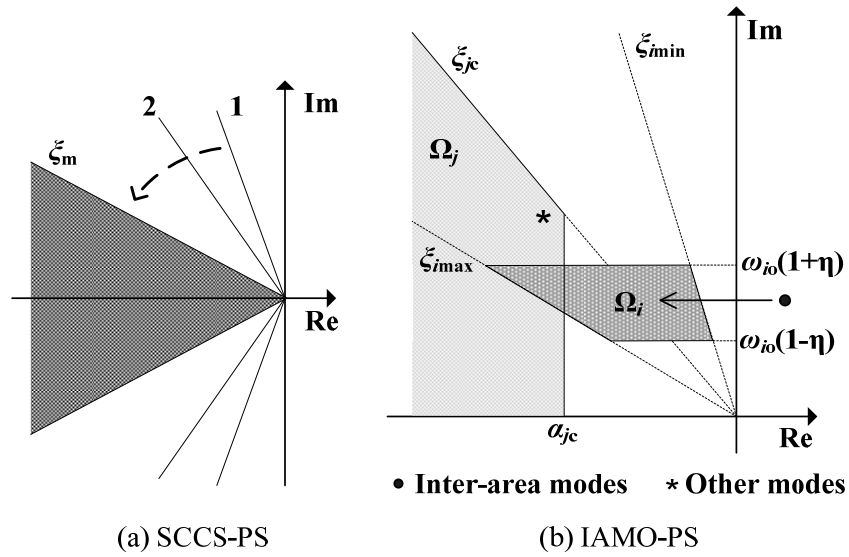
Fig. 4.1. Pole placement strategies of the two methods.

The SQP, which represents the state-of-the-art in numerical optimization, is employed to solve (4.4); its brief procedure for solving a constrained nonlinear programming problem has been given in Subsection 3.4.2. Thus, ξ_m will be sequentially increased during the optimization. This is visually interpreted as the conic section shown in Fig. 4.1(a) is sequentially compressed, i.e. from position

1 to 2. Consequently, accompanying this compressing process, all poles shift gradually towards the left hand side of the complex plane under the force of the constraints, until they finally locate within the conic section represented by the maximum ξ_m. The upper limit of ξ_m is simply set to 1.0 in this study. Specifically, for given initial controller parameters, all poles and their damping ratios are computed. The minimum damping ratio is then chosen as the lower limit of ξ_m and it is also used as the initial value of ξ_m, so that the starting point for the SQP method is feasible.

4.2.2 Discussion

The maximum ξ_m obtained from solution of (4.4) indicates that the inter-area modes will have damping ratios not less than ξ_m. Nevertheless, due to the same damping ratio requirement imposed on all modes, improvement of inter-area modes may be considerably limited because the controllers may be ineffective in controlling some other modes. Obviously, if so, SCCS-PS can easily find these modes because they will reside on the border of the conic section. Generally, for some modes with high frequencies, it is unnecessary to require damping ratios as large as the inter-area modes. Excessively changing the damping of these high frequency modes will waste the limited available control capacities and may exacerbate the control effect for the inter-area modes. Hence, it is expected that inter-area modes can be treated as different from other modes. Besides, some additional considerations are usually preferred in design of controllers for inter-area oscillations. Based on these points of view, a more elaborate method is proposed in the next section.

4.3　IAMO-PS with Coordination of Control Efforts

4.3.1　Control Effort Measurement

Generally, measurement of the control effort of the kth controller can be explicitly defined as:

$$CE_k = \int_0^\infty u_k^2 \mathrm{d}t \qquad \mathbf{x}\big|_{t=0} = \mathbf{x}_0 \qquad\qquad (4.5)$$

where $\mathbf{x}_0$ is the initial state of the closed loop system (4.1)-(4.2). It represents the initial disturbed deviation from the operating point, and thus cannot be determined in advance. It is ineffective to use CE_k directly for the control design because of its dependence on the undermined $\mathbf{x}_0$. When all eigenvalues of $\mathbf{A}$ have negative real parts, however, (4.5) can be transformed into the following form:

$$
\begin{aligned}
CE_k &= \int_0^\infty u_k^2 \mathrm{d}t = \int_0^\infty \left(\mathbf{E}_k \mathbf{x}\right)^{\mathrm{H}}\left(\mathbf{E}_k \mathbf{x}\right)\mathrm{d}t \\
&= \int_0^\infty \mathbf{x}^{\mathrm{H}} \mathbf{E}_k^{\mathrm{H}} \mathbf{E}_k \mathbf{x}\mathrm{d}t \\
&= \int_0^\infty \mathbf{x}_0^{\mathrm{H}} \mathbf{V}^{\mathrm{H}} e^{\mathbf{\Lambda}^{\mathrm{H}} t} \mathbf{U}^{\mathrm{H}} \mathbf{E}_k^{\mathrm{H}} \mathbf{E}_k \mathbf{U} e^{\mathbf{\Lambda} t} \mathbf{V}\mathbf{x}_0 \mathrm{d}t \\
&= \mathbf{x}_0^{\mathrm{H}} \mathbf{V}^{\mathrm{H}} \left[\int_0^\infty e^{\mathbf{\Lambda}^{\mathrm{H}} t} \mathbf{U}^{\mathrm{H}} \mathbf{E}_k^{\mathrm{H}} \mathbf{E}_k \mathbf{U} e^{\mathbf{\Lambda} t} \mathrm{d}t \right] \mathbf{V}\mathbf{x}_0 \qquad (4.6)\\
&= \mathbf{x}_0^{\mathrm{H}} \mathbf{V}^{\mathrm{H}} \left[\left(\mathbf{U}^{\mathrm{H}} \mathbf{E}_k^{\mathrm{H}} \mathbf{E}_k \mathbf{U}\right) \cdot \int_0^\infty e^{\left(\mathbf{\Lambda}^{\mathrm{H}}+\mathbf{\Lambda}\right) t} \mathrm{d}t \right] \mathbf{V}\mathbf{x}_0 \\
&= \mathbf{x}_0^{\mathrm{H}} \mathbf{V}^{\mathrm{H}} \left[\left(\mathbf{U}^{\mathrm{H}} \mathbf{E}_k^{\mathrm{H}} \mathbf{E}_k \mathbf{U}\right) \cdot \mathbf{L} \right] \mathbf{V}\mathbf{x}_0 \\
&= \mathbf{x}_0^{\mathrm{H}} \mathbf{M}_k \mathbf{x}_0
\end{aligned}
$$

where H is the conjugate transpose operator; $\mathbf{M}_k$ is a positive definite matrix with the following definition:

$$\mathbf{M}_k = \mathbf{V}^{\mathrm{H}} \left[\left(\mathbf{U}^{\mathrm{H}} \mathbf{E}_k^{\mathrm{H}} \mathbf{E}_k \mathbf{U}\right) \cdot \mathbf{L} \right] \mathbf{V} \qquad\qquad (4.7)$$

where $\cdot$ denotes dot production; $\mathbf{U}$ and $\mathbf{V}$ are right and left eigenvector matrices, respectively, of $\mathbf{A}$; $\mathbf{E}_k$ is the kth row vector of $\mathbf{E}$; $\mathbf{L}$ is a Hermite matrix, whose entry in the position of iith row, jjth column is defined as,

$$\mathrm{L}(ii, jj) = -\frac{1}{\lambda_{ii}^* + \lambda_{jj}} \qquad ii = 1, 2, ..., \mathrm{n} \qquad jj = 1, 2, ..., \mathrm{n} \quad (4.8)$$

where * is the conjugate operator. Accordingly, (4.6) can be decomposed as follows:

$$CE_k = \mathbf{z}_0^{\mathrm{H}} \mathbf{N}_k \mathbf{z}_0 \qquad\qquad (4.9)$$

where $\mathbf{N}_k$ is a diagonal matrix with the following definition:

$$\mathbf{N}_k = \mathrm{diag}(\sigma_{1k}, \sigma_{2k}, ..., \sigma_{nk}) \qquad \sigma_{1k} \geq \sigma_{2k} \geq \cdots \geq \sigma_{nk} > 0 \quad (4.10)$$

where $\sigma_{1k}, \sigma_{2k}, ..., \sigma_{nk}$ are eigenvalues of $\mathbf{M}_k$, and thus $\mathbf{z}_0$ is the coordinate vector when projecting $\mathbf{x}_0$ onto the orthogonal basis spanned by the right eigenvectors of $\mathbf{M}_k$. Transforming $\mathbf{x}_0$ into $\mathbf{z}_0$ is an orthogonal transformation which will not change the length of the vector. Thus, based on (4.9) and (4.10), it can be inferred that reducing $\sigma_{1k}, \sigma_{2k}, ..., \sigma_{nk}$ can equivalently decrease CE_k for the undermined $\mathbf{x}_0$, and vice versa. Consequently, instead of using CE_k, a novel index, which has no relationship with $\mathbf{x}_0$, is proposed for measuring the control effort of the kth controller in this chapter:

$$f_k = \sum_{i=1}^{\mathrm{n}} \sigma_{ik} \qquad\qquad (4.11)$$

Based on index f_k, IAMO-PS is proposed. It is formulated as a two-stage mathematical programming problem where optimization in the first stage is solved to provide a feasible starting point for the second stage optimization, so as to facilitate its application. In other words, all poles are moved in the first stage (introduced in Subsection 4.3.3) to meet the specific pole placement suitable for controlling inter-area oscillations. Then, subjected to constraints for such pole placement, control efforts of different controllers are coordinated in the second stage, which is discussed in the following subsection.

4.3.2 Coordinating Control Efforts of Different Controllers

$$\min_{\mathbf{p}} \sum_{k=1}^{m} \mathrm{w}_k f_k \tag{4.12a}$$

$$\text{s.t.} \quad \xi_{i\min} \leq \xi_i \leq \xi_{i\max} \qquad i = 1, 2, \ldots, \mathrm{n_i} \tag{4.12b}$$

$$\omega_{io}\left(1-\eta\right) \leq \omega_i \leq \omega_{io}\left(1+\eta\right) \tag{4.12c}$$

$$\xi_{jc} - \xi_j \leq 0 \qquad \lambda_j \in \pi_{c1} \tag{4.12d}$$

$$\alpha_j - \alpha_{jc} \leq 0 \tag{4.12e}$$

$$\mathbf{p}_{\min} \leq \mathbf{p} \leq \mathbf{p}_{\max} \tag{4.12f}$$

where w_k is the weight of the kth controller; subscripts i refers to the weakly damped inter-area mode and the first $\mathrm{n_i}$ eigenvalues are such mode; the other modes are referred by subscript j; ω_i is the imaginary part of λ_i, while α_j is the real part of λ_j; ω_{io} is the special value of ω_i when no damping controller is installed; η is a small positive number; $\xi_{i\min}$ and $\xi_{i\max}$ are the lower and upper limits, respectively, of ξ_i; ξ_{jc} and α_{jc} are the critical values of ξ_j and α_j, respectively; π_{c1} is the set of modes which may be greatly deteriorated after optimization.

Constraint (4.12c) on frequencies of inter-area modes is used to avoid excessive over- or under-phase compensations which may significantly alter synchronizing damping torques of the generators. $\xi_{i\min}$ is generally set to guarantee that the settling time of the ith mode is less than a required value, while $\xi_{i\max}$ is set to prevent excessive control efforts. Therefore, (4.12b) and (4.12c) ensure that the inter-area mode can locate in area Ω_i, indicating acceptable dynamics, as shown in Fig. 4.1(b). For modes in π_{c1}, ξ_{jc} is chosen to be slightly less than the initial value of ξ_j, which is calculated when the initial controller parameters are used. Likewise, α_{jc} is set to be slightly larger than the

initial value of α_j. Thus, according to Fig. 4.1(b), (4.12d) and (4.12e) are able to constrain this mode within area Ω_j after optimization, which can avoid excessive negative effects on it brought by tuning of the controllers.

It is noted that the contribution of each controller to the specific pole placement can be altered by adjusting weight w$_k$ in (4.12a). Thus, the control burden can be reasonably allocated among the controllers, which obviously makes more practical sense when considering limited available capacities of the controllers, as well as some operational requirements.

Unfortunately, unlike (4.4), it is usually not easy to obtain a feasible starting point (initial controller parameters) when employing the SQP method to solve (4.12) because (4.12b) and (4.12c) cannot be well satisfied simultaneously by using a simple tuning method. What is more, a starting point far from the feasible region is prone to cause the search process of the SQP to diverge. Therefore, the optimization process proposed in the following subsection serves to provide the starting point for (4.12), and to enhance its convergence.

4.3.3 Inter-Area Mode Oriented Pole Shifting

$$\min_{\mathbf{p}} \quad -\sum_{i=1}^{n_i} \xi_i \tag{4.13a}$$

$$\text{s.t.} \quad \xi_i \leq \xi_{i\max} \qquad i = 1, 2, ..., n_i \tag{4.13b}$$

$$\omega_{i\mathrm{o}}\left(1-\eta\right) \leq \omega_i \leq \omega_{i\mathrm{o}}\left(1+\eta\right) \tag{4.13c}$$

$$\xi_{jc} - \xi_j \leq 0 \qquad \lambda_j \in \pi_{c2} \tag{4.13d}$$

$$\alpha_j - \alpha_{jc} \leq 0 \tag{4.13e}$$

$$\mathbf{p}_{\min} \leq \mathbf{p} \leq \mathbf{p}_{\max} \tag{4.13f}$$

where π_{c2} has the same meaning as π_{c1}. Process of determining ξ_{jc} and α_{jc} in (4.13)

is the same as that in (4.12). Obviously, compared to the difficulty in directly obtaining a feasible starting point for (4.12), it is quite straightforward to provide a feasible starting point which can simultaneously satisfy (4.13b) and (4.13c), when using the SQP method to solve (4.13). For example, the initial controller parameters can be easily determined with the phase compensation technique. Therefore, a feasible starting point formed by these practically meaningful parameters (or with some adjustments) can generally lead to sequential movement of inter-area modes into the specific region shown in Fig. 4.1(b), which indicates that the final solution of (4.13) can be used as the feasible starting point for (4.12).

4.3.4 Implementation Procedure of IAMO-PS

Because most modes are generally either quite deeply damped or insensitive to controllers, π_{c1} and π_{c2} contain only a small number of modes, and they are determined in an iterative manner during implementation of IAMO-PS, which includes the following steps:

S.1) Select a feasible starting point for (4.13).

S.2) Depending on the starting point, π_{c2} is initially set to consist of modes whose frequencies locate in the studied range, say 0.2 to 1.0Hz;

S.3) Solve (4.13) based on the starting point and π_{c2};

S.4) Find modes which are significantly deteriorated after solving (4.13). These modes are added to π_{c2} and then go to S.3. If no such mode is found, go to the next step;

S.5) Check whether inter-area modes have been moved to the specific regions. If not, adjust the starting point and go to S.2, or derive the solution and go to the next step;

S.6) Use the solution of (4.13) as the starting point for (4.12). π_{c1} is initially set to be equal to π_{c2};

S.7) Solve (4.12) based on the starting point and π_{c1};

S.8) Find modes which are significantly deteriorated after solving (4.12). Add these modes to π_{c1} and then go to S.7. If no such mode is found, obtain the solution and the computation is terminated.

4.3.5 Discussion

For damping control of inter-area oscillations, IAMO-PS is much more objective-oriented than SCCS-PS. Besides offering the inter-area modes satisfactory damping ratios, coordination of control efforts, limiting frequency drifts of inter-area modes, and impacts of controllers on other non-inter-area modes are also explicitly considered in IAMO-PS. Moreover, due to use of the two-stage optimization procedure, a feasible starting point for IAMO-PS (actually for (4.13)), which enables its convergence, can be readily obtained, which makes its practical application as easy as that of SCCS-PS. Subsequently, SCCS-PS and IAMO-PS are compared in the next section on the basis of applications to coordinated design of a SDC for the TCSC and a PSS to damp inter-area oscillations in the New York and New England interconnected system.

4.4 Investigated System

The modified version of the New England and New York interconnected system (Fig. 3.8) used in the previous chapter is employed again to demonstrate the proposed control design methods. Similarly, a TCSC is installed in line 50-18 to compensate 40% of its reactance in the steady state. The minimum and

maximum allowable dynamic compensation of the TCSC are 25% and 65%, respectively, of line reactance. Fig. 4.2(a) shows the TCSC dynamic model with time constant T_{tc} equal to 10ms. The large loads are modeled as a combination of constant impedances (50%) and classic third-order induction motors (50%), while the remaining is modeled as constant impedance. Consequently, the open loop system model has a dimension of 236.
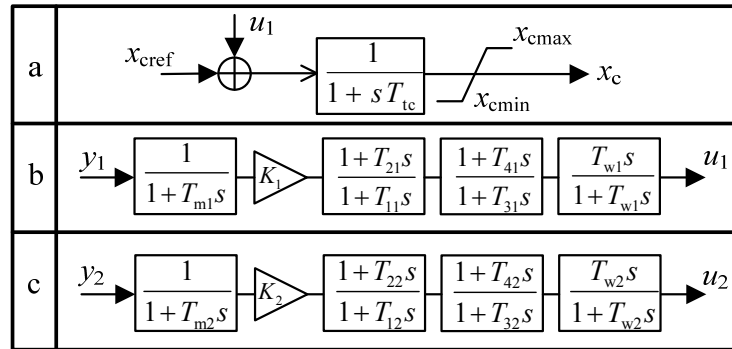
Fig. 4.2. Block diagrams (a: TCSC; b: SDC; c: PSS).

According to the geographic distribution, this system can be partitioned into five areas, of which Areas A_3, A_4 and A_5 are represented by a single aggregated generator. In the steady state, a total of about 2860MW power is imported to Area A_2; 715MW from Area A_1 and 2145MW from A_3, A_4 and A_5. The high level of power transmission between interconnected areas has given rise to two poorly damped oscillations of inter-area modes M_1 and M_2. M_1 with frequency at about 0.65Hz dominates the power oscillation between A_1 and A_2, while M_2 oscillating at frequency of about 0.32Hz mainly depicts the power oscillation between A_1, A_2 and the rest of the system. Hence, in order to damp these two modes, a wide-area signal based PSS is installed in Generator 13 which greatly participates in M_1 and M_2. Moreover, since the TCSC locates at the key transmission corridor, a SDC is installed in it to share the control burden of the

PSS.

Model structures of SDC and PSS are presented in Fig. 4.2(b) and (c), respectively: tunable controller parameters are K_1, T_{11}, T_{21}, T_{31}, T_{41}, K_2, T_{12}, T_{22}, T_{32}, and T_{42}; filter constant (T_{m1} and T_{m2}) and washout time constant (T_{w1} and T_{w2}) are preset to be 0.012s and 10s, respectively, and they remain fixed during the design. The detailed process of obtaining upper and lower limits of $\mathbf{p}$ can refer to Subsection 3.4.1. Residue analysis indicates that the signal of active power in line 13-17 is the most effective signal in damping of inter-area oscillations by both controllers; it is selected as the controllers' input. Moreover, the time-delay related to sending the wide-area signal to the remote SDC site through a dedicated fiber-optic communication channel is assumed to be 80ms, and it is assumed that no time-delay exists in feedback signal for the PSS. The time-delay is approximated by a second order Pade formula.

Model reduction should consider that inter-area modes are well preserved in the reduced-order model because the proposed methods are based on eigenvalues. Therefore, a 26-order reduced model, which has almost the same inter-area modes as those in the full model, is obtained by using the Schur balanced model truncation algorithm [86]. The step responses from u_2 to y_1 of both models are illustrated in Fig. 4.3. The two almost overlapped curves further confirm that the reduced-order model can accurately approximate the full model within the frequency range of studied dynamics. In fact, the same phenomenon has been observed in the step response experiments conducted respectively with the other three input-output pairs (u_1-y_1, u_1-y_2 and u_2-y_2).

It is commonly expected that oscillations of inter-area modes can settle down within 10s. Thus, the minimum damping ratios of M_1 and M_2 are set to be 10%

and 18%, respectively, in IAMO-PS. Moreover, the upper limit is 25% for M_1, and it is 30% for M_2. η is chosen to be 5%. For modes in π_{c1} and π_{c2}, both α_{jc} and ξ_{jc} are chosen to be 95% of their initial values.
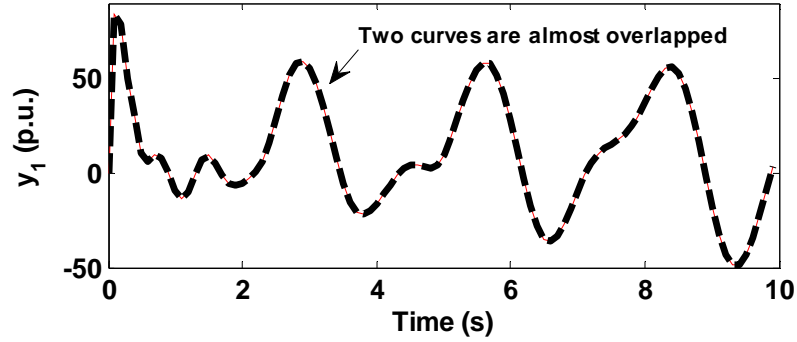
Fig. 4.3. Step response from input u_2 to output y_1 (thick dash line: reduced; thin solid line: full).

4.5 Simulation Results and Analysis

4.5.1 Control Effect Comparisons between Two Methods

For both SCCS-PS and IAMO-PS, a feasible starting point is required. Firstly, T_{11} to T_{41} are selected to compensate phase of the residue from u_1 to y_1, with respect to M_2, to -180˚. Likewise, T_{12} to T_{42} are determined for the SDC, with respect to M_1. Then, K_1 and K_2 are simply set to be zero, which disables the controllers. Thus, M_1 and M_2 in the system with these controller parameters will apparently be the same as that in the open loop system. Consequently, these initial parameters serve to form the starting point for both methods (Table 4.1).

The optimization process of SCCS-PS is illustrated in Fig. 4.4. It is seen that the SQP method is quite efficient in solving (4.4) and the maximum ξ_m is 0.0383. The inequality constraint in (4.4b) associated with mode (-0.3636+9.4600i) is activated at the final solution, which means it locates on the border of the conic section. For IAMO-PS, evolutions of both inter-area modes during optimization are depicted in Fig. 4.5. The first 41 iterations are at the first stage, while the

second stage costs 9 iterations to converge. Clearly, damping ratios of the two modes are efficiently improved and, during this process, their frequency drifts are also well controlled. The final tuned controller parameters for SCCS-PS and IAMO-PS are presented in Table 4.1. In addition, Table 4.2 compares the control results in terms of inter-area modes. It is easy to check that both M_1 and M_2 have been moved to the expected region by controllers designed by IAMO-PS. Furthermore, although SCCS-PS can design controllers that are able to stabilize the unstable open loop system, they cannot perform as well as controllers tuned by IAMO-PS. Damping ratios of M_1 and M_2 are only 0.0418 and 0.1348, respectively. Moreover, it is easily observed that frequencies of M_1 and M_2 have been significantly altered, compared to the case with IAMO-PS.

TABLE 4.1 INITIAL AND TUNED CONTROLLER PARAMETERS

	LB	UB	Initial	SCCS-PS	IAMO-PS
K_1	0.0000	0.0500	0.0000	0.0124	0.0163
T_{11}	0.1100	1.0300	0.7851	0.8929	0.6884
T_{21}	0.0800	0.7400	0.2275	0.1067	0.0800
T_{31}	0.1100	1.0300	0.7851	0.8929	0.6884
T_{41}	0.0800	0.7400	0.2275	0.1067	0.0800
K_2	0.0000	0.1200	0.0000	0.0365	0.0248
T_{12}	0.1100	1.0300	0.4054	0.5995	0.3139
T_{22}	0.0800	0.7400	0.1244	0.5593	0.0800
T_{32}	0.1100	1.0300	0.4054	0.5995	0.3139
T_{42}	0.0800	0.7400	0.1244	0.5593	0.0800
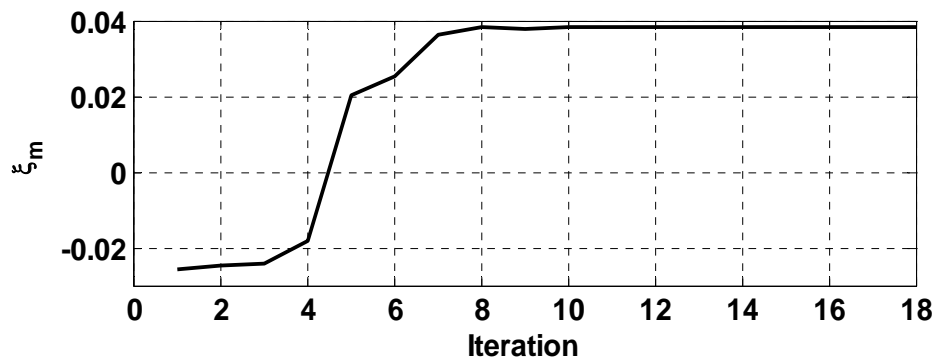
Fig. 4.4. Optimization process of SCCS-PS.
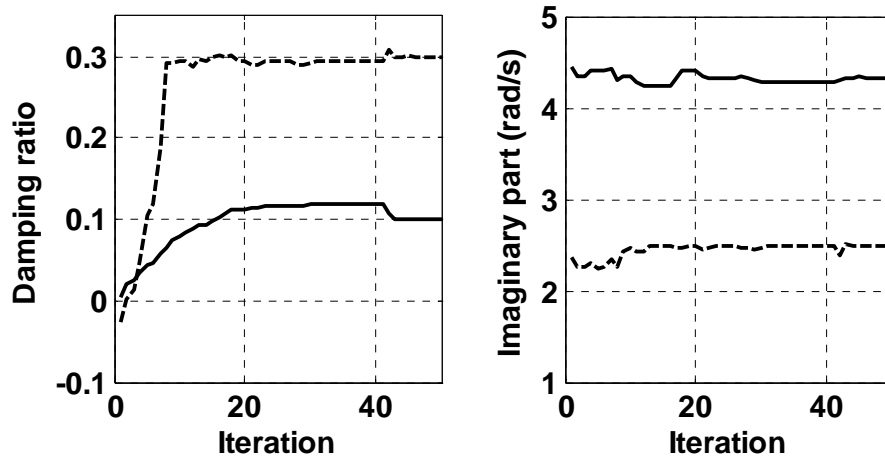
Fig. 4.5. Evolutions of inter-area modes during optimization (solid line: M1; dash line: M2).

TABLE 4.2 CONTROL RESULTS FOR THE INTER-AREA MODES

Mode	Open loop	SCCS-PS	IAMO-PS
M_1	-0.0118±4.4531i	-0.1689±4.0328i	-0.4348±4.3259i
M_2	0.0655±2.3660i	-0.2790±1.9792i	-0.7850±2.5001i

Nonlinear numerical simulations are conducted to further demonstrate the control effects. A three phase short circuit fault occurs at Bus 60 at 1.0s and it is cleared 100ms later by removing one of transmission lines between Buses 60 and 61. This key corridor located fault can effectively excite two inter-area mode oscillations in the system. Thus, Fig. 4.6 depicts the relative power angle oscillations of all generators with respect to Generator 13 when subject to the disturbance. It is clear that the oscillatory instability has emerged in the open loop system owing to the unstable mode M_2. Nevertheless, these sustainable oscillations can be suppressed by the coordinated SDC and PSS tuned by SCCS-PS or IAMO-PS. Even so, it is obvious that oscillations of both inter-area and local modes in the system under control of IAMO-PS tuned controllers decay much faster (within 10s) than those in the system with controllers designed by SCCS-PS. Curves of relative power angle of Generators 6 and 15 (Fig. 4.7) strongly confirm the conclusion that IAMO-PS is more suitable for coordinating

controllers aiming at inter-area oscillations. Furthermore, the dynamic compensation of the TCSC, as well as the PSS output during the transient, is also shown in Fig. 4.7. When SCCS-PS is employed, control effort of the TCSC is rather lightly exerted, compared with the PSS. This is because SCCS-PS only focuses on the pole placement and lacks of mechanism to distribute control burden among different controllers. However, it is also noted that this issue does not exist in controllers designed by IAMO-PS. In this study, w_1 and w_2 are selected to be 1 and 0.8, respectively, which can appropriately utilize the available capacity of the TCSC to help relieve the control burden of the PSS.
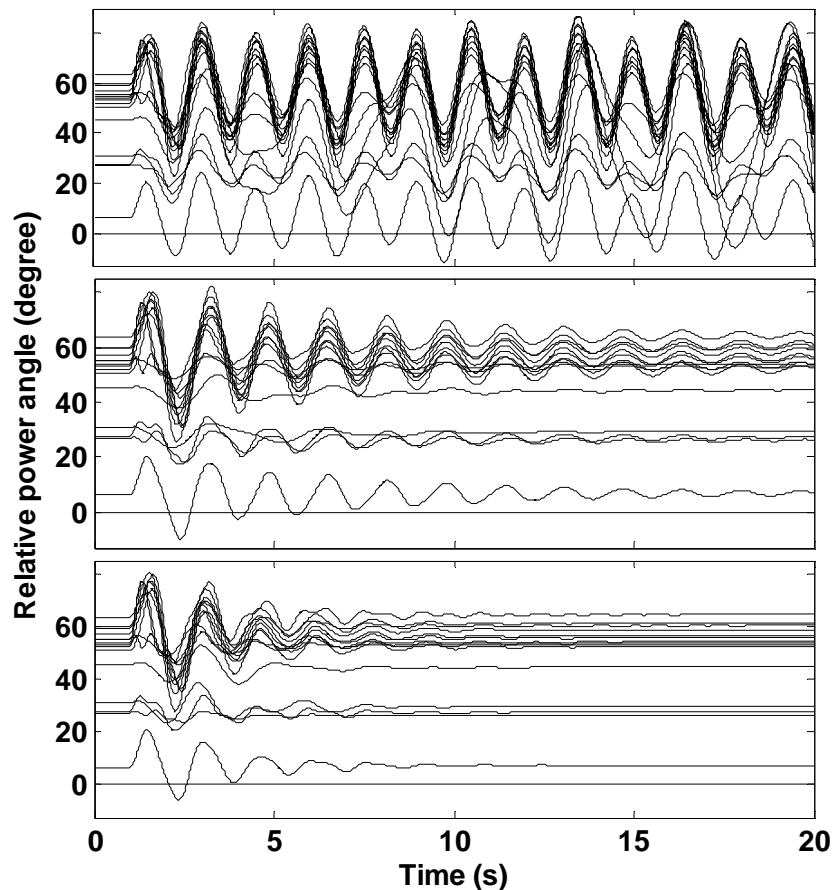
Fig. 4.6. Power angle oscillations of all generators with respect to Generator 13 (upper plot: no controller; middle plot: SCCS-PS; lower plot: IAMO-PS).
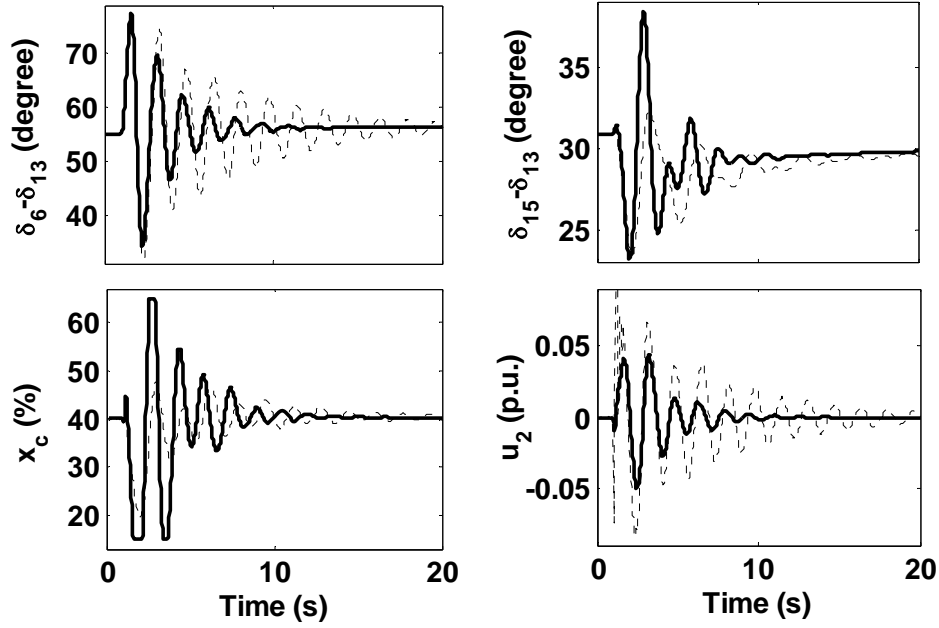
Fig. 4.7. Partial system dynamics (dot line: SCCS-PS; solid line: IAMO-PS).

4.5.2 Comparison with the PSS in Service Only

In the heuristic sense, a much larger w_1 will greatly constrain the control effort of the SDC, and vice versa. Obviously, the same principle holds for the PSS. Thus, an extreme case with $w_1=1$ and $w_2=0$ is employed for test, which predicts that only control effort of the SDC is limited and the PSS can freely meet the pole placement requirement. Using the same initial controller parameters as shown in Table 4.1, the final tuned parameters in such cases are calculated and given in Table 4.3. Interestingly, it is noted that K_1 has been driven to zero by optimization, which is qualitatively different from that when $w_1=1$ and $w_2=0.8$; it can be understood as implying that the SDC will be out of service (no control effort) and the PSS can take the whole responsibility to damp inter-area oscillations. Obviously, this is in accordance with the aforementioned prediction, and thus validates the notion that the index f_k is effective in measuring the control effort, and IAMO-PS employing this index can properly coordinate control efforts of different controllers.

80

TABLE 4.3 CONTROLLER PARAMETERS FOR DIFFERENT WEIGHTS

	$w_1=1$ $w_2=0.8$	$w_1=1$ $w_2=0$
K_1	0.0163	0.0000
T_{11}	0.6884	0.2518
T_{21}	0.0800	0.2528
T_{31}	0.6884	0.2539
T_{41}	0.0800	0.2528
K_2	0.0248	0.0717
T_{12}	0.3139	0.4695
T_{22}	0.0800	0.0802
T_{32}	0.3139	0.7233
T_{42}	0.0800	0.1499

Comparisons of the PSS output as well as the terminal voltage of Generator 13 in the two cases are given in Fig. 4.8, when the system is subject to the same disturbance as that in Section 4.5.1. It is seen that although the PSS can work alone to suppress the oscillations, it has to sacrifice the voltage dynamics of the generator. However, when the control burden has been shared appropriately by the TCSC, control effort of the PSS is reduced, resulting in the terminal voltage profile obviously improving.
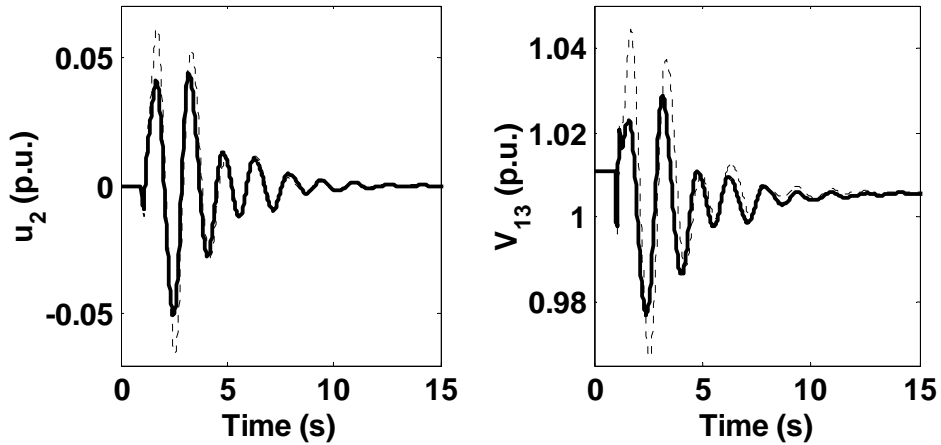
Fig. 4.8. PSS output and terminal voltage of Generator 13 (solid line: $w_1=1$ and $w_2=0.8$; dot line: $w_1=1$ and $w_2=0$).

81

4.5.3 Study of Influence of Other Modes on Control of Inter-Area Modes in SCCS-PS

25 sets of controller parameters are randomly generated, within the range of parameter limits. In each of them, K_1 and K_2 are fixed to be zeros. Each set of parameters is used to form the starting point for both methods. It is found that regardless of their randomness, optimizations of both methods are able to converge for all sets of parameters. Moreover, in SCCS-PS, the maximum ξ_m stays always around 0.0383 for all tested starting points and a mode with imaginary part of about 9.4600 always locates on the border of the conic section. Therefore, it is inferred that this mode should be the obstacle for SCCS-PS to further enhance system stability because the controllers are unable to significantly improve its damping ratio.

Damping ratios of the two inter-area modes at the final solution are shown in Fig. 4.9. It is seen that when SCCS-PS is utilized, M_1 and M_2 can obtain damping ratios not less than 0.0383 in all cases, but they appear to be greatly dependent on the initial controller parameters. This is because although poorly damped M_1 and M_2 are moved towards the high damping ratio region at the initial stage of the optimization, they are not 'specially cared' afterward, once their damping ratios are larger than other modes. Their final locations may not be within the expected region and are considerably affected by the initial controller parameters. However, it is noted that M_1 and M_2 are with satisfactory damping ratios when the system is under control of controllers tuned by IAMO-PS, which is an inter-area mode oriented method. Handling inter-area modes and other modes differently enables IAMO-PS to concentrate on control of M_1 and M_2.
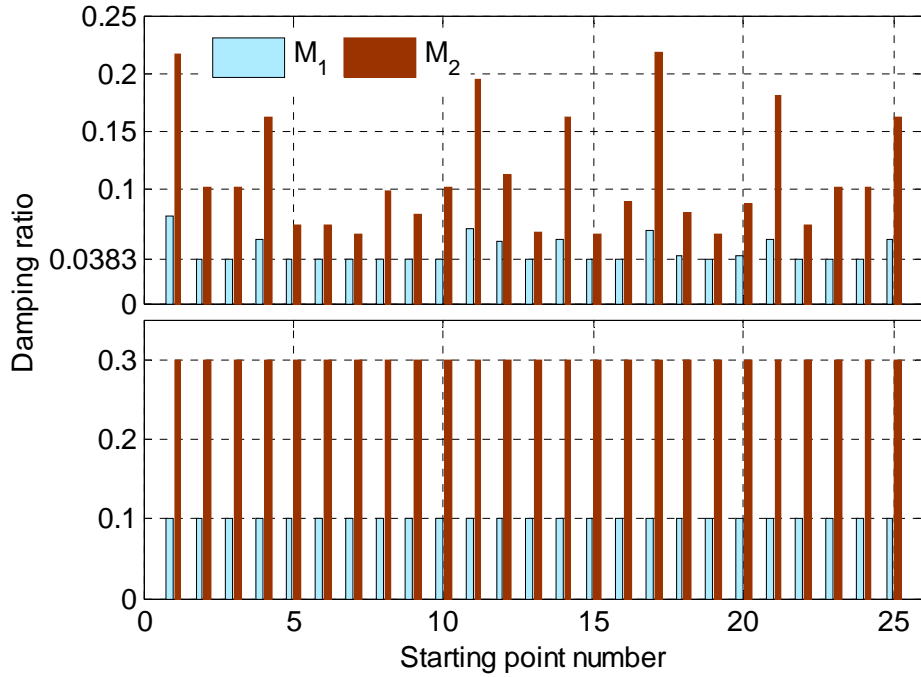
Fig. 4.9. Damping ratios of the two inter-area modes for different starting points (upper plot: SCCS-PS; lower plot: IAMO-PS).

4.6 Summary

This chapter first proposes the SQP based SCCS-PS, which tunes the controllers by moving all poles to a sequentially compressed conic section, in order to provide insights into the impacts of other modes on control of inter-area modes. Inspired by analysis of SCCS-PS, IAMO-PS is then specifically proposed for damping control design to suppress inter-area oscillations. The pole placement in IAMO-PS makes the controllers focus on controlling inter-area modes. Moreover, it flexibly allocates the control burden among different controllers. The two-stage SQP proposed for IAMO-PS enables easy selection of the starting point, which makes it convenient for application. Both methods were applied to coordinate the PSS and the SDC for the TCSC in the New England and New York interconnected system. SCCS-PS has disclosed that improvements of inter-area modes could be considerably limited by some other

high frequency modes if all poles are pushed into a conic section because the controllers cannot significantly impact these modes. However, IAMO-PS yielded quite satisfactory control effects for inter-area modes. Successfully relieving the control effort of the PSS by properly allocating some of its control burden to the SDC by IAMO-PS, which reduces its adverse effects on the system operation, has shown that measuring and coordinating control efforts of different controllers is important and practically meaningful in pole placement based damping control designs.

Chapter 5

Optimal Design of Controllers for DFIG-based WTG to Damp Inter-Area Oscillations

5.1 Introduction

Besides extensive works have been devoted to investigate effects of continuously increased wind power penetration on the transient stability, voltage stability and frequency dynamics, its impacts on power system oscillations have also drawn much concern from power researchers [42, 43, 131-136]. Interestingly, it is in general accepted that the wind power proliferation is benefit to the damping of electromechanical oscillations [137, 138]. This can be conceptually explained under the assumption that the increased WTGs replace some conventional synchronous generators to supply the grid. Thus, the remaining synchronous generators become relatively smaller with respect to the impedance of the grid. This actually strengthens their mutual coupling, which in most cases improves the damping of any oscillations that occur between the synchronous generators. Moreover, it is also advocated in [138] that the fixed speed WTGs affect the damping of power system oscillations more than the variable speed WTGs because the former are directly connected to the grid while the latter are decoupled from the grid by the power electronic converter. However, these are just heuristic conclusions used for a meaningful schematic

understanding. In fact, sensitivities studies in [139] indicate that the damping performance of the New Zealand system is not materially affected by a high level of wind generation as well as the types of WTGs. Moreover, Reference [140] reports that increased wind power penetration causes congestion at weak interconnection lines that leads to reduced damping. Therefore, the real situation of wind power penetration influencing the system small signal stability should depend on the concrete study background.

Reference [141] has summarized four mechanisms by which DFIGs can affect the damping of electromechanical modes: (1) displacing synchronous machines thereby affecting the modes; (2) impacting major path flows thereby affecting the synchronizing forces; (3) displacing synchronous machines that have PSSs; (4) DFIG controls interacting with the damping torque on nearby large synchronous generators. Generally, replacement of synchronous generators by WTGs leads to the reduction of system effective inertia. Therefore, the eigenvalue sensitivities with respect to the inertia of synchronous generators are calculated in [141] to predict impacts of the augmented wind power on electromechanical modes. Apart from these replacement caused impacts, it is pointed out in [45] that, as the DFIG-based wind power penetration increases, its reactive power control loop have more obvious impacts on inter-area oscillations than other control loops such as phase-locked loop (PLL) and pitch angle control. Furthermore, Reference [142] has shown that when the reactive power control loop works at voltage control (VC) mode, its impacts are quite sensitive to the parameter setting and if inappropriate tuned, certain penetration levels will bring considerable adverse effects to the damping of inter-area modes.

In heuristic sense, as the active power injected by the WTG decreases, the

synchronous generator power is increased, which leads to deceleration of its rotor. Based on this physical consideration, in order to provide a novel source of oscillation damping and reinforce the positive damping effect of the DFIG, a simple stabilizer which adds an auxiliary signal proportional to the frequency deviation to the active power reference has been proposed in [143]. Moreover, the rate of change of the PLL angle which is equivalent to the DFIG bus frequency deviation is employed in [144] as an available input signal to the stabilizer. From another perspective, this type of damping controllers actually provides additional equivalent inertia to the system, probably benefitting the inertia response during the transient [43]. Reference [145] has proposed a control strategy to mitigate the impact of reduced inertia due to DFIGs by adjusting pitch compensation and maximum active power order. Consequently, the improvements of system dynamics in terms of power oscillation damping have been observed in a large power system. However, since these damping control methods are just based on general physical interpretations, it is easily found that their control effects may not be comparable with those of approaches employing SDCs designed based on exact control theories and system models, as in [44, 46, 74]. Therefore, installation of SDCs to DFIG-based WTGs is a common way to engage them active participation in system damping control.

According to the above statement, an optimal control design is employed for the DFIG-based WTG in this chapter to systematically demonstrate its capability of damping inter-area oscillations. Firstly, the operating modes of the DFIG at the steady state are discussed. The simplified dynamic models of the WTG are then introduced. Subsequently, an optimization problem is constructed for damping control where parameters of the power and voltage (PV) controllers and

the SDC are simultaneously adjusted by using differential evolution (DE), which is a simple but yet powerful evolutionary optimization algorithm, especially for problems with real-valued parameters. A two-area system is employed at final stage to verify the design and draw some profitable conclusions.

5.2 Steady-State Operation of DFIG

At the steady state, DFIG operates to influence the system load flow. It is necessary to obtain the steady-state model of DFIG for load flow calculation as well as system initialization for further dynamic analysis [146, 147]. Additionally, the process of internal energy transfer in the DFIG can be thoroughly perceived based on the steady-state analysis of DFIG. Normally, the DFIG steady-state operation can be mathematically described by the following equations in the synchronously rotating d-q reference frame [39]:

$$v_{ds} = -r_s i_{ds} + \omega_s L_{ss} i_{qs} - \omega_s L_m i_{qr} \tag{5.1}$$

$$v_{qs} = -r_s i_{qs} - \omega_s L_{ss} i_{ds} + \omega_s L_m i_{dr} \tag{5.2}$$

$$v_{dr} = r_r i_{dr} - s\omega_s L_{rr} i_{qr} + s\omega_s L_m i_{qs} \tag{5.3}$$

$$v_{qr} = r_r i_{qr} + s\omega_s L_{rr} i_{dr} - s\omega_s L_m i_{ds} \tag{5.4}$$

where v_{ds} and v_{qs} are d and q components, respectively, of stator voltage; v_{dr} and v_{qr} are d and q components of rotor voltage; i_{ds} and i_{qs} are d and q components of stator current; i_{dr} and i_{qr} are d and q components of rotor current; L_{ss} and L_{rr} are the stator and rotor inductances, respectively; L_m is the magnetizing inductance; r_s and r_r are stator and rotor resistances, respectively; ω_s is the synchronous speed; and s is the slip. All variables and parameters are expressed in per-unit terms in this chapter, if not specified.

Based on (5.1)-(5.4), by expressing all voltage and current as phasors in terms of their d and q components, the equivalent circuit of DFIG at the steady state is illustrated in Fig. 5.1 where L_s and L_r are stator and rotor leakage inductances, respectively; P_e, P_m and P_r represent air-gap power delivered from rotor to stator, mechanical power and injected rotor active power, respectively. Thus, according to this diagram, these three kinds of power are calculated as follows:

$$P_e = \mathrm{Re}\left(\frac{\dot{v}_r}{s}\dot{I}_r^* - \frac{r_r}{s}I_r^2\right) \tag{5.5}$$

$$P_m = \mathrm{Re}\left(\frac{(1-s)\dot{v}_r}{s}\dot{I}_r^* - \frac{(1-s)r_r}{s}I_r^2\right) \tag{5.6}$$

$$P_r = \mathrm{Re}\left(\dot{v}_r\dot{I}_r^*\right) \tag{5.7}$$

where Re(.) is the operator that obtains the real part of a complex number. Obviously, the following relationships are hold among them:

$$P_e = P_m + P_r - r_r I_r^2 \tag{5.8}$$

$$P_m = (1-s)P_e \tag{5.9}$$

$$P_r = sP_e + r_r I_r^2 \tag{5.10}$$

From (5.8), it is told that the power passing from rotor to stator via the air gap is the sum of mechanical power and injected rotor active power minus the power loss at the rotor resistance. Moreover, since the mechanical power should be always larger than zero ($P_m>0$), from (5.9) and (5.10), it is readily concluded that there are five types of operating modes for the DFIG at the steady state according to its internal power flow directions, as follows:

(1) Subsynchronous mode ($0<s<1$): an amount of active power is injected into

the rotor from the external network. A part of them will be consumed by the rotor resistance and the remaining together with the mechanical power will be delivered to the stator through the air gap.

(2)   Synchronous mode ($s=0$): the injected rotor active power exactly counteracts the power consumed by the rotor resistance. Only mechanical power will be delivered to the stator.

(3)   Supersynchronous mode ($s<0$) and $P_r>0$: a part of mechanical power plus the active power injected from the external network into the rotor is consumed by the rotor resistance and the rest of mechanical power is delivered to the stator.

(4)   Supersynchronous mode ($s<0$) and $P_r=0$: the power consumed by the rotor resistance is exactly balanced by a part of mechanical power and no active power is exchanged between the rotor and the external network.

(5)   Supersynchronous mode ($s<0$) and $P_r<0$: deducting the power consumed by the rotor resistance, the mechanical power will be partly delivered to the external network through the rotor in addition to the part delivered through the stator.

$$\dot{v}_s = v_{ds} + jv_{qs} \qquad \dot{I}_s = i_{ds} + ji_{qs} \qquad L_{ss} = L_s + L_m$$
$$\dot{v}_r = v_{dr} + jv_{qr} \qquad \dot{I}_r = i_{dr} + ji_{qr} \qquad L_{rr} = L_r + L_m$$
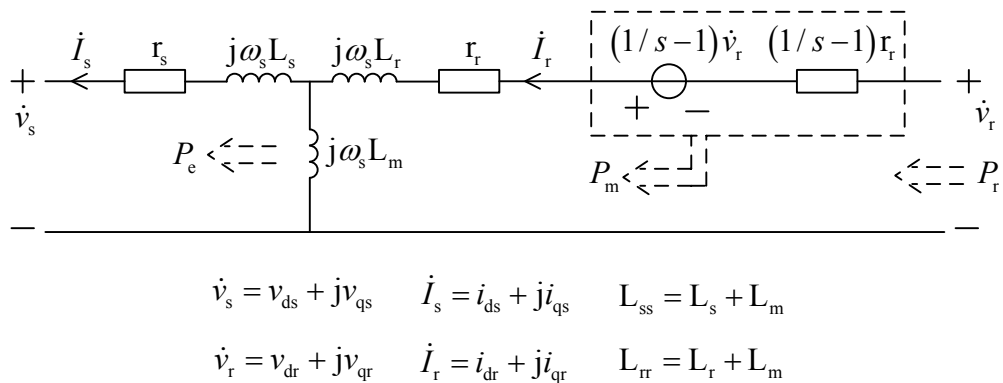
Fig. 5.1. Steady-state equivalent circuit of DFIG

Clearly, it is found that given the stator voltage, the active and reactive power outputs of the DFIG can be flexibly controlled by adjusting the magnitude and phase angle of the rotor voltage. This indicates that the bus incorporating the DFIG can be modeled as the machine or load bus in the load flow calculation. Moreover, to take into account more real scenarios, it is also possible to use the wind speed as an input variable for the load flow [147]. In such case, the steady-state model (5.1)-(5.4) of the DFIG should be necessarily involved in the iterations of load flow computation.

5.3 Dynamic Models of DFIG-based WTG

5.3.1 Simplified DFIG Model

The sketch diagram of a DFIG-based WTG is shown in Fig. 5.2. In this study, the dynamics of the DC capacitor are neglected; the active power on the RSC is assumed to be equal to the active power on the grid side converter (GSC). Moreover, the GSC is manipulated ideally to ensure that no reactive power is exchanged with the grid during the transient and the reactive power support is totally accomplished by the stator. By ignoring dynamics of the stator current and assuming a lumped-mass shaft model, the simplified third-order model of DFIG is derived as follows:

$$\frac{1}{\omega_b}\frac{de_d}{dt} = -\frac{1}{T_0}\left[e_d - (X-X')i_{qs}\right] + s\omega_s e_q - \omega_s \frac{L_m}{L_r + L_m}v_{qr} \tag{5.11}$$

$$\frac{1}{\omega_b}\frac{de_q}{dt} = -\frac{1}{T_0}\left[e_q + (X-X')i_{ds}\right] - s\omega_s e_d + \omega_s \frac{L_m}{L_r + L_m}v_{dr} \tag{5.12}$$

$$\frac{d\omega_r}{dt} = \frac{1}{2H}\left[T_m - \frac{e_d i_{ds} + e_q i_{qs}}{\omega_s}\right] \tag{5.13}$$

$$v_{ds} = -r_s i_{ds} + X' i_{qs} + e_d \qquad (5.14)$$

$$v_{qs} = -r_s i_{qs} - X' i_{ds} + e_q \qquad (5.15)$$

$$i_{dr} = \frac{1}{\omega_s L_m} e_q + \frac{L_m}{L_r + L_m} i_{ds} \qquad (5.16)$$

$$i_{qr} = \frac{-1}{\omega_s L_m} e_d + \frac{L_m}{L_r + L_m} i_{qs} \qquad (5.17)$$

$$P_g = v_{ds} i_{ds} + v_{qs} i_{qs} - v_{dr} i_{dr} - v_{qr} i_{qr} \qquad (5.18)$$

$$Q_g = v_{qs} i_{ds} - v_{ds} i_{qs} \qquad (5.19)$$

where

$$e_d = -\omega_s L_m / (L_m + L_r) \psi_{qr} \qquad (5.20)$$

$$e_q = \omega_s L_m / (L_m + L_r) \psi_{dr} \qquad (5.21)$$

$$X' = \omega_s \left(L_s + L_m - L_m^2 / (L_m + L_r) \right) \qquad (5.22)$$

$$X = \omega_s (L_s + L_m) \qquad (5.23)$$

$$T_0 = (L_r + L_m) / r_r \qquad (5.24)$$

where ψ_{dr} and ψ_{qr} are d and q components, respectively, of rotor flux; e_d and e_q are d and q components, respectively, of internally generated voltage; P_g and Q_g are active and reactive power output of DFIG; ω_r is the rotor speed; X and X' are open-circuit and short-circuit reactance; T_0 is the transient open-circuit time constant; H is the inertia constant in unit of second; T_m is the mechanical torque; and ω_b is the system speed base in unit of rad/s. Specifically, as the ones used in References [46] and [148], such simplified model suffices for manifestation of the capability of WTGs in suppression of inter-area oscillations with the merit of facilitation of control design.
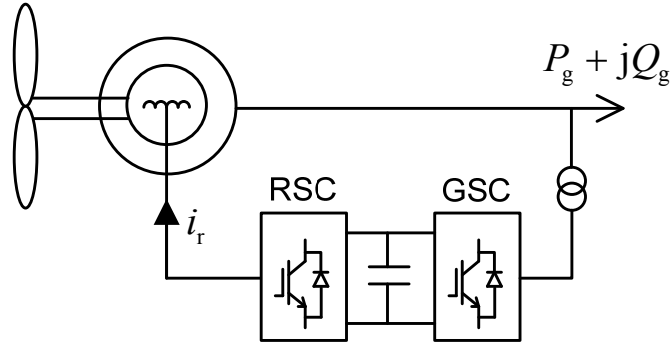
Fig. 5.2. Sketch diagram of DFIG-based WTG

The dynamic equivalent circuit and vector diagram of DFIG are shown in Fig. 5.3. The mechanical torque generated by the wind turbine is modeled as follows:

$$T_\mathrm{m} = \frac{0.5 \rho \pi \mathrm{R}^2 C_\mathrm{p} \mathrm{V}_\mathrm{w}^3}{\omega_\mathrm{r}} \tag{5.25}$$

where R is the wind turbine radius; V_w is wind speed; ρ is the air mass density; and C_p is the power coefficient, defined as follows:

$$C_\mathrm{p} = 0.5 \left(\frac{\mathrm{R}}{\gamma} - 0.022 \beta^2 - 5.6 \right) \mathrm{e}^{-\frac{0.17\mathrm{R}}{\gamma}} \tag{5.26}$$

where γ is the tip speed ratio and β is the pitch angle which is set to 0.2349 and kept fixed during the study process.

(a) eqiuvalent circuit   (b)vector diagram
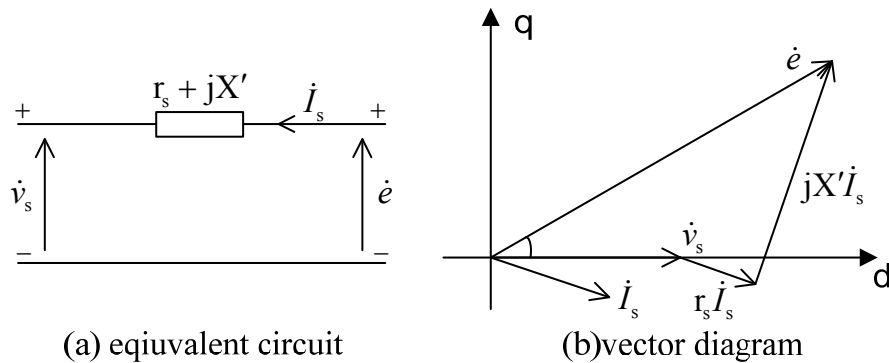
Fig. 5.3. Dynamic equivalent circuit and vector diagram of DFIG

5.3.2 Power and Voltage Control Systems

The control system for DFIG should be able to deal with wind speed variation and extract maximum electric power under different wind speeds. Furthermore reactive power support should be provided by DFIG to maintain the terminal voltage. In this study, the rotor flux magnitude and angle control (FMAC) method is applied to accomplish these two tasks.

From the equivalent circuit and vector diagram in Fig. 5.3, it can be observed that internally generated voltage $\dot{e}$ plays a role in induction generator that is similar to the role of q-axis transient electric potential in a synchronous generator. Therefore, the angle of $\dot{e}$ is employed to control the active power output of DFIG, while its magnitude is applied for maintaining terminal voltage in DFIG.

The block diagram of PV control system for DFIG is shown in Fig. 5.4. E_e and δ_e are magnitude and angle, respectively, of $\dot{e}$. v_{ref} is the terminal voltage reference of DFIG. P_{opm} is the optimal reference power output, which is calculated from the power-speed function of the wind turbine, for maximum power extraction. T_v is the time constant used to approximate the time delay between the control signal and the real output of the converter. u_{pss} is the signal provided by the SDC for the DFIG.

5.3.3 SDC for DFIG

The SDC with the traditional lead-lag compensation structure is shown in Fig. 5.5. Through investigation it is found that it is more effective to add supplementary damping signal in the power control loop for increasing damping of the inter-area mode, compared with adding it in the voltage control loop. Moreover in the steady state u_{pss} is zero so that it will not impact the maximum power extraction function of the power control loop. Also because of the high

visibility of the inter-area mode in the terminal voltage signal, it is selected as the control input for the damping controller in this study.
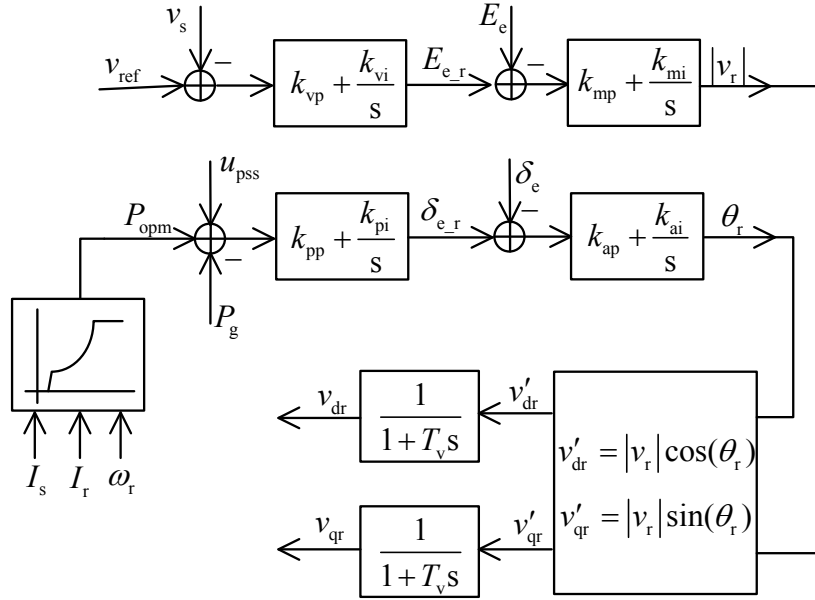
Fig. 5.4. Power and voltage control loops for DFIG
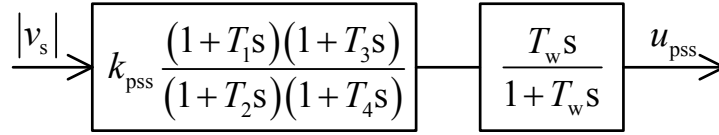
Fig. 5.5. Supplementary damping controller for DFIG

5.4 Controller Tuning and Differential Evolution

5.4.1 Problem Formulation

The tunable parameters of the PV controllers and the SDC are adjusted simultaneously to ensure dynamic performance of the system, especially for suppressing inter-area oscillation. This indicates that eigenvalues of the final tuned closed loop system are expected to locate in the shadowed D-shaped region S^* in Fig. 5.6, where α_c and ξ_c are acceptable limits for the damping constant and the damping ratio, respectively, to guarantee that the system can settle down as

soon as possible after disturbances [116].
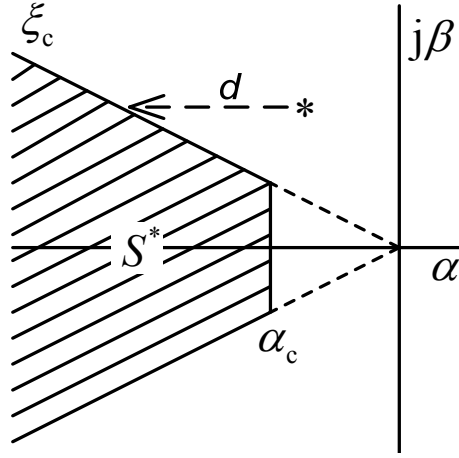
Fig. 5.6. Desired eigenvalues distribution region

The controllers should be tuned aiming at shifting eigenvalues outside the region into the region. This results in the following optimization problem:

$$\min f(\mathbf{p}) = \sum_{i \notin S^*} d_i \qquad (5.27)$$

$$\text{s.t.} \quad \mathbf{p}^{\min} \leq \mathbf{p} \leq \mathbf{p}^{\max}$$

where d_i is the horizontal distance from the ith eigenvalue which locates outside S^*, toward the boundary of S^*, and $\mathbf{p}$ is the parameter vector defined as

$$\mathbf{p} = \left[k_{pp}, k_{pi}, k_{vp}, k_{vi}, k_{mp}, k_{mi}, k_{ap}, k_{ai}, k_{pss}, T_1, T_2, T_3, T_4 \right]^{\mathrm{T}} \qquad (5.28)$$

where $\mathbf{p}^{\max}$ and $\mathbf{p}^{\min}$ are the upper and lower limits, respectively, of the parameter vector. From the theoretical viewpoint, the controllers tuned by this optimization based method may not be as efficient as the ones tuned by the method of IAMO-PS presented in Chapter 4 in controlling inter-area modes. However, it is indeed found that this method seldom obstructs from showing the damping control capability of WTGs. Moreover, the optimization problem formulated in such a simple form facilitates employment of DE as the solver which can endeavor to seek the global optimal solution.

5.4.2 Solving the Optimization Problem Using DE

To minimize the objective function (5.27), the following classic DE procedure is employed [73]:

S.1) Initialization of the population: Each individual representing a parameter vector as (5.28) can be randomly generated, for a population with NP individuals, as follows:

$$p_{i,j}^{(0)} = p_j^{\min} + r \cdot (p_j^{\max} - p_j^{\min}) \tag{5.29}$$

where $p_{i,j}^{(0)}$ denotes the jth controller parameter (gene or chromosome) of the ith parameter vector (individual) $\mathbf{p}_i^{(0)}$ in the first generation, and $p_j^{\min}$ and $p_j^{\max}$ are the lower and upper limits of the jth controller parameter, respectively. r is a uniformly distributed random value over the range of [0, 1].

S.2) Differential mutation: The ith mutant $\mathbf{v}_i^{(n)}$ (parameter vector) in generation n is produced according to the following formula:

$$\mathbf{v}_i^{(n)} = \mathbf{p}_i^{(n)} + K_b \left(\mathbf{p}_{\text{best}}^{(n)} - \mathbf{p}_i^{(n)} \right) + F_m \left(\mathbf{p}_{r_1}^{(n)} - \mathbf{p}_{r_2}^{(n)} \right) \tag{5.30}$$

where $\mathbf{p}_{\text{best}}^{(n)}$ is the best individual among the population in generation n. K_b and F_m are constants in [0, 1]. r_1 and r_2 are two randomly generated integers between 1 and NP. $\mathbf{p}_i^{(n)}$, $\mathbf{p}_{r_1}^{(n)}$ and $\mathbf{p}_{r_2}^{(n)}$ are the ith, r_1th and r_2th individuals, respectively, in the population.

S.3) Crossover: The ith mutant $\mathbf{v}_i^{(n)}$ (father) is then mated with individual $\mathbf{p}_i^{(n)}$ (mother) to produce child $\mathbf{c}_i^{(n+1)}$ in generation n+1. The One-Point crossover strategy is used in this study.

S.4) Selection: The mother-child competition is applied for generating

individual $\mathbf{p}_i^{(n+1)}$ in generation n+1, which can be expressed mathematically as follows:

$$\mathbf{p}_i^{(n+1)} = \begin{cases} \mathbf{c}_i^{(n+1)} & \text{if} \quad f\left(\mathbf{c}_i^{(n+1)}\right) < f\left(\mathbf{p}_i^{(n)}\right) \\ \mathbf{p}_i^{(n)} & \text{otherwise} \end{cases} \tag{5.31}$$

Repeat Steps 2 to 4 until the objective function in (5.27) becomes zero or the specified maximum number of generation is reached. Then the individual with minimum objective function in final generation will be selected as the controller parameters.

5.5 Simulation Studies

5.5.1 System Introduction

A two-area system (Fig. 5.7) derived from the two-area four-machine system used in Chapter 3 is employed for demonstration. They share the most data but with exception in this chapter that a DFIG-based WTG is connected to the grid in Area 1 and it outputs 411MW to the system in normal operating condition while the other four synchronous generators' output are: P_{G1}=494MW, P_{G2}=494MW, P_{G3}=700MW and P_{G4}=700MW. The DFIG parameters are given in Table 5.1.

Wind power penetration is about 30% of the power generated in Area 1; about 400MW of power is transferred from Area 1 to Area 2. An inter-area mode with frequency of about 0.7 Hz exists in the relative motion of generators in Area 1 with respect to generators in Area 2. In addition, there are two local modes at about 1.3 Hz and they depict the relative motion between generators in each area. Wind speed is assumed to remain constant.
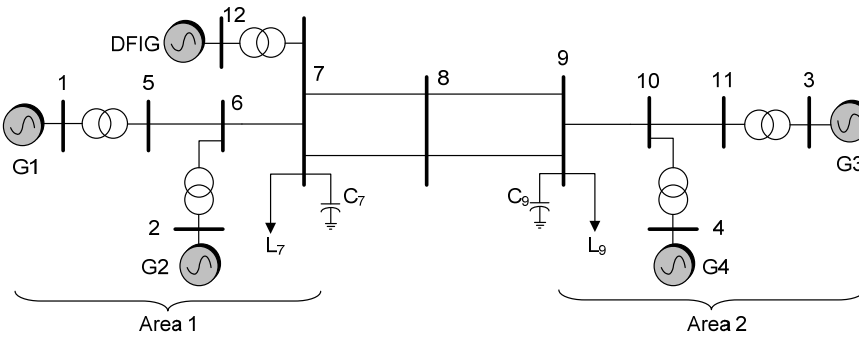
Fig. 5.7. Two-area system with a DFIG-based WTG

TABLE 5.1 DFIG PARAMETERS (POWER RATING: 900MVA)

H (s)	r_s	r_r	x_s	x_r	x_m
5.0444	0.0088	0.1060	0.1663	0.1793	7.1168

5.5.2 Simulation Results and Discussion

In order to verify the effectiveness of the optimal control design in damping inter-area oscillation, two experiments are carried out. The first experiment is conducted on the DFIG with only PV controllers whose parameters are carefully tuned to ensure satisfactory DFIG dynamics [39]. Then in the second experiment, the PV controllers and the SDC are installed to control the DFIG, and the optimal parameter vector **p** is derived by using DE.

The average converging curves of the search process of DE are given in Fig. 5.8. In this case, both K_b and F_m are chosen to be 0.9, and the population size NP is set to 50. It is clear that the objective function can reach zero after about 450 generations of evolution. The optimization results are presented in Table 5.2. When only PV controllers are installed, the tuned parameters are given in this table as well.
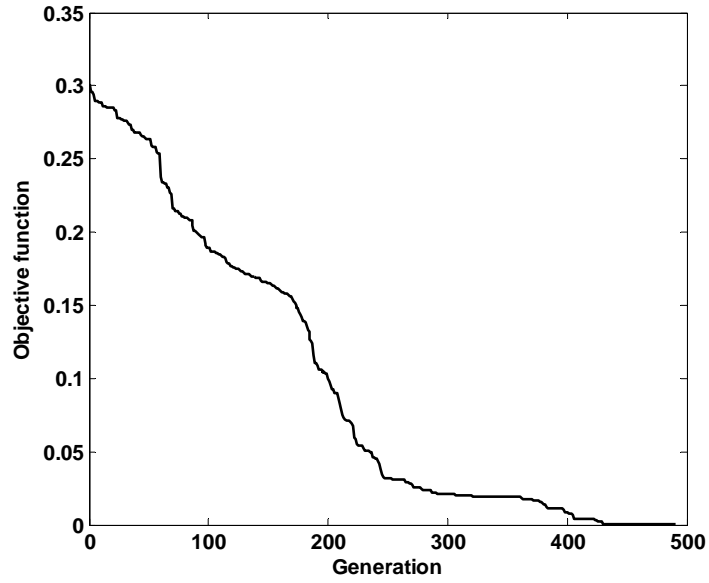
Fig. 5.8. Objective function converging curves of DE.

TABEL 5.2 CONTROLLER PARAMETERS

	k_{pp}	k_{pi}	k_{vp}	k_{vi}	k_{mp}	k_{mi}
PV+SDC	2.8815	0.2955	0.0297	2.2012	0.0014	0.1187
PV	0.6527	0.5043	0.8832	0.4155	0.0083	0.0223
Range	[0,5]	[0,5]	[0,5]	[0,5]	[0,5]	[0,5]

k_{ap}	k_{ai}	k_{pss}	T_1	T_2	T_3	T_4
0.2541	3.4238	0.9968	0.9962	0.9965	0.0530	0.0952
0.9833	0.6997	-	-	-	-	-
[0,5]	[0,5]	[0,1]	[0,1]	[0,1]	[0,1]	[0,1]

Distribution of partial eigenvalues for the two experiments is shown in Fig. 5.9. It is rather obvious that when there are only PV controllers for the DFIG, the inter-area oscillation is poorly damped. In contrast, the coordinatedly tuned PV controllers and SDC can move all eigenvalues to the desired region.

To further demonstrate the effectiveness of the employed optimal control design, numerical simulations are conducted. A three-phase fault takes place at bus 9 at 1.0s and it is cleared 50ms later. The relative power angle dynamics of the synchronous generators are illustrated in Fig. 5.10. It is seen that the system can settle down much faster in the case with optimal PV controllers and SDC than with only PV controllers. This can be further confirmed by generators'

active power output as shown in Fig. 5.11. This implies that the PV controllers and the SDC equipped in the DFIG can work cooperatively to damp the inter-area oscillation.
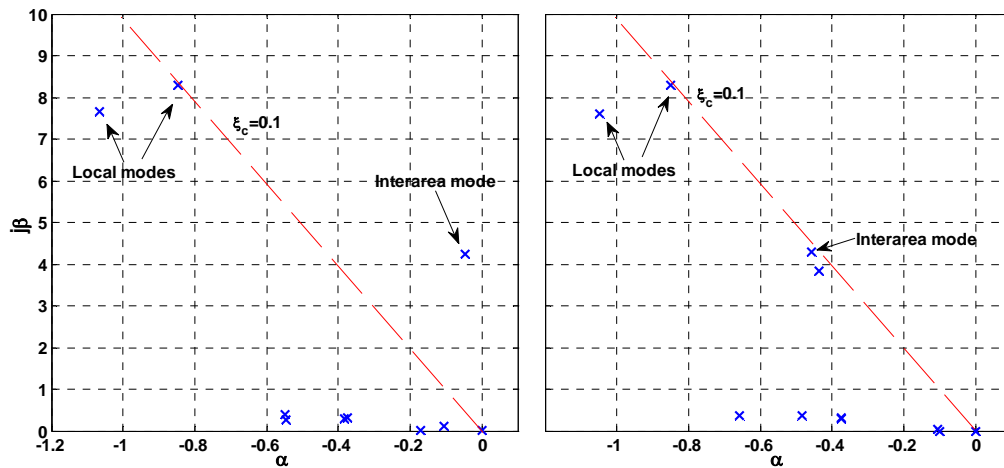
Fig. 5.9. Distribution of partial eigenvalues (left plot: no SDC; right plot: optimal PV controllers and SDC).
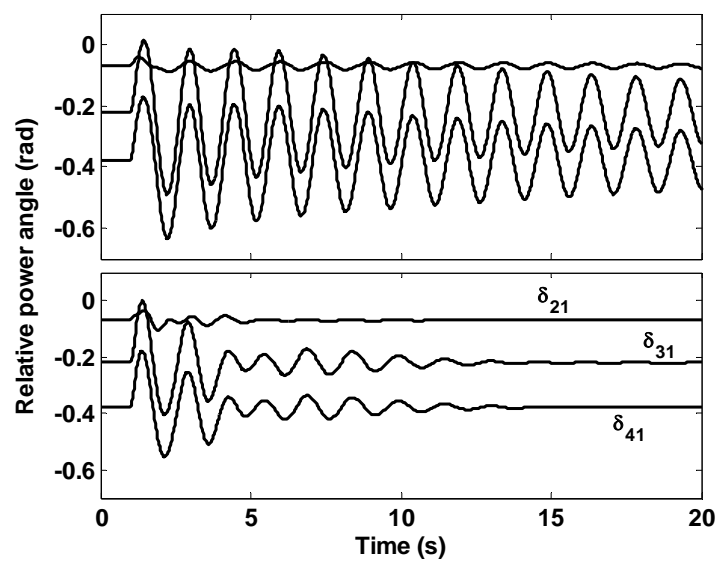
Fig. 5.10. Relative power angle oscillation curves (upper plot: no SDC; lower plot: optimal PV controllers and SDC).

Apparently, it is seen from Fig. 5.11 that the active power output of DFIG with PV controllers and SDC is a little more fluctuant than that of DFIG with only PV controllers, at the initial stage after disturbance. This means damping

control is achieved via DFIG's active power modulation. However, this fluctuation can disappear rather quickly because of the sufficient damping of the system.
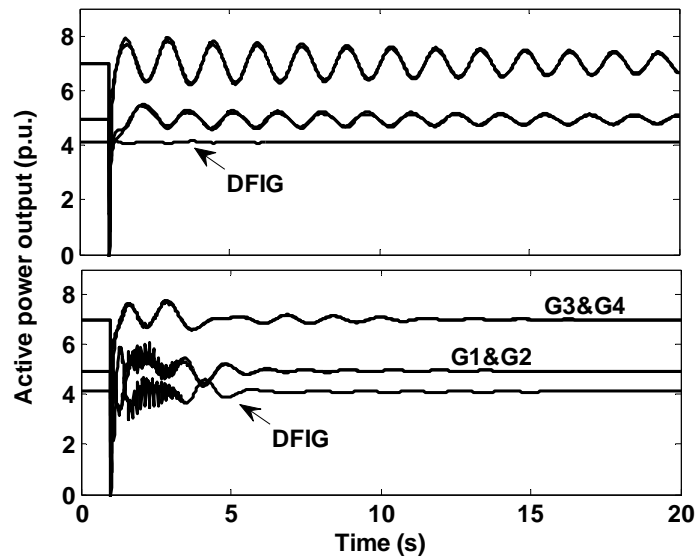
Fig. 5.11. Generator power oscillation curves (upper plot: no SDC; lower plot: optimal PV controllers and SDC).

Dynamics of DFIG rotor voltage magnitude, rotor speed and stator voltage magnitude are depicted in Fig. 5.12. It is easily found from the plot of rotor voltage magnitude that much more control efforts have been generated by the PV controllers and the SDC to drive the DFIG so as to help increase the damping of the system, compared to those when only PV control is implemented for the DFIG. Nevertheless, such large control effort will very likely deteriorate the dynamic performance of the DFIG. Actually, this is confirmed by the further observation that the rotor speed and the stator voltage magnitude oscillate fiercely at the beginning, when the DFIG is controlled by the PV controllers and the SDC. Therefore, it can be concluded that the DFIG has to sacrifice its dynamic performance when it is employed for providing additional damping to the system. However as mentioned before, these dynamics caused by the

presence of these controllers can vanish quite fast due to the increased damping
of the system.
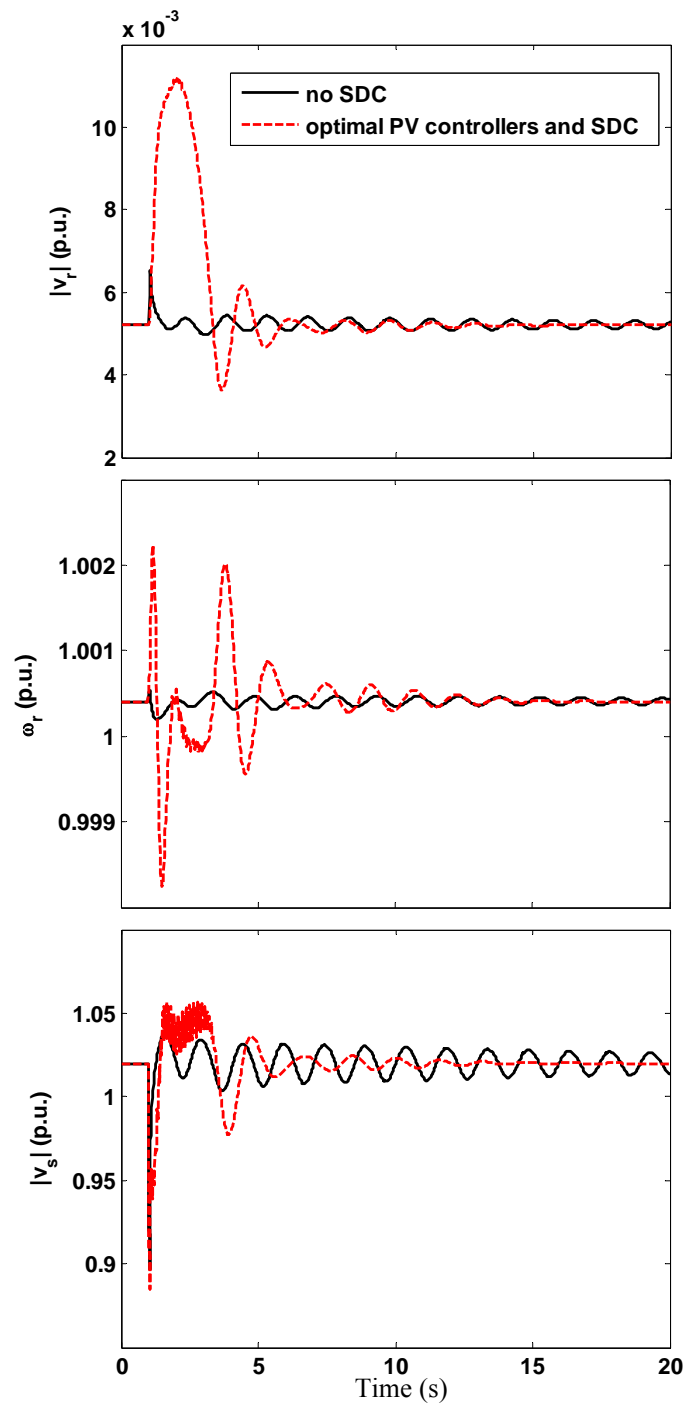
Fig. 5.12. Partial dynamics of DFIG (upper plot: rotor voltage magnitude; middle plot: rotor
speed; lower plot: stator voltage magnitude).

5.6 Summary

In this chapter, simultaneous tuning of PV controllers and the SDC for the DFIG has been performed to increase the damping of the system in a high wind power penetration scenario. The classic FMAC method has been employed for PV control. Furthermore a SDC has been added to work in coordination with PV controllers to damp the inter-area oscillation of the system. Simultaneous tuning of parameters of these controllers is accomplished by using DE. The simulation results on a two-area system demonstrate the effectiveness of the proposed control scheme.

Chapter 6

Optimal Coordination of Active and Reactive Power Modulation of DFIG-Based WTG to Damp Inter-Area Oscillations

6.1 Introduction

It has been solidly corroborated by the works conducted in Chapter 5 that DFIG-based WTGs can be employed to damp inter-area oscillations. Actually, as early as in 2006, Reference [44] already formally proposed the concept of PSS specifically for a wind turbine employing DFIG to damp electromechanical oscillations. Such PSS employed a conventional structure used by the PSSs for synchronous generators, producing an auxiliary damping signal added to the control input of rotor voltage phase angle. The phase compensation technique was utilized to tune the PSS. In this context, Reference [149] further investigated the impacts of tower shadow and wind turbulence on performance of the PSS when stator power, rotor speed of the DFIG and grid frequency were employed as the control input of the PSS, respectively. It was shown that the tower shadow deteriorated performance of the rotor speed based PSS but enforced little effect on the other two, and the influence caused by the wind turbulence was almost trivial. Furthermore, by using the partial eigenstructure assignment technique, the

active damping controller for DFIG in [52] is devised in cooperation with the PSSs (for the synchronous generators) to mitigate torsional as well as electromechanical oscillations.

As the basis of the supplementary damping control, the power and voltage control of the DFIG in [44, 52, 149] is implemented via the FMAC scheme. Nevertheless, it has been verified in [150] that there is a strong coupling between the voltage control loop and the power control loop which weakens robustness of the controllers and makes the controller design more difficult. In fact, the majority of power and voltage control schemes for DFIG including the commercial products are based on stator voltage oriented vector control which comprises well decoupled active and reactive power control loops [151-153]. Accordingly, taking advantage of the vector control, Reference [46] adds the auxiliary damping signal produced by a SDC to the power reference of the active power control loop to modulate active power output of the DFIG to suppress the inter-area oscillation. Although the SDC is acceptably tuned by the classic root locus method, a washout block that is necessary to avoid influences of the SDC on the power outputs of DFIG at the steady state is not included in [46]. In contrast, similar works are carried out in [47] with the main exception that the damping signal is added to the reactive power reference so that reactive power output of the DFIG is modulated. Afterwards, by using a two-mass shaft model instead of the one-mass shaft model used in [46] where no torsional mode exists, Reference [51] presents a systematic comparison of these two types of power modulation methods on their effectiveness in damping inter-area oscillations and their interaction with wind turbine's shaft dynamics. It is found that although both modulation methods can effectively enhance the damping of inter-area

modes, the active power modulation (PM) has the risk of adversely interacting with the shaft dynamics but imposes little impact on the stator voltage, whereas the reactive power modulation (QM) is naturally immune to such interaction but significantly worsens the stator voltage dynamics. Hence, Reference [154] presents the proposal of hybrid modulation of active and reactive power of DFIG for damping control. Furthermore, optimization techniques have also revealed considerable perspective in design of damping controllers for DFIGs [74, 155, 156]. For example, Reference [148] introduces an evolutionary particle swarm optimization algorithm to design robust damping controllers for DFIGs under multiple operating conditions.

As discussed in Chapter 1, unlike the FACTS devices, the DFIG cannot be modeled as a static or quasi-static device when it participates in control of electromechanical dynamics, at least the shaft dynamics should be preserved in the simplified model [157]. Even though above mentioned literatures have successfully applied the DFIGs to damp inter-area oscillations, they commonly overlook to confront a problem, as shown in Chapter 5 that the DFIGs need to sacrifice the dynamic performance for the engagement in damping control. In fact, this phenomenon can be clearly observed in [44, 46, 47, 51, 74, 149]. On the other hand, the dynamics of DFIGs without SDC generally rarely interacts with the external electromechanical dynamics. Therefore, these indicate that there is a trade-off for DFIG between damping control and dynamic performance. From another point of view, it should be feasible that the damping control capability of the DFIG is moderately exploited by the SDC so as to just provide required additional damping to the inter-area mode. In such situation, besides to drive the DFIG to supply desired damping, there is still extra freedom for the design of the

SDC to optimize the DFIG dynamics.

Based on a dual-channel SDC, PM and QM will be coordinated for DFIG to damp inter-area oscillations in this chapter. Moreover, because DFIG dynamics are strongly coupled with its active and reactive power outputs, the control efforts of PM and QM which are measured by eigenstructure-based indexes during the damping control process will also be optimized. Thus, the DFIG dynamics in such case will be significantly improved, compared to those in the case that PM and QM are just simply coordinated. Specifically, a revised version of IAMO-PS which has been introduced in Chapter 4, will be utilized to tune the SDC which are able to simultaneously control the inter-area mode and result in optimal DFIG dynamics.

This chapter is organized as follows. Firstly, the stator voltage oriented vector control scheme which is used for design of the power and voltage controllers for DFIG will be briefly introduced. Subsequently, since DFIG dynamics are the investigated objective in this study, the models that describe these dynamics will be presented. A classic two-area system is then employed to show the process for optimally coordinate PM and QM of DFIG to damp inter-area oscillations. The simulation results and discussion are presented at the final stage.

6.2 Stator Voltage Oriented Vector Control

The advantage of the stator voltage oriented vector control is that the electrical torque and the stator reactive power can be managed in an almost decoupled manner by controlling the q-axis and d-axis rotor currents, respectively. However, for this control scheme, the q-axis of the synchronously rotating d-q reference frame should be aligned in the direction of the stator

voltage so that $v_{ds}=0$ and $v_{qs}=v_s$ (It should be noted that the same symbols appeared in this chapter and Chapter 5 have the same meaning, if not specified). The phase locked loop which is able to rapidly track the direction of the rotor voltage is normally employed to perform the orientation task.

In general, the stator resistance of an induction generator is much smaller than the stator leakage reactance and the magnetizing reactance. Thus, by neglecting the term associated with stator resistance in (5.1), the following equation is derived:

$$v_{ds} = \omega_s L_{ss} i_{qs} - \omega_s L_m i_{qr} \tag{6.1}$$

Then, under the condition of $v_{ds}=0$, the q-axis stator current can be expressed in terms of the q-axis rotor current as follows:

$$i_{qs} = \frac{i_{qr} L_m}{L_{ss}} \tag{6.2}$$

Similarly, the d-axis stator current can be represented by the d-axis rotor current by neglecting the stator resistance and applying $v_{qs}=v_s$ in (5.2), as follows:

$$i_{ds} = -\frac{v_s}{\omega_s L_{ss}} + \frac{L_m}{L_{ss}} i_{dr} \tag{6.3}$$

Moreover, the general expression for the electrical torque T_e is as follows:

$$T_e = L_m \left(i_{dr} i_{qs} - i_{qr} i_{ds} \right) \tag{6.4}$$

Then, substituting (6.2) and (6.3) into (6.4) yields,

$$T_e = \frac{v_s L_m}{\omega_s L_{ss}} i_{qr} \tag{6.5}$$

Generally, in any d-q reference frame the stator reactive power output Q_{sg} can be calculated as follows:

$$Q_{sg} = v_{qs} i_{ds} - v_{ds} i_{qs} \tag{6.6}$$

In particular, with consideration of $v_{ds}=0$ and $v_{qs}=v_s$, and substitution of (6.3) for i_{qs} in (6.6), the following equation is obtained:

$$Q_{sg} = -\frac{v_s^2}{\omega_s L_{ss}} + \frac{L_m v_s}{L_{ss}} i_{dr} \tag{6.7}$$

Obviously, given a constant stator voltage v_s, it is observed from (6.5) and (6.7) that T_e and Q_{sg} are in linear relationship with i_{qr} and i_{dr}, respectively, in the stator voltage oriented vector control scheme. Therefore, through manipulation of d and q components of the rotor current, the terminal voltage and active power output of the DFIG can be flexibly and independently controlled.

6.3 General Model of DFIG-based WTG

The WTG is complicated equipment which is concerned with mechanics, electrics and magnetics. It is definitely unnecessary to model all dynamics of the equipment in full time scale when only electromechanical dynamics are the focus [158]. As done in Chapter 5, various simplified models have been utilized to describe the dynamics of DFIG-based WTGs [45, 157, 159-163]. For example, Reference [146] ignores the dynamics of the rotor and its current control loops and models the rotor circuit as a controlled current source. Nevertheless, unlike the situation in Chapter 5 where a simplified WTG model can be used because it mainly concerns the impacts of the WTG on electromechanical dynamics of the system and intends to show the damping control function of WTG, a more detailed model describing WTG dynamics should be utilized in this chapter which focuses on dynamics of both WTG and system as well as their interactions. Actually, a more general model with proper descriptions of rotor dynamics for the DFIG-based WTG has been employed in studies of electromechanical

transient [39, 46, 47, 51, 155, 156, 159, 164, 165]. Therefore, without loss of generality, this chapter continues to use this model for demonstration. Fig. 6.1 shows a WTG with DFIG whose components are introduced in the following subsections.
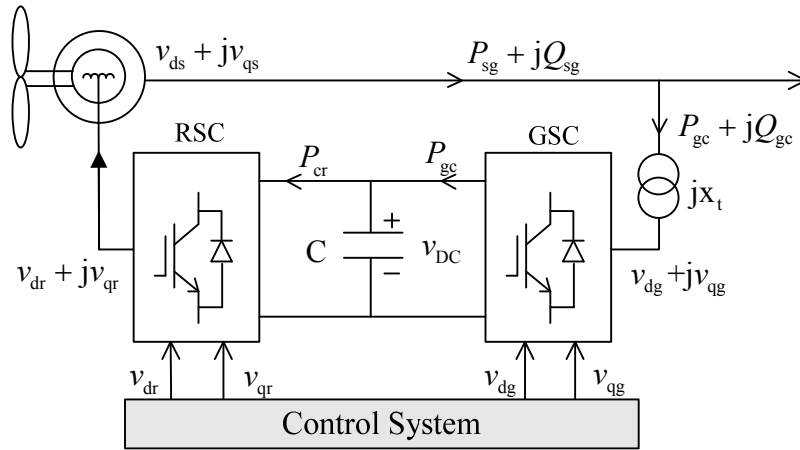
Fig. 6.1. Detailed structure of a DFIG-based WTG

6.3.1 Drive Train Model

The mechanical system of the WTG mainly consists of the generator rotor, turbine shaft, gear box, and blades. Generally, there are two major mechanical modes in this system. One corresponds to the oscillation of the blades with respect to the hub where they are mounted. This mode arises due to the fact that the blades are not rigid and could be bended. Another mode depicts the torsional motion between the generator rotor and the turbine shaft which are connected via the gear box. The frequency of this torsional mode greatly depends on the stiffness and mass of the whole shaft. In general, the presence of the gear box makes the shaft more slender and reduces the shaft stiffness. Moreover, increased individual wind turbine capacity leads to use of turbine shaft with quite large mass, which also augments the distinction in mass between the turbine shaft and the generator rotor. As a result, the frequency of the torsional mode is rather low

and well within the bandwidth that is normally considered in power system dynamic analysis (0.1-10 Hz).

Except for some special researches that need to use a three-mass drive train model to take into account the bending flexibility and the torsional flexibility, most literatures employs a two-mass model to capture the concerned torsional dynamics because the mode associated the blade-hub system is generally well damped and out of the frequency range of interest as well. Thus, the two-mass drive train model is used in this chapter as follows:

$$\frac{\mathrm{d}\theta_{\mathrm{tw}}}{\mathrm{d}t} = \omega_{\mathrm{b}}\left(\omega_{\mathrm{t}} - \omega_{\mathrm{r}}\right) \tag{6.8}$$

$$\frac{\mathrm{d}\omega_{\mathrm{t}}}{\mathrm{d}t} = \frac{1}{2\mathrm{H}_{\mathrm{t}}}\left[T_{\mathrm{m}} - \mathrm{K}_{\mathrm{tw}}\theta_{\mathrm{tw}} - \mathrm{D}_{\mathrm{tw}}\left(\omega_{\mathrm{t}} - \omega_{\mathrm{r}}\right)\right] \tag{6.9}$$

$$\frac{\mathrm{d}\omega_{\mathrm{r}}}{\mathrm{d}t} = \frac{1}{2\mathrm{H}_{\mathrm{g}}}\left[\mathrm{K}_{\mathrm{tw}}\theta_{\mathrm{tw}} + \mathrm{D}_{\mathrm{tw}}\left(\omega_{\mathrm{t}} - \omega_{\mathrm{r}}\right) - T_{\mathrm{e}}\right] \tag{6.10}$$

where ω_{t} is the turbine speed; θ_{tw} (rad) is the shaft twist angle; K_{tw} (p.u./rad) and D_{tw} are the shaft stiffness and mechanical damping coefficients, respectively; H_{t} (s) and H_{g} (s) are the wind turbine and generator inertia constants, respectively.

6.3.2 DFIG Model

In power system electromechanical transient simulations, the fast stator dynamics of induction generators are normally neglected to ensure compatibility with the models representing other system components, particularly the transmission network. Therefore, the model describing the dynamics of DFIG is given as follows:

$$\frac{1}{\omega_{\mathrm{b}}}\frac{\mathrm{d}e_{\mathrm{d}}}{\mathrm{d}t} = -\frac{1}{\mathrm{T}_{0}}\left[e_{\mathrm{d}} - \left(\mathrm{X} - \mathrm{X}'\right)i_{\mathrm{qs}}\right] + s\omega_{\mathrm{s}}e_{\mathrm{q}} - \omega_{\mathrm{s}}\frac{\mathrm{L}_{\mathrm{m}}}{\mathrm{L}_{\mathrm{r}} + \mathrm{L}_{\mathrm{m}}}v_{\mathrm{qr}} \tag{6.11}$$

$$\frac{1}{\omega_b}\frac{de_q}{dt} = -\frac{1}{T_0}\left[e_q + \left(X - X'\right)i_{ds}\right] - s\omega_s e_d + \omega_s \frac{L_m}{L_r + L_m}v_{dr} \qquad (6.12)$$

$$v_{ds} = -r_s i_{ds} + X' i_{qs} + e_d \qquad (6.13)$$

$$v_{qs} = -r_s i_{qs} - X' i_{ds} + e_q \qquad (6.14)$$

$$i_{dr} = \frac{1}{\omega_s L_m}e_q + \frac{L_m}{L_r + L_m}i_{ds} \qquad (6.15)$$

$$i_{qr} = \frac{-1}{\omega_s L_m}e_d + \frac{L_m}{L_r + L_m}i_{qs} \qquad (6.16)$$

As shown in Fig. 6.1, the stator active power output P_{sg} and reactive power output Q_{sg} are calculated as follows:

$$P_{sg} = v_{ds}i_{ds} + v_{qs}i_{qs} \qquad (6.17)$$

$$Q_{sg} = v_{qs}i_{ds} - v_{ds}i_{qs} \qquad (6.18)$$

6.3.3   Models of Converters and DC Capacitor

The dynamics of the dc capacitor between the RSC and GSC are described by the following equation:

$$\frac{dv_{dc}}{dt} = \frac{1}{C}\left(\frac{P_{gc} - P_{cr}}{v_{dc}}\right) \qquad (6.19)$$

where v_{dc} is the voltage across the dc link; C (s) is the capacitance; P_{cr} is the power delivered from the dc capacitor to the RSC, while P_{gc} is the power injected to the dc capacitor from the GSC. In this study, the RSC and GSC are modeled as lossless devices so that P_{cr} is equal to the active power injected to the rotor and P_{gc} is equal to the active power exchanged between the GSC and the external network through a transformer shown in Fig. 6.1. Thereby, P_{cr} and P_{gc} can be calculated as follows:

$$P_{cr} = v_{dr}i_{dr} + v_{qr}i_{qr} \tag{6.20}$$

$$P_{gc} = \frac{v_{qs}v_{dg} - v_{ds}v_{qg}}{x_t} \tag{6.21}$$

where v_{dg} and v_{qg} are the d and q components, respectively, of the GSC voltage; x_t is the reactance of the transformer. Moreover, the reactive power Q_{gc} absorbed from the external network is given as follows:

$$Q_{gc} = \frac{v_{ds}^2 + v_{qs}^2 - v_{ds}v_{dg} - v_{qs}v_{qg}}{x_t} \tag{6.22}$$

The switching dynamics of the power electronic converters are much faster than the concerned dynamics in the stability studies. Thus, the RSC and GSC are in general modeled as static devices which can instantaneously change the output in response to the control input.

6.3.4 Power and Voltage Control Systems

According to the principle introduced in Section 6.2, the management of power and voltage of the DFIG is accomplished through implementation of the stator voltage oriented vector control on the RSC. The Block diagrams of the RSC controllers are shown in Fig. 6.2 where u_p and u_q are the supplementary damping signals added to the power and voltage control loops, respectively.

The GSC controllers take responsibilities to maintain the voltage of the dc capacitor as well as to make sure no reactive power injected into (or absorbed from) external network by the GSC in this study. From (6.21) and (6.22) it is deduced that P_{gc} and Q_{gc} can be independently controlled by v_{dg} and v_{qg}, respectively, in the stator voltage oriented vector control scheme. Moreover, it is known from (6.19) that increasing P_{gc} will raise the voltage of the dc capacitor, and vice versa. Thus, the GSC controllers are designed as shown in Fig. 6.3.
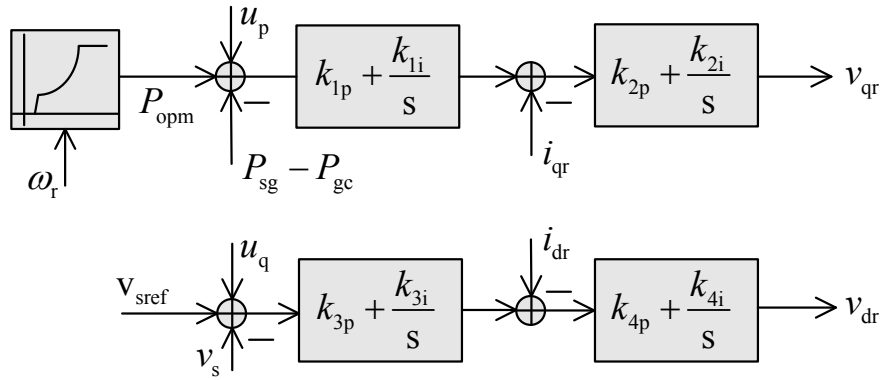
Fig. 6.2. Block diagram of RSC controllers
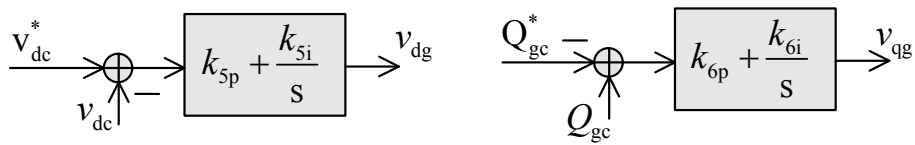
Fig. 6.3. Block diagram of GSC controllers

6.4 Optimal Coordination of PM and QM of DFIG

6.4.1 Investigated System

The two-area system with the same configuration (Fig. 5.1) as that used in Chapter 5 will be employed in this chapter for demonstration of optimally coordinating PM and QM of DFIG to damp inter-area oscillations. Except for the WTG, all other system components as well as the steady state operating condition are the same as those used in Chapter 5. The DFIG-based WTG used in this system is represented by the model described in Section 6.3 and its data are given in Table 6.1. As normal, the RSC and GSC controllers are tuned in advance to ensure the control performance for management of the power and voltage of the DFIG. Actually, several effective PID controller tuning methods can be utilized [46, 162, 166], and the tuned parameters are presented in Table 6.2. Subsequently, small signal stability analysis shows that besides the two adequately damped local modes, a 0.68 Hz poorly damped inter-area mode

115

resides in this system as well. Therefore, to increase the damping of this mode, the DFIG is equipped with a dual-channel SDC which is introduced in the following subsection.

TABLE 6.1 PARAMETERS OF DFIG-BASED WTG (POWER RATING: 700MVA)

r_s	r_r	x_s	x_r	x_m	H_g
0.00488	0.00590	0.09241	0.09955	3.95379	0.4

H_t	K_{tw}	D_{tw}	x_t	C
3.8	0.6	0.45	0.0550	0.0410

TABLE 6.2 PARAMETERS OF RSC AND GSC CONTROLLERS

k_{1p}	k_{1i}	k_{2p}	k_{2i}	k_{3p}	k_{3i}
0.6742	0.9252	0.0588	0.7857	0.8492	0.8640

k_{4p}	k_{4i}	k_{5p}	k_{5i}	k_{6p}	k_{6i}
0.1744	0.6829	0.0124	0.0297	0.4270	0.5156

6.4.2 Dual-Channel SDC

Since the active and reactive power controls are nearly decoupled in the vector control scheme, it has been observed in [46] and [47] that the SDC attached to the power control loop of the DFIG mainly impacts its active power output while the SDC installed in the voltage control loop principally influences the reactive power output. Therefore, in order to make utilization of both PM and QM of the DFIG for damping control possible, a dual-channel SDC whose structure is illustrated in Fig. 6.4 is proposed. It is seen that the DFIG active and reactive power can be modulated by the controller since both control loops are compensated. Each channel is constituted by a gain and two same phase lead-lag compensation blocks that can supple necessary phase compensation to the inter-area mode. K_p, T_{p1}, T_{p2}, K_q, T_{q1} and T_{q2} are the adjustable parameters. One washout block is shared by the two channels to annihilate the steady-state offset of the control input so that the SDC will have no effect on the steady-state power

and voltage control results.

Remote signals which have a quite high visibility of inter-area modes are generally much more effective control inputs for damping controllers installed in DFIGs than local signals [167]. In the investigated system, the power angle difference between Generator 1 and 3 is the most direct and effective signal to observe the inter-area mode, and thus it is selected as control input of the SDC. Specifically, time delays introduced by usage of the remote signal are ignored since they could be dealt with by many techniques in practice which will seldom challenge the demonstration theme of this study [46, 47, 51].
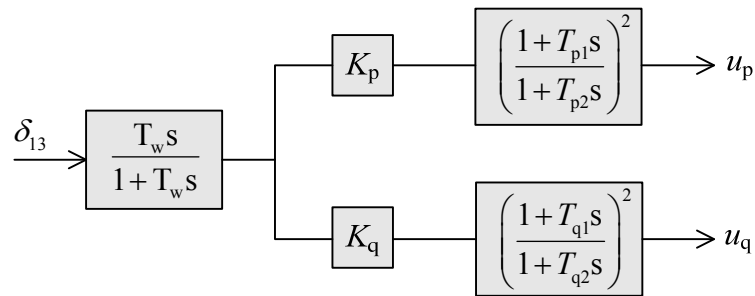
Fig. 6.4. Dual-channel SDC

6.4.3   Measurements of PM and QM Control Efforts

By support from the dual-channel structure of the SDC, it is possible to flexibly allocate control burden between PM and QM of the DFIG for damping the inter-area oscillation. However, to do this, the premise is the availability of indexes that can effectively indicate the control efforts of PM and QM during the transient. Therefore, inspired by the studies carried out in Chapter 1 and 2, the eigenstructure-base indexes are proposed to perform measurements of PM and QM control efforts.

The linearized closed loop system incorporating the SDC around the operating point can be described by the following equations:

$$\dot{\mathbf{x}} = \mathbf{A}\mathbf{x} \tag{6.23}$$

$$P_{\mathrm{g}} = \mathbf{E}_{\mathrm{p}}\mathbf{x} \tag{6.24}$$

$$Q_{\mathrm{g}} = \mathbf{E}_{\mathrm{q}}\mathbf{x} \tag{6.25}$$

where $\mathbf{x}$ is the state vector of the closed loop system; $\mathbf{A}$ is the state matrix; P_{g} and Q_{g} are the deviations of the DFIG active and reactive power outputs, respectively, from the equilibrium point; and $\mathbf{E}_{\mathrm{p}}$ and $\mathbf{E}_{\mathrm{q}}$ are the corresponding output matrices. Thus, in the normal case that $\mathbf{A}$ can be similarly diagonalized and the closed loop system is stable, the index f_{p} measuring the PM control effort is defined as follows:

$$f_{\mathrm{p}} = \sum_{k=1}^{n} \sigma_{\mathrm{p}k} \tag{6.26}$$

where n is the dimension of the closed loop system. $\sigma_{\mathrm{p}k}$ is the kth eigenvalue of the cost matrix $\mathbf{M}_{\mathrm{p}}$ which is constructed as follows:

$$\mathbf{M}_{\mathrm{p}} = \mathbf{V}^{\mathrm{H}}\left[\left(\mathbf{U}^{\mathrm{H}}\mathbf{E}_{\mathrm{p}}^{\mathrm{H}}\mathbf{E}_{\mathrm{p}}\mathbf{U}\right)\cdot\mathbf{L}\right]\mathbf{V} \tag{6.27}$$

where $\mathbf{U}$ and $\mathbf{V}$ are right and left eigenvector matrices, respectively, of $\mathbf{A}$; H is the conjugate transpose operator, while $\cdot$ denotes dot production; and $\mathbf{L}$ is an n×n Hermite matrix, whose entry in the position of iith row, jjth column is defined as,

$$L(ii, jj) = -\frac{1}{\lambda_{ii}^{*} + \lambda_{jj}} \tag{6.28}$$

where * is the conjugate operator; λ_{ii} is the iith eigenvalue of $\mathbf{A}$. The deduction process of f_{p} can be similarly derived according to Equations (3.4)-(3.14) presented in Chapter 3. It is known from the deduction process that f_{p} is derived from the time domain cost function $cost_{\mathrm{p}}$ defined in the following and can perform resembling it to indicate the control effort of PM of the DFIG:

$$cost_{\mathrm{p}} = \int_0^{\infty} P_{\mathrm{g}}^2 \mathrm{d}t \qquad\qquad (6.29)$$

Obviously, the advantage of f_{p} over $cost_{\mathrm{p}}$ is that the former is independent to the initial state of the system which is required by calculation of the latter. It is clear that the system initial state which is related to the disturbance is actually undetermined. Thus, it will be ineffective to directly apply $cost_{\mathrm{p}}$ to the design of the controller, whereas use of f_{p} can satisfactorily overcome this problem since it depends only on the eigenstructure of the closed loop system.

Similar to the definition of f_{p}, an eigenstructure-based index f_{q} is defined to measure the control effort of QM of the DFIG. All above discussion is applicable to f_{q} only with proper substitutions, for example, using $\mathbf{E}_{\mathrm{q}}$ to replace $\mathbf{E}_{\mathrm{p}}$.

6.4.4 Tuning Method for the SDC and Interpretation

The tuning method used in this chapter will refer to the method of IAMO-PS introduced in Chapter 4. A derivative version of IAMO-PS with coordination of PM and QM of the DFIG will be employed for tuning of the SDC. Likewise, the tuning method is formulated as a two-stage mathematical programming problem in which the optimization in the first stage serves to offer a starting point for the optimization in the second stage. Physically, the SDC is tuned in the first stage to move all closed loop poles to fulfill the specific pole placement requirements. Then, subjected to constraints of such pole placement, the SDC is further tuned in the second stage so that the coordination of PM and QM is optimized.

In the first stage, the inter-area mode is moved to the specific region that indicates acceptable dynamics of the inter-area oscillation by solving a minimization problem as follows:

$$\min_{\mathbf{p}} \; \left(\alpha_{\mathrm{io}} - \alpha_{\mathrm{exp}} \right)^2 \qquad\qquad (6.30a)$$

s. t. $\alpha_{iomin} \le \alpha_{io}$ (6.30b)

$\omega_{iomin} \le \omega_{io} \le \omega_{iomax}$ (6.30c)

$\alpha_j \le \alpha_{jc} \qquad \lambda_j \in \pi_{c2}$ (6.30d)

$\omega_{jmin} \le \omega_j \le \omega_{jmax}$ (6.30e)

$\mathbf{p}_{min} \le \mathbf{p} \le \mathbf{p}_{max}$ (6.30f)

where α_{io} and ω_{io} is the real and imaginary parts, respectively, of the inter-area mode; α_{iomin} is the lower limit of α_{io} to prevent from exploiting too much control effort of the DFIG and it is set to -0.5; α_{exp} is the expected value of α_{io} and it is selected to be -0.42; ω_{iomin} and ω_{iomax} are the lower and upper limits, respectively, of ω_{io} to avoid unexpected frequency drift; π_{c2} is the set consisting of modes such as λ_j, that may be significantly deteriorated after the optimization; α_j and ω_j are the real and imaginary parts, respectively, of λ_j; α_{jc} is the critical value of α_j, while ω_{jmin} and ω_{jmax} are the lower and upper limits, respectively, of ω_j; and $\mathbf{p}$ is the tunable controller parameters defined as follows:

$$\mathbf{p} = \left[K_p, T_{p1}, T_{p2}, K_q, T_{q1}, T_{q2} \right]^T$$ (6.31)

To ensure that λ_j is not obviously exacerbated by the SDC, α_{jc} is set to be slightly larger than the initial value of α_j which is obtained when the system is open loop. Similarly, ω_{jmin} and ω_{jmax} are chosen to be properly smaller and larger, respectively, than the initial value of ω_j. In particular, the same iterative process as that used in Chapter 4 will be employed to determine π_{c2}.

The optimization problem (6.30) will be solved by the SQP method for which a feasible starting point can be readily provided to enhance its reliability in convergence by setting K_p and K_q to zeros. Furthermore, if the final solution can

120

ensure that the settling time of the inter-area oscillation is less than a required value, i.e. $\alpha_{io} \leq \alpha_{iomax}$, then it can be used as the starting point for the optimization to coordinate PM and QM in the second stage, as follows:

$$\min_{\mathbf{p}} \ \mathrm{w}_p f_p + \mathrm{w}_q f_q \tag{6.32a}$$

$$\text{s. t. } \alpha_{iomin} \leq \alpha_{io} \leq \alpha_{iomax} \tag{6.32b}$$

$$\omega_{iomin} \leq \omega_{io} \leq \omega_{iomax} \tag{6.32c}$$

$$\alpha_j \leq \alpha_{jc} \qquad \lambda_j \in \pi_{c1} \tag{6.32d}$$

$$\omega_{jmin} \leq \omega_j \leq \omega_{jmax} \tag{6.32e}$$

$$\mathbf{p}_{min} \leq \mathbf{p} \leq \mathbf{p}_{max} \tag{6.32f}$$

where w_p and w_q are the weights of f_p and f_q, respectively; π_{c1} has the same meaning as π_{c2} and is initially equal to final π_{c2}. Moreover, the iterative process used for determining π_{c2} is also applicable to π_{c1}. In this study, α_{iomax} is chosen to be -0.4 since the inter-area oscillation is normally expected to settle down within about 10s. Likewise, the SQP method is used to solve (6.32).

It is known that by only satisfying the constraints (6.32b)-(6.32f), the inter-area mode will be acceptably damped. The frequency drift and impacts on the other modes caused by the SDC can also be considered and limited. Moreover, owing to the dual-channel structure of the SDC, both PM and QM of the DFIG can be utilized in a coordinated manner for the damping function. However, it is clear that the active and reactive power outputs of the DFIG during the transient are not optimized. Thus, the dynamics of the DFIG will not be optimal correspondently because they are tightly coupled with the power outputs. In contrast, by additionally incorporating the objective of (6.32a), the coordinated

PM and QM according to the given w_p and w_q will be further explicitly optimized, leading to the improved DFIG dynamics.

The natures of w_p and w_q are apparent in this study. Larger w_p indicates that the damping function of the DFIG will be more reliant on PM, which tends to bring more impacts to the DFIG dynamics associated with the active power output, for example, the rotor dynamics. On the other hand, QM will be more dominant in controlling the inter-area mode when w_q is quite larger. Consequently, the DFIG dynamics related to the reactive power output such as the rotor voltage will be more obviously influenced. Accordingly, the control efforts of damping the inter-area mode can be flexibly distributed between PM and QM of the DFIG by adjusting w_p and w_q. Nevertheless, it may be naturally expected that all kinds of dynamics can be evenly sacrificed when the DFIG contributes to the damping control. Apparently, such control objective can be readily achieved through appropriate selection of w_p and w_q.

6.5 Simulation Results and Discussions

In order to enhance the quality of final solution, several different starting points will be tried for the optimization to avoid the unacceptable local minimum which is the intrinsic insufficiency of the SQP method. Moreover, P_g and Q_g are normalized respectively so that f_p and f_q will be in the same order of magnitude, which can facilitate the selection of w_p and w_q. Furthermore, according to the aforementioned rules of adjustment for w_p and w_q, it is easily found that the SDC obtained with $w_p=0.8$ and $w_q=1.0$ can fairly and optimally coordinate PM and QM of the DFIG to damp the inter-area mode. As a targeted comparison, the case in which the only objective is to damp the inter-area mode by the coordinated

PM and QM and no optimization of the DFIG dynamics is performed is also studied. In such case, only optimization problem (6.30) is solved with different starting points and among all solutions, the one which results in $\alpha_{io} \leq \alpha_{iomax}$ and relatively fair control efforts between PM and QM will be chosen as the parameters of the SDC. For these two cases, the corresponding SDC parameters are given in Table 6.3.

TABLE 6.3 TUNED PARAMETERS OF SDC

	K_p	T_{p1}	T_{p2}	K_q	T_{q1}	T_{q2}
Coordination	2.4544	0.7504	0.3117	6.7454	0.5861	0.5441
w_p=0.8, w_q=1.0	0.2879	0.9885	0.1646	3.4389	0.0100	0.0749

During the SDC tuning process, besides the inter-area mode, it has to pay special attention to other four modes which have the risk of being significantly altered by the SDC since their frequencies lay within the frequency range of electromechanical dynamics. These modes are listed in Table 6.4 where M_1 is the inter-area mode; M_2 is the torsional mode; M_3 and M_4 are the two local modes; and M_5 is the mode greatly participated by the dc capacitor dynamics. It is seen that in both cases, the inter-area mode has received required damping enhancement with quite limited frequency drift (maximum about 5%). Moreover, M_2 to M_5 are also not considerably changed by the SDC, compared to their open loop values. These indicate that the inter-area oscillation will be acceptably damped by the SDC and the adverse effects of the SDC on the other modes are also well controlled via the explicit constraints imposed on the shifting of these modes in the employed pole placement strategy.

In the case of optimal coordination of PM and QM (w_p=0.8 and w_q=1.0), the evolutions of the inter-area mode and M_2 to M_5 during the searching process are illustrated in Fig. 6.5 and 6.6, respectively. Clearly, the effectiveness and

efficiency of the two-stage optimization based IAMO-PS in tuning the SDC for

the DFIG can be confirmed from these diagrams.

TABLE 6.4 CONCERNED MODES

	Open loop	Coordination	Optimal Coordination
M_1	-0.0629+4.2446i	-0.4199+4.4748i	-0.4000+4.2415i
M_2	-1.8982+11.4654i	-2.0186+11.4981i	-1.9550+11.3964i
M_3	-1.0770+7.6569i	-1.1145+7.5305i	-1.0041+7.6069i
M_4	-0.8471+8.2977i	-0.8396+8.3014i	-0.8441+8.3053i
M_5	-2.9699+21.7083i	-2.9703+21.7074i	-2.9700+21.7073i
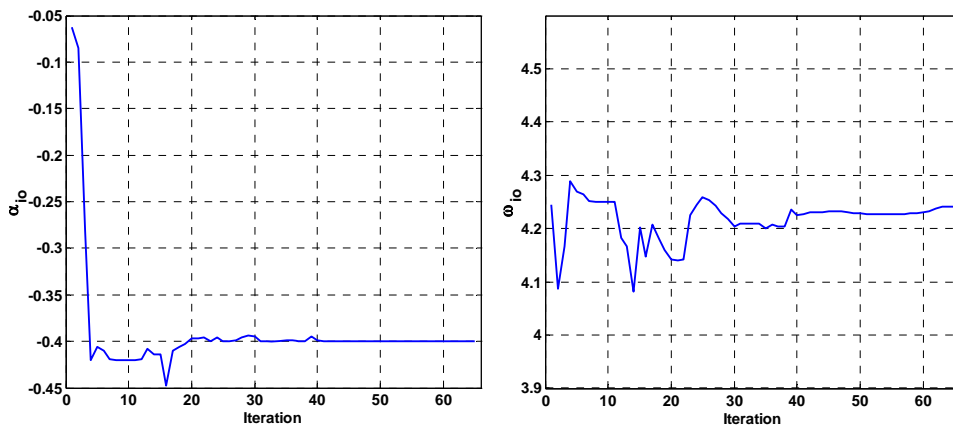
Fig. 6.5. Evolution of the inter-area mode during the searching process (left plot: real part; right plot: imaginary part).
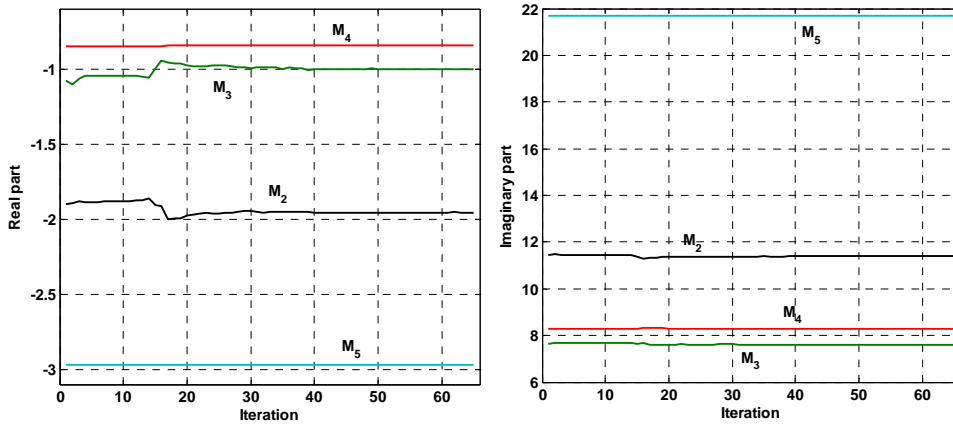
Fig. 6.6. Evolution of the other modes during the searching process (left plot: real part; right plot: imaginary part).

The eigenvalues of $\mathbf{M}_p$ and $\mathbf{M}_q$ in the two cases are calculated and depicted in

Fig. 6.7. Only the first eight eigenvalues are displayed since they are much larger

than the remaining. It is found that the dominant (the first two) eigenvalues of $\mathbf{M}_p$ in the optimal coordination case are markedly smaller than those in the coordination case. The same observation can be found for the first three dominant eigenvalues of $\mathbf{M}_q$. Consequently, according to (6.26), it is inferred that f_p (or f_q) in the optimal coordination case will be much smaller than f_p (or f_q) in the coordination case. This essentially indicates that the power output dynamics of the DFIG in the optimal coordination case will be comparatively better than those in the coordination case.
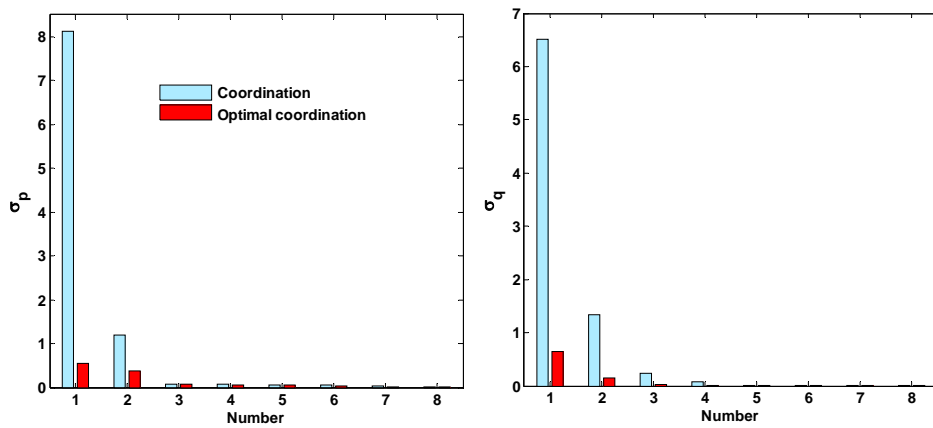
Fig. 6.7. Partial eigenvalues of cost matrices (left plot: $\mathbf{M}_p$; right plot: $\mathbf{M}_q$)

In order to confirm the above inferences, the time domain simulation is conducted. A three-phase short circuit fault occurs at Bus 9 at 1.0s and it is cleared 50ms later. The relative power angles of all synchronous generators are illustrated in Fig. 6.8. It is easily observed that in both cases, the inter-area oscillation can quickly settle down within 10s after the disturbance. From the viewpoint of increasing the damping of the inter-area oscillation, the SDCs used in the two cases have little distinction. Together with the eigen-analysis shown in Table 6.4, it manifests that by only implementing the pole placement strategy irrespective of the DFIG dynamics, as done in many literatures, the SDC can

undoubtedly be satisfactorily tuned to drive the DFIG to provide required damping to the inter-area oscillation. However, by additionally optimizing the power outputs of the DFIG, it is quite clearly observed in Fig. 6.9 that the DFIG dynamics are considerably improved in the optimal coordination case, compared to those in the coordination case. This phenomenon is exactly consistent with the inference drawn from Fig. 6.7, which in turn substantiates the effectiveness of the eigenstructure-based indexes f_p and f_q in measuring the control efforts of PM and QM. Furthermore, comparisons of the DFIG dynamics in the system with the SDC and those in the open loop system again confirm the conclusion that the DFIG will sacrifice its dynamic performance for contribution to the damping control.
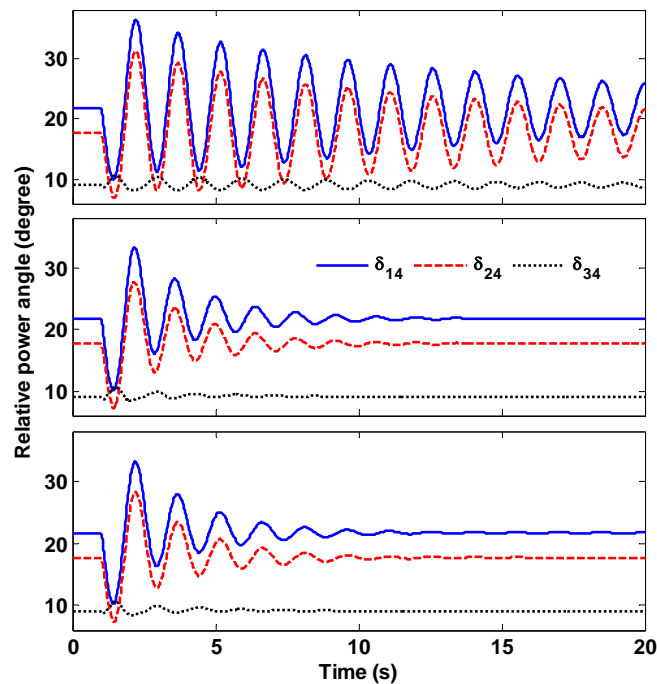
Fig. 6.8. Power angle oscillation curves of all generators with respect to Generator 4 (upper plot: open loop; middle plot: coordination; lower plot: optimal coordination).
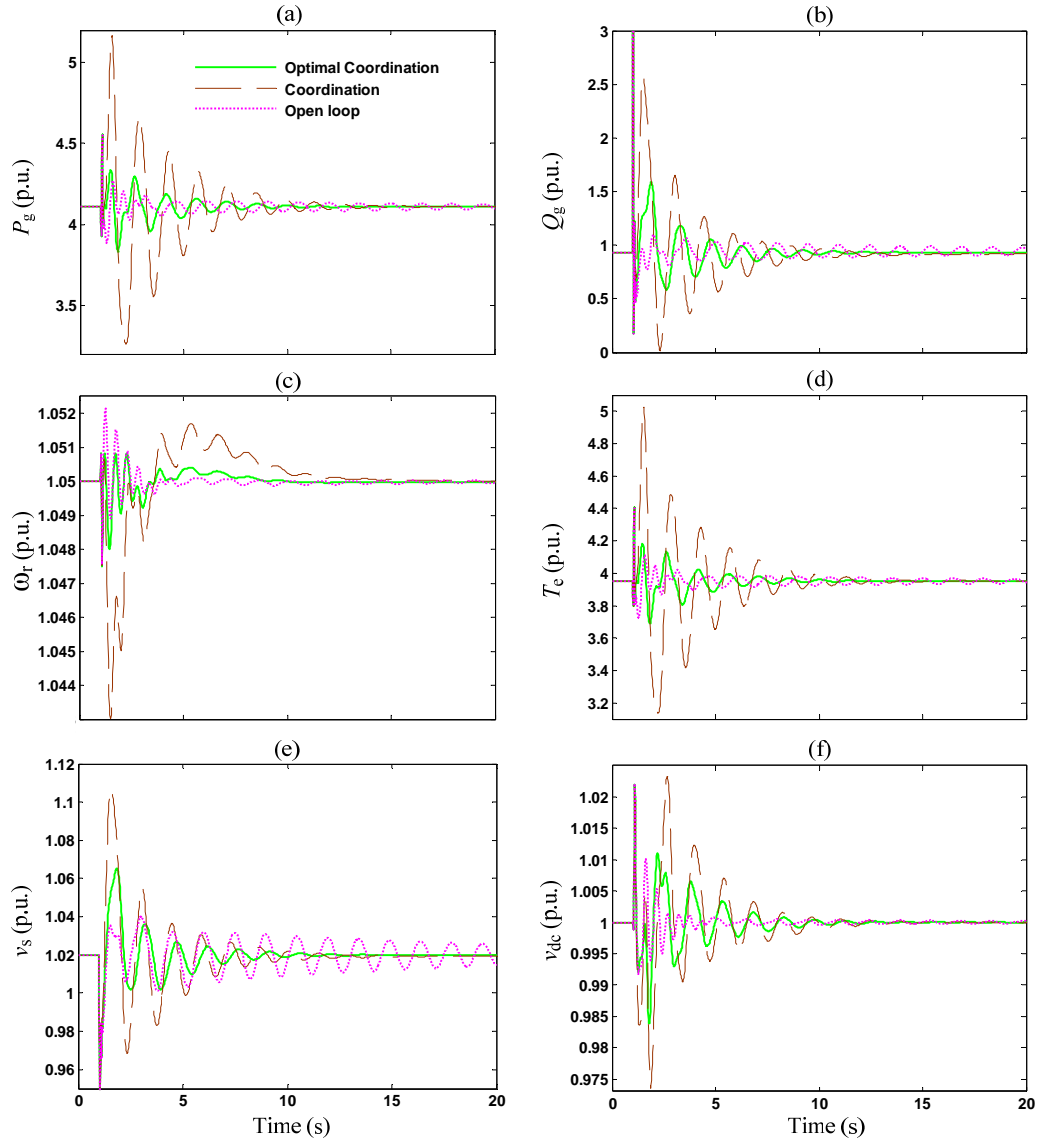
Fig. 6.9. Partial DFIG dynamics ((a) active power output; (b) reactive power output; (c) rotor speed; (d) electrical torque; (e) rotor voltage; (f) dc capacitor voltage).

6.6 Summary

In this chapter, it has been demonstrated in a two-area system that PM and QM of the DFIG can be optimally coordinated to damp the inter-area oscillation. Firstly, the dual-channel SDC is employed for the DFIG to enable coordination of PM and QM. Furthermore, based on the eigenstructure-based indexes which accurately indicate the control efforts of PM and QM, the power outputs of the DFIG during the transient are optimized when it is driven by the SDC to provide

expected damping to the inter-area mode. Therefore, in such case the DFIG dynamics which are tightly associated with the power outputs are significantly improved, compared to those in the case where PM and QM of the DFIG are only coordinated to perform the damping function.

Chapter 7

Conclusion and Future Work

7.1 Conclusion

In power systems all over the world, medium-size local electricity networks are increasingly being interconnected by long-distance transmission lines for stabilizing the demand-supply balance by transportation power from resource centers to all sorts of load centers. Such interconnections have given rise to emergence of very large scale power systems where safety of operations is often threatened by low frequency power oscillations of inter-area modes. Heuristically, as the quantum of power transmitted between interconnected areas and transmission distances increases, management of inter-area power oscillations is becoming increasingly important and difficult. Thus, design of damping controllers for damping of inter-area oscillations has received increasing attention from academic researchers. Damping of inter-area oscillations is the major theme of this thesis, with considerable innovation and improvements proposed on the basis of pioneering research works already conducted.

The eigenstructures (both eigenvalues and eigenvectors) of closed loop systems have been innovatively utilized in the design of damping controllers, compared to the conventional methods which are mostly based on eigenvalues but rarely consider eigenvectors. By a novel way, eigenvalues and eigenvectors

are synthesized into indexes which are equivalent to corresponding cost functions defined in time domain, in terms of measuring system dynamic performance. Nevertheless, unlike the cost functions, the eigenstructure-based indexes have no relationship with system initial states which are actually undermined in the control design. Moreover, calculation of these indexes has no bearing on structures of damping controllers, which enables applications for solving structurally constrained control problems. Thus, due to these favorable features, eigenstructure-based indexes have been utilized throughout the thesis for design of damping controllers.

An eigenstructure-based index jointly measuring the dynamic performance of inter-area oscillations and control efforts has been employed in coordinated tuning of PSSs and SDCs for FACTS devices under multiple operating conditions. Both PSSs and SDCs use control structures as a classic simple SISO phase lead-lag compensator, and wide-area signals are employed as inputs to enhance their effectiveness in controlling inter-area modes. Time delays caused by introduction of the wide-area signals are also approximately considered in the design. These structurally constrained controllers have been successfully tuned by solving a nonlinear optimization problem which takes the eigenstructure-based index as the objective function. Specifically, weights of the objective function have been determined by a systematic procedure to ensure acceptable damping of inter-area modes and coordinating control efforts although it may be a little onerous. Furthermore, regarding coordination of PSSs and SDCs, the method of SCCS-PS has been utilized to demonstrate that control of inter-area modes by moving all closed loop poles to a conic section in the complex plane may be significantly impacted by other modes. Accordingly, the method of

IAMO-PS, a two-stage optimization method in which the inter-area mode oriented pole placement is implemented in the first stage, is used for damping control. Control efforts measured by the eigenstructure-based indexes are coordinated in the second stage under constraints such as pole placement. This has been proved to be a satisfactory alternative.

Compared to the conventional applications of PSSs and/or SDCs for FACTS devices in damping of inter-area oscillations, installing SDCs in DFIG-based WTGs for the damping function is a relatively new background. Through simultaneously optimizing parameters of SDCs and PV controllers of DFIGs by the DE algorithm, capabilities of DFIGs in damping inter-area oscillations have been demonstrated. However, it has been obviously addressed and emphasized that employing DFIG for damping control means sacrificing its dynamic performance. Furthermore, control efforts of active and reactive power modulation of DFIG have been measured by the eigenstructure-based indexes. Thus, by the method of IAMO-PS with optimal coordination of active and reactive power modulation, the dual-channel SDC has been designed for DFIG to optimize its power outputs as it is controlled to provide the required damping to inter-area modes. Consequently, in such a case, the dynamics of DFIG have been significantly improved since they are tightly coupled with power outputs of DFIG, in contrast with the case where the DFIG is employed for damping control but without optimizing its power outputs.

7.2 Future Work

This thesis has laid a substantial foundation for application of eigenstructure-based indexes to design damping controllers to suppress inter-area oscillations.

However, the following three aspects may be worthy of further research in the future:

(1) Extension of the IAMO-PS method to the robust design. Although this method has been proven to be successful for a single operating condition, multiple operating conditions should be taken into account during the design to ensure robustness of the final tuned controllers.

(2) Application of the proposed methods to real large scale power systems, such as the China southern power grid, which quite possibly suffers the threat of low frequency oscillations. However, in order to facilitate the applications, proper low-order system models should be derived. The identification based techniques should be promising in model reduction as they just process data of time domain responses from real measurements or numerical simulation programs which can deal with large scale power systems.

(3) Design of SDCs for DFIGs in more complex scenarios. It is known that wind energy is an intermittent type of energy, and the wind speed varies from time to time. The SDC designed for a given constant wind speed may not be robust enough in other wind speeds. Thus, consideration of wind speed variation in the design of SDCs for DFIGs to increase damping of inter-area modes is necessary. Moreover, SDCs for DFIGs should also be designed to operate in coordination with PSSs and SDCs for FACTS devices.

Appendix

A. Core of Deduction

For the diagonal matrix $\mathbf{\Lambda}_j$, the following equation holds:

$$e^{\mathbf{\Lambda}_j t} = \begin{bmatrix} e^{\lambda_{1j}t} & & & \\ & e^{\lambda_{2j}t} & & \\ & & \ddots & \\ & & & e^{\lambda_{nj}t} \end{bmatrix} \tag{A.1}$$

Moreover, an auxiliary matrix is defined as follows:

$$\mathbf{U}_j^{\mathrm{H}}\mathbf{P}_j\mathbf{U}_j = \begin{bmatrix} a_{11}, a_{12}, ..., a_{1n} \\ a_{21}, a_{22}, ..., a_{2n} \\ \vdots \\ a_{n1}, a_{n2}, ..., a_{nn} \end{bmatrix} \tag{A.2}$$

It is found that the core of (3.9) is the calculation of the following equation:

$$\int_0^\infty \left(e^{\mathbf{\Lambda}_j^{\mathrm{H}}t}\mathbf{U}_j^{\mathrm{H}}\mathbf{P}_j\mathbf{U}_j e^{\mathbf{\Lambda}_j t} \right) \mathrm{d}t \tag{A.3}$$

Therefore, by substituting (A.1) and (A.2) into (A.3), the following transformation can be derived:

$$\begin{aligned} &\int_0^\infty \left(e^{\mathbf{\Lambda}_j^{\mathrm{H}}t}\mathbf{U}_j^{\mathrm{H}}\mathbf{P}_j\mathbf{U}_j e^{\mathbf{\Lambda}_j t} \right) \mathrm{d}t \\ &= \int_0^\infty \begin{bmatrix} e^{\lambda_{1j}^* t} & & & \\ & e^{\lambda_{2j}^* t} & & \\ & & \ddots & \\ & & & e^{\lambda_{nj}^* t} \end{bmatrix} \begin{bmatrix} a_{11}, a_{12}, ..., a_{1n} \\ a_{21}, a_{22}, ..., a_{2n} \\ \vdots \\ a_{n1}, a_{n2}, ..., a_{nn} \end{bmatrix} \begin{bmatrix} e^{\lambda_{1j}t} & & & \\ & e^{\lambda_{2j}t} & & \\ & & \ddots & \\ & & & e^{\lambda_{nj}t} \end{bmatrix} \mathrm{d}t \\ &= \int_0^\infty \begin{bmatrix} a_{11}e^{\lambda_{1j}^* t}e^{\lambda_{1j}t}, a_{12}e^{\lambda_{1j}^* t}e^{\lambda_{2j}t}, ..., a_{1n}e^{\lambda_{1j}^* t}e^{\lambda_{nj}t} \\ a_{21}e^{\lambda_{2j}^* t}e^{\lambda_{1j}t}, a_{22}e^{\lambda_{2j}^* t}e^{\lambda_{2j}t}, ..., a_{2n}e^{\lambda_{2j}^* t}e^{\lambda_{nj}t} \\ \vdots \\ a_{n1}e^{\lambda_{nj}^* t}e^{\lambda_{1j}t}, a_{n2}e^{\lambda_{nj}^* t}e^{\lambda_{2j}t}, ..., a_{nn}e^{\lambda_{nj}^* t}e^{\lambda_{nj}t} \end{bmatrix} \mathrm{d}t \end{aligned} \tag{A.4}$$

$$= \begin{bmatrix} a_{11}\int_0^\infty e^{\left(\lambda_{1j}^* + \lambda_{1j}\right)t}\,\mathrm{d}t, a_{12}\int_0^\infty e^{\left(\lambda_{1j}^* + \lambda_{2j}\right)t}\,\mathrm{d}t, ..., a_{1n}\int_0^\infty e^{\left(\lambda_{1j}^* + \lambda_{nj}\right)t}\,\mathrm{d}t \\ a_{21}\int_0^\infty e^{\left(\lambda_{2j}^* + \lambda_{1j}\right)t}\,\mathrm{d}t, a_{22}\int_0^\infty e^{\left(\lambda_{2j}^* + \lambda_{2j}\right)t}\,\mathrm{d}t, ..., a_{2n}\int_0^\infty e^{\left(\lambda_{2j}^* + \lambda_{nj}\right)t}\,\mathrm{d}t \\ \vdots \\ a_{n1}\int_0^\infty e^{\left(\lambda_{nj}^* + \lambda_{1j}\right)t}\,\mathrm{d}t, a_{n2}\int_0^\infty e^{\left(\lambda_{nj}^* + \lambda_{2j}\right)t}\,\mathrm{d}t, ..., a_{nn}\int_0^\infty e^{\left(\lambda_{nj}^* + \lambda_{nj}\right)t}\,\mathrm{d}t \end{bmatrix}$$

$$= \begin{bmatrix} \left(\dfrac{-a_{11}}{\lambda_{1j}^* + \lambda_{1j}}\right), \left(\dfrac{-a_{12}}{\lambda_{1j}^* + \lambda_{2j}}\right), ..., \left(\dfrac{-a_{1n}}{\lambda_{1j}^* + \lambda_{nj}}\right) \\ \left(\dfrac{-a_{21}}{\lambda_{2j}^* + \lambda_{1j}}\right), \left(\dfrac{-a_{22}}{\lambda_{2j}^* + \lambda_{2j}}\right), ..., \left(\dfrac{-a_{2n}}{\lambda_{2j}^* + \lambda_{nj}}\right) \\ \vdots \\ \left(\dfrac{-a_{n1}}{\lambda_{nj}^* + \lambda_{1j}}\right), \left(\dfrac{-a_{n2}}{\lambda_{nj}^* + \lambda_{2j}}\right), ..., \left(\dfrac{-a_{nn}}{\lambda_{nj}^* + \lambda_{nj}}\right) \end{bmatrix}$$

$$= \begin{bmatrix} a_{11}, a_{12}, ..., a_{1n} \\ a_{21}, a_{22}, ..., a_{2n} \\ \vdots \\ a_{n1}, a_{n2}, ..., a_{nn} \end{bmatrix} \square \begin{bmatrix} \dfrac{-1}{\lambda_{1j}^* + \lambda_{1j}}, \dfrac{-1}{\lambda_{1j}^* + \lambda_{2j}}, ..., \dfrac{-1}{\lambda_{1j}^* + \lambda_{nj}} \\ \dfrac{-1}{\lambda_{2j}^* + \lambda_{1j}}, \dfrac{-1}{\lambda_{2j}^* + \lambda_{2j}}, ..., \dfrac{-1}{\lambda_{2j}^* + \lambda_{nj}} \\ \vdots \\ \dfrac{-1}{\lambda_{nj}^* + \lambda_{1j}}, \dfrac{-1}{\lambda_{nj}^* + \lambda_{2j}}, ..., \dfrac{-1}{\lambda_{nj}^* + \lambda_{nj}} \end{bmatrix}$$

B. Data of Four-Machine Two-Area System

Note: If not specified, all data in per unit are calculated on the basis of power rating of 100MVA and voltage rating of 230KV.

TABLE A.1 MACHINE BUS DATA

Bus	Voltage (p.u.)	Power generation (p.u.)
1	1.0300	7.0000
2	1.0100	7.0000
3	1.0300	7.1900
4	1.0100	7.0000

TABLE A.2 LOAD BUS DATA

Bus	Real load (p.u.)	Reactive load (p.u.)
7	9.7600	7.0000
9	17.6700	7.0000

TABLE A.3 SHUNT COMPENSATION

Bus	Compensation (p.u.)
7	2.0000
9	3.5000

TABLE A.4 TRANSMISSION LINE DATA

From Bus	To Bus	Resistance(p.u.)	Reactance (p.u.)	Line Charging (p.u.)
5	6	0.0025	0.0250	0.04375
6	7	0.0010	0.0100	0.0175
9	8	0.0110	0.1100	0.1925
7	8	0.0110	0.1100	0.1925
11	10	0.0025	0.0250	0.04375
10	9	0.0010	0.0100	0.0175
9	8	0.0110	0.1100	0.1925
7	8	0.0110	0.1100	0.1925

TABLE A.5 TRANSFORMER DATA (POWER RATING: 900MVA)

From Bus	To Bus	Reactance (p.u.)	Tap ratio (p.u.)
1	5	0.1500	1.0000
2	6	0.1500	1.0000
4	10	0.1500	1.0000
3	11	0.1500	1.0000

TABLE A.6 MACHINE DATA (POWER RATING: 900MVA AND VOLTAGE RATING: 20KV)

Bus	x_l	r	x_d	x'_d	x''_d	T'_{d0} (s)	T''_{d0} (s)
1	0.2000	0.0025	1.8000	0.3000	0.2500	8.0000	0.0300
2	0.2000	0.0025	1.8000	0.3000	0.2500	8.0000	0.0300
3	0.2000	0.0025	1.8000	0.3000	0.2500	8.0000	0.0300
4	0.2000	0.0025	1.8000	0.3000	0.2500	8.0000	0.0300

x_q	x'_q	x''_q	T'_{q0} (s)	T''_{q0} (s)	H(s)
1.7000	0.5500	0.2500	0.4000	0.0500	6.5000
1.7000	0.5500	0.2500	0.4000	0.0500	6.5000
1.7000	0.5500	0.2500	0.4000	0.0500	6.1750
1.7000	0.5500	0.2500	0.4000	0.0500	6.1750

TABLE A.7 DC EXCITATION SYSTEM DATA

Bus	V_{rmax}	V_{rmin}	K_A	T_A (s)	K_F	T_F (s)	T_E (s)	T_R (s)	A_{ex}	B_{ex}
1	5	-5	20.000	0.0550	0.1250	1.8000	0.3600	0.0500	0.0056	1.0750
2	5	-5	20.000	0.0550	0.1250	1.8000	0.3600	0.0500	0.0056	1.0750
3	5	-5	20.000	0.0550	0.1250	1.8000	0.3600	0.0500	0.0056	1.0750
4	5	-5	20.000	0.0550	0.1250	1.8000	0.3600	0.0500	0.0056	1.0750

C. Data of New England and New York Interconnected System

Note: If not specified, all data in per unit are calculated on the basis of power rating of 100MVA.

TABLE A.8 MACHINE BUS DATA

Bus	Voltage (p.u.)	Power generation (p.u.)
1	1.0450	2.5000
2	0.9800	5.4500
3	0.9830	6.5000
4	0.9970	6.3200
5	1.0110	5.0500
6	1.0500	7.0000
7	1.0630	5.6000
8	1.0300	5.4000
9	1.0250	8.0000
10	1.0100	5.0000
11	1.0000	10.0000
12	1.0156	13.5000
13	1.0110	35.9100
14	1.0000	17.8500
15	1.0000	10.0000
16	1.0000	40.0000

TABLE A.9 LOAD BUS DATA

Bus	Real load (p.u.)	Reactive load (p.u.)
17	60.0000	3.0000
18	24.7000	1.2300
20	6.8000	1.0300
21	2.7400	1.1500
23	2.4800	0.8500
24	3.0900	-0.9200
25	2.2400	0.4700
26	1.3900	0.1700
27	2.8100	0.7600
28	2.0600	0.2800
29	2.8400	0.2700
33	1.1200	0.0000
36	1.0200	-0.1946
39	2.6700	0.1260
40	0.6563	0.2353
41	10.0000	2.5000
42	11.5000	2.5000
44	2.6755	0.0484
45	2.0800	0.2100
46	1.5070	0.2850
47	2.0312	0.3259
48	2.4120	0.0220
49	1.6400	0.2900
50	1.0000	-1.4700
51	3.3700	-1.2200

	52	1.5800	0.3000
	53	2.5270	1.1856
	55	3.2200	0.0200
	56	2.0000	0.7360
	59	2.3400	0.8400
	60	2.0880	0.7080
	61	1.0400	1.2500
	64	0.0900	0.8800
	67	3.2000	1.5300
	68	3.2900	0.3200

TABLE A.10 TRANSMISSION LINE (TRANSFORMER) DATA

From Bus	To Bus	Resistance(p.u.)	Reactance (p.u.)	Line Charging (p.u.)	Tap ratio
54	1	0.0000	0.0181	0.0000	1.0250
58	2	0.0000	0.0250	0.0000	1.0700
62	3	0.0000	0.0200	0.0000	1.0700
19	4	0.0007	0.0142	0.0000	1.0700
20	5	0.0009	0.0180	0.0000	1.0090
22	6	0.0000	0.0143	0.0000	1.0250
23	7	0.0005	0.0272	0.0000	1.0000
25	8	0.0006	0.0232	0.0000	1.0250
29	9	0.0008	0.0156	0.0000	1.0250
31	10	0.0000	0.0260	0.0000	1.0400
32	11	0.0000	0.0130	0.0000	1.0400
36	12	0.0000	0.0075	0.0000	1.0400
17	13	0.0000	0.0033	0.0000	1.0400
41	14	0.0000	0.0015	0.0000	1.0000
42	15	0.0000	0.0015	0.0000	1.0000
18	16	0.0000	0.0030	0.0000	1.0000
36	17	0.0005	0.0045	0.3200	1.0000
49	18	0.0076	0.1141	1.1600	1.0000
68	19	0.0016	0.0195	0.3040	1.0000
19	20	0.0007	0.0138	0.0000	1.0600
68	21	0.0008	0.0135	0.2548	1.0000
21	22	0.0008	0.0140	0.2565	1.0000
22	23	0.0006	0.0096	0.1846	1.0000
23	24	0.0022	0.0350	0.3610	1.0000
68	24	0.0003	0.0059	0.0680	1.0000
54	25	0.0070	0.0086	0.1460	1.0000
25	26	0.0032	0.0323	0.5310	1.0000
37	27	0.0013	0.0173	0.3216	1.0000
26	27	0.0014	0.0147	0.2396	1.0000
26	28	0.0043	0.0474	0.7802	1.0000
26	29	0.0057	0.0625	1.0290	1.0000
28	29	0.0014	0.0151	0.2490	1.0000
53	30	0.0008	0.0074	0.4800	1.0000
61	30	0.0019	0.0183	0.2900	1.0000
61	30	0.0019	0.0183	0.2900	1.0000
30	31	0.0013	0.0187	0.3330	1.0000
53	31	0.0016	0.0163	0.2500	1.0000
30	32	0.0024	0.0288	0.4880	1.0000
32	33	0.0008	0.0099	0.1680	1.0000
33	34	0.0011	0.0157	0.2020	1.0000
35	34	0.0001	0.0074	0.0000	0.9460
34	36	0.0033	0.0111	1.4500	1.0000

61	36	0.0022	0.0196	0.3400	1.0000
61	36	0.0022	0.0196	0.3400	1.0000
68	37	0.0007	0.0089	0.1342	1.0000
31	38	0.0011	0.0147	0.2470	1.0000
33	38	0.0036	0.0444	0.6930	1.0000
41	40	0.0060	0.0840	3.1500	1.0000
48	40	0.0020	0.0220	1.2800	1.0000
42	41	0.0040	0.0600	2.2500	1.0000
18	42	0.0040	0.0600	2.2500	1.0000
17	43	0.0005	0.0276	0.0000	1.0000
39	44	0.0000	0.0411	0.0000	1.0000
43	44	0.0001	0.0011	0.0000	1.0000
35	45	0.0007	0.0175	1.3900	1.0000
39	45	0.0000	0.0839	0.0000	1.0000
44	45	0.0025	0.0730	0.0000	1.0000
38	46	0.0022	0.0284	0.4300	1.0000
53	47	0.0013	0.0188	1.3100	1.0000
47	48	0.0025	0.0268	0.4000	1.0000
47	48	0.0025	0.0268	0.4000	1.0000
46	49	0.0018	0.0274	0.2700	1.0000
45	51	0.0004	0.0105	0.7200	1.0000
50	51	0.0009	0.0221	1.6200	1.0000
37	52	0.0007	0.0082	0.1319	1.0000
55	52	0.0011	0.0133	0.2138	1.0000
53	54	0.0035	0.0411	0.6987	1.0000
54	55	0.0013	0.0151	0.2572	1.0000
55	56	0.0013	0.0213	0.2214	1.0000
56	57	0.0008	0.0128	0.1342	1.0000
57	58	0.0002	0.0026	0.0434	1.0000
58	59	0.0006	0.0092	0.1130	1.0000
57	60	0.0008	0.0112	0.1476	1.0000
59	60	0.0004	0.0046	0.0780	1.0000
60	61	0.0023	0.0363	0.3804	1.0000
58	63	0.0007	0.0082	0.1389	1.0000
62	63	0.0004	0.0043	0.0729	1.0000
64	63	0.0016	0.0435	0.0000	1.0600
62	65	0.0004	0.0043	0.0729	1.0000
64	65	0.0016	0.0435	0.0000	1.0000
56	66	0.0008	0.0129	0.1382	1.0000
65	66	0.0009	0.0101	0.1723	1.0000
66	67	0.0018	0.0217	0.3660	1.0000
67	68	0.0009	0.0094	0.1710	1.0000
53	27	0.0320	0.3200	0.4100	1.0000
69	18	0.0006	0.0144	1.0300	1.0000
50	69	0.0006	0.0144	1.0300	1.0000

TABLE A.11 MACHINE DATA

Bus	Base MVA	x_l	r	x_d	x'_d	x''_d	T'_{d0} (s)	T''_{d0} (s)
1	100	0.0125	0.0000	0.1000	0.0310	0.0250	10.2000	0.0500
2	100	0.0350	0.0000	0.2950	0.0697	0.0500	6.5600	0.0500
3	100	0.0304	0.0000	0.2495	0.0531	0.0450	5.7000	0.0500
4	100	0.0295	0.0000	0.2620	0.0436	0.0350	5.6900	0.0500
5	100	0.0270	0.0000	0.3300	0.0660	0.0500	5.4000	0.0500
6	100	0.0224	0.0000	0.2540	0.0500	0.0400	7.3000	0.0500

7	100	0.0322	0.0000	0.2950	0.0490	0.0400	5.6600	0.0500
8	100	0.0280	0.0000	0.2900	0.0570	0.0450	6.7000	0.0500
9	100	0.0298	0.0000	0.2106	0.0570	0.0450	4.7900	0.0500
10	100	0.0199	0.0000	0.1690	0.0457	0.0400	9.3700	0.0500
11	100	0.0103	0.0000	0.1280	0.0180	0.0120	4.1000	0.0500
12	100	0.0220	0.0000	0.1010	0.0310	0.0250	7.4000	0.0500
13	200	0.0030	0.0000	0.0296	0.0055	0.0040	5.9000	0.0500
14	100	0.0017	0.0000	0.0180	0.00285	0.0023	4.1000	0.0500
15	100	0.0017	0.0000	0.0180	0.00285	0.0023	4.1000	0.0500
16	200	0.0041	0.0000	0.0356	0.0071	0.0055	7.800	0.0500

x_q	x'_q	x''_q	T'_{q0} (s)	T''_{q0} (s)	H(s)	D
0.0690	0.0280	0.0250	1.5000	0.0350	42.0	4.0000
0.2820	0.0600	0.0500	1.5000	0.0350	30.2	9.7500
0.2370	0.0500	0.0450	1.5000	0.0350	35.8	10.0000
0.2580	0.0400	0.0350	1.5000	0.0350	28.6	0.0000
0.3100	0.0600	0.0500	0.4400	0.0350	26.0	3.0000
0.2410	0.0450	0.0400	0.4000	0.0350	34.8	0.0000
0.2920	0.0450	0.0400	1.5000	0.0350	26.4	0.0000
0.2800	0.0500	0.0450	0.4100	0.0350	24.3	9.0000
0.2050	0.0500	0.0450	1.9600	0.0350	34.5	14.0000
0.1150	0.0450	0.0400	1.5000	0.0350	31.0	0.0000
0.1230	0.0150	0.0120	1.5000	0.0350	28.2	13.6000
0.0950	0.0280	0.0250	1.5000	0.0350	92.3	0.0000
0.0286	0.0050	0.0040	1.5000	0.0350	248.0	0.0000
0.0173	0.0025	0.0023	1.5000	0.0350	300.0	0.0000
0.0173	0.0025	0.0023	1.5000	0.0350	300.0	0.0000
0.0334	0.0060	0.0055	1.5000	0.0350	225.0	0.0000

TABLE A.12 DC EXCITATION SYSTEM DATA

Bus	V_{rmax}	V_{rmin}	K_A	T_A (s)	K_F	T_F (s)	T_E (s)	T_R (s)	A_{ex}	B_{ex}
1	10	-10	40.000	0.0200	0.0000	1.0000	0.7850	0.0100	0.07	0.9100
2	10	-10	40.000	0.0200	0.0000	1.0000	0.7850	0.0100	0.07	0.9100
3	10	-10	40.000	0.0200	0.0000	1.0000	0.7850	0.0100	0.07	0.9100
4	10	-10	40.000	0.0200	0.0000	1.0000	0.7850	0.0100	0.07	0.9100
5	10	-10	40.000	0.0200	0.0000	1.0000	0.7850	0.0100	0.07	0.9100
6	10	-10	40.000	0.0200	0.0000	1.0000	0.7850	0.0100	0.07	0.9100
7	10	-10	40.000	0.0200	0.0000	1.0000	0.7850	0.0100	0.07	0.9100
8	10	-10	40.000	0.0200	0.0000	1.0000	0.7850	0.0100	0.07	0.9100

TABLE A.13 STATIC EXCITATION SYSTEM DATA

Bus	V_{rmax}	V_{rmin}	K_A	T_A (s)	T_R (s)
9	5	-5	200.0	0.0001	0.0100
10	5	-5	200.0	0.0001	0.0100
11	5	-5	200.0	0.0001	0.0100
12	5	-5	200.0	0.0001	0.0100
13	5	-5	200.0	0.0001	0.0100
14	5	-5	200.0	0.0001	0.0100
15	5	-5	200.0	0.0001	0.0100
16	5	-5	200.0	0.0001	0.0100

TABLE A.14 LOCAL SPEED BASED PSS DATA (MODEL STRUCTURE SHOWN IN FIG. 2.4)

Bus	V_{rmax}	V_{rmin}	T_w	K_{pss}	T_1 (s)	T_2 (s)	T_3 (s)	T_4 (s)
10	0.1	-0.1	10.0	1.5000	0.1631	0.0746	0.1631	0.0746
13	0.1	-0.1	10.0	18.000	0.2936	0.2856	0.2936	0.2856
15	0.1	-0.1	10.0	28.000	0.2196	0.2021	0.2196	0.2021
16	0.1	-0.1	10.0	20.000	0.3280	0.2941	0.3280	0.2941

Reference

[1] G. Andersson, P. Donalek, R. Farmer, N. Hatziargyriou, I. Kamwa, P. Kundur, N. Martins, J. Paserba, P. Pourbeik, J. Sanchez-Gasca, R. Schulz, A. Stankovic, C. Taylor, and V. Vittal, "Causes of the 2003 major grid blackouts in north America and Europe, and recommended means to improve system dynamic performance," *IEEE Trans. Power Syst.,* vol. 20, no. 4, pp. 1922-1928, Nov. 2005.

[2] U. S.-Canada Power System Outage Task Force, "Final report on the August 14, 2003 blackout in the United States and Canada: causes and recommendations," *https://reports.energy.gov/,* 2004.

[3] IEEE/CIGRE joint task force on stability terms and definitions, "Definition and classification of power system stability," *IEEE Trans. Power Syst.,* vol. 19, no. 2, pp. 1387-1401, May 2004.

[4] G. Rogers, *Power system oscillations*. Bostan: Kluwer Academic, 2000.

[5] P. Kundur, *Power system stability and control*. New York: McGraw-Hill, 1994.

[6] B. Pal and B. Chaudhuri, *Robust control in power systems*. New York: Springer, 2005.

[7] M. Klein, G. J. Rogers, and P. Kundur, "A fundamental study of inter-area oscillations in power systems," *IEEE Trans. Power Syst.,* vol. 6, no. 3, pp. 914-921, Aug. 1991.

[8] M. Klein, G. J. Rogers, S. Mooty, and P. Kundur, "Analytical investigation

of factors influencing power system stabilizers performance," *IEEE Trans. Energy Conversion,* vol. 7, no. 3, pp. 382-390, Sep. 1992.

[9]   F. R. Schleif and J. H. White, "Damping for northwest-southwest tie line oscillations-an analogue study," *IEEE Trans. Power Apparatus and Systems,* vol. PAS-85, no. 12, pp. 1239-1247, Dec. 1966.

[10] J. He, C. Lu, X. Wu, P. Li, and J. Wu, "Design and experiment of wide area HVDC supplementary damping controller considering time delay in China southern power grid," *IET Gener. Transm. Distrib.,* vol. 3, no. 1, pp. 17-25, 2009.

[11] P. Li, X. Wu, C. Lu, J. Shi, J. Hu, J. He, Y. Zhao, and A. Xu, "Implementation of CSG's wide-area damping control system: overview and experience " in *Power Systems Conference and Exposition*, 2009.

[12] X. M. Zhang, Y. Zhang, L. Guan, and X. C. Wu, "Coordinated control of interarea oscillation in the China Southern Power Grid," *IEEE Trans. Power Syst.,* vol. 21, no. 2, pp. 845-852, May 2006.

[13] A. M. Simoes, D. C. Savelli, P. C. Pellanda, N. Martins, and P. Apkarian, "Robust design of a TCSC oscillation damping controllers in a weak 500-kV interconnection considering multiple power flow scenarios and external disturbances," *IEEE Trans. Power Syst.,* vol. 24, no.1, pp. 226-236, Feb. 2009.

[14] N. Martins, A. A. Barbosa, J. C. R. Ferraz, M. G. dos Santos, A. L. B. Bergamo, C. S. Yung, V. R. Oliveira, and N. J. P. Macedo, "Retuning stabilizers for the north-south Brazilian interconnection," in *IEEE PES Summer Meeting*, 1999.

[15] B. M. Nomikos, M. E. Kouveletsou, and C. D. Vournas, "PSS design for

the Hellenic system with partial interconnection to Turkey," in *IEEE Power Tech*, 2009.

[16] C. D. Vournas, A. Metsiou, and B. M. Nomikos, "Analysis of intra-area and interarea oscillations in South-Eastern UCTE interconnection," in *IEEE PES General Meeting*, 2009.

[17] F. P. Demello and C. Concordia, "Concepts of synchronous machine stability as affected by excitation control," *IEEE Trans. Power App. Syst.*, vol. PAS-88, no. 4, pp. 316-329, Apr. 1969.

[18] IEEE Standard 421.5, "IEEE recommend practice for excitation system models for power system stability studies," Aug. 1992.

[19] IEEE Digital Excitation Task Force of the Equipment Working Group of the IEEE/PES Excitation System Subcommittee, "Computer model for representation of digital-based excitation systems," *IEEE Trans. Energy Conversion,* vol. 11, no. 3, pp. 607-615, Sep. 1996.

[20] E. V. Larsen and D. A. Swann, "Applying power system stabilizers Part I: general concepts," *IEEE Trans. Power App. Syst.,* vol. PAS-100, no. 6, pp. 3017-3024, Jun. 1981.

[21] E. V. Larsen and D. A. Swann, "Applying power system stabilizers Part II: performance objectives and tuning concepts," *IEEE Trans. Power App. Syst.,* vol. PAS-100, no. 6, pp. 3025-3033, Jun. 1981.

[22] E. V. Larsen and D. A. Swann, "Applying power system stabilizers Part III: practical considerations," *IEEE Trans. Power App. Syst.,* vol. PAS-100, no. 6, pp. 3034-3046, Jun. 1981.

[23] Y. H. Song and A. T. Johns, *Flexible ac transmission systems (FACTS)*. London: Institution of Electrical Engineers, 1999.

[24] N. Flourentzou, V. G. Agelidis, and G. D. Demetriades, "VSC-based HVDC power transmission systems: an overview," *IEEE Trans. Power Electron.,* vol. 24, no. 3, pp. 592-602, Mar. 2009.

[25] Y. Xiao, Y. H. Song, C.-C. Liu, and Y. Z. Sun, "Available transfer capability enhancement using facts devices," *IEEE Trans. Power Syst.,* vol. 18, no. 1, pp. 305-312, Feb. 2003.

[26] N. Yorino, E. E. El-Araby, H. Sasaki, and S. Harada, "A new formulation for FACTS allocation for security enhancement against voltage collapse," *IEEE Trans. Power Syst.,* vol. 18, no. 1, pp. 3-10, Feb. 2003.

[27] C. A. Canizares and Z. T. Faur, "Analysis of SVC and TCSC controllers in voltage collapse," *IEEE Trans. Power Syst.,* vol. 14, no. 1, pp. 158-165, Feb. 1999.

[28] P. Pourbeik and M. J. Gibbard, "Damping and synchronizing torques induced on generators by FACTS stabilizers in multimachine power systems," *IEEE Trans. Power Syst.,* vol. 11, no. 4, pp. 1920-1925, Nov. 1996.

[29] R. L. Lee, M. J. Beshir, A. T. Finley, D. R. Hayes, J. C. Hsu, H. R. Peterson, G. L. DeShazo, and D. W. Gerlach, "Application of static var compensators for the dynamic performance of the mead-adelanto and mead-phoenix transmission projects," *IEEE Trans. Power Delivery,* vol. 10, no. 1, pp. 459-466, Jan. 1995.

[30] C. Gama, L. Angquist, G. Ingestrom, and M. Noroozian, "Commissioning and operative experience of TCSC for damping power oscillation in the Brazilian north-south interconnection," in *Proc. CIGRE*, France, 2000.

[31] H. F. Wang and F. J. Swift, "Capability of the static VAr compensator in

damping power system oscillations," *IEE Proc.-Gener. Transm. Distrib.,* vol. 143, no. 4, Jul. 1996.

[32] B. Chaudhuri, R. Majumder, and B. C. Pal, "Robust damping of multiple swing modes employing global stabilizing signals with a TCSC," *IEEE Trans. Power Syst.,* vol. 19, no. 1, pp. 499-506, Feb. 2004.

[33] S. Mohagheghi, G. K. Venayagamoorthy, and R. G. Harley, "Optimal wide area controller and state predictor for a power system," *IEEE Trans. Power Syst.,* vol. 22, no. 2, pp. 693-705, May 2007.

[34] D. Rai, S. O. Faried, G. Ramakrishna, and A.-A. Edris, "Damping inter-area oscillations using phase imbalanced series compensation schemes," *IEEE Trans. Power Syst.,* vol. 26, no. 3, pp. 1753-1761, Aug. 2011.

[35] Z. Y. Huang, Y. X. Ni, C. M. Shen, F. F. Wu, S. S. Chen, and B. L. Zhang, "Application of unified power flow controller in interconnected power systems—modeling, interface, control strategy, and case study," *IEEE Trans. Power Syst.,* vol. 15, no. 2, pp. 817-824, May 2000.

[36] S. Mishra, P. K. Dash, P. K. Hota, and M. Tripathy, "Genetically optimized neuro-fuzzy IPFC for damping modal oscillations of power system," *IEEE Trans. Power Syst.,* vol. 17, no. 4, pp. 1140-1147, Nov. 2002.

[37] L. Anquist, B. Lundin, and J. Samuelsson, "Power oscillation damping using controlled reactive power compensation: a comparison between series and shunt approaches," *IEEE Trans. Power Syst.,* vol. 8, no. 2, pp. 687-699, May 1993.

[38] T. Ackermann, *Wind power in power systems.* Chichester: John Wiley, 2005.

[39] O. Anaya-Lara, N. Jenkins, J. Ekanayake, P. Cartwright, and M. Hughes,

Wind energy generation—modelling and control. Chichester, U.K.: John&Sons, 2009.

[40] L. Holdsworth, X. G. Wu, J. B. Ekanayake, and N. Jenkins, "Comparison of fixed speed and doubly-fed induction wind turbines during power system disturbances," *IEE Proc.-Gener. Transm. Distrib.,* vol. 150, no. 3, pp. 343-352, May, 2003.

[41] O. Anaya-Lara, F. M. Hughes, N. Jenkins, and G. Strbac, "Rotor flux magnitude and angle control strategy for doubly fed induction generators," *Wind Energy,* vol. 9, no. 5, 2006.

[42] E. Vittal, M. O'Malley, and A. Keane, "A steady-state voltage stability analysis of power systems with high penetrations of wind," *IEEE Trans. Power Syst.,* vol. 25, no.1, pp. 433-442, Feb. 2010.

[43] J. Morren, S. W. H. Haan, W. L. Kling, and J. A. Ferreira, "Wind turbines emulating inertia and supporting primary frequency control," *IEEE Trans. Power Syst.,* vol. 21, no. 1, pp. 433-434, Feb. 2006.

[44] F. M. Hughes, O. Anaya-Lara, N. Jenkins, and G. Strbac, "A power system stabilizer for DFIG-based wind generation," *IEEE Trans. Power Syst.,* vol. 21, no. 2, pp. 763-772, May 2006.

[45] L. Fan, Z. Miao, and D. Osborn, "Impact of doubly fed wind turbine generation on inter-area oscillation damping," in *IEEE PES General Meeting*, 2008.

[46] Z. Miao, L. Fan, D. Osborn, and S. Yuvarajan, "Control of DFIG-based wind generation to improve inter-area oscillation damping," *IEEE Trans. Energy Conversion,* vol. 24, no. 2, pp. 415-422, Jun. 2009.

[47] H. Yin, L. Fan, and Z. Miao, "Reactive power modulation for inter-area

oscillation damping of DFIG-based wind generation," in *IEEE PES General Meeting*,2010.

[48] H. F. Wang and F. J. Swift, "A unified model for the analysis of FACTS devices in damping power system oscillations part I: single-machine infinite bus power systems," *IEEE Trans. Power Delivery,* vol. 12, no. 2, pp. 941-946, Apr. 1997.

[49] H. F. Wang, F. J. Swift, and M. Li, "A unified model for the analysis of FACTS devices in damping power system oscillations part II: multi-machine power systems," *IEEE Trans. Power Delivery,* vol. 13, no. 4, pp. 1355-1362, Oct. 1998.

[50] H. F. Wang, "A unified model for the analysis of FACTS devices in damping power system oscillations—part III: unified power flow controller," *IEEE Trans. Power Delivery,* vol. 15, no. 3, pp. 978-983, Jul. 2000.

[51] L. Fan, H. Yin, and Z. Miao, "On active/reactive power modulation of DFIG-based wind generation for interarea oscillation damping," *IEEE Trans. Energy Conversion,* vol. 26, no. 2, pp. 513-521, Jun. 2011.

[52] N. Kshatriya, U. D. Annakkage, F. M. Hughes, and A. M. Gole, "Optimized partial eigenstructure assignment-based design of a combined PSS and active damping controller for a DFIG," *IEEE Trans. Power Syst.,* vol. 25, no. 2, pp. 866-876, May 2010.

[53] M. J. Gibbard and D. J. Vowles, "Reconciliation of methods of compensation for PSSs in multimachine systems," *IEEE Trans. Power Syst.,* vol. 19, no. 1, pp. 463-472, Feb. 2004.

[54] M. J. Gibbard, N. Martins, J. J. Sanchez-Gasca, N. Uchida, V. Vittal, and L.

Wang, "Recent application of linear analysis techniques," *IEEE Trans. Power Syst.,* vol. 16, no. 1, pp. 154-162, Feb. 2001.

[55] N. Martins, S. Corsi, G. Andersson, and M. J. Gibbard, "Impact of the interaction among power system controls," CIGRE Special Publication 38.02.16, Technical Brochure, 2000.

[56] L. Rouco, "Eigenvalue-based methods for analysis and control of power system oscillations," in *IEE Colloguium on Power System Dynamics Stabilization,* 1998.

[57] M. A. Abido, "Optimal design of power-system stabilizers using particle swarm optimization," *IEEE Trans. Energy Conversion,* vol. 17, no. 3, pp. 406-413, Sep. 2002.

[58] J. H. Chow and J. J. Sanchez-Gasca, "Pole-placement designs of power system stabilizers," *IEEE Trans. Power Syst.,* vol. 4, no. 1, pp. 271-277, Feb. 1989.

[59] Y.-N. Yu and Q.-H. Li, "Pole-placement power system stabilizers design of an unstable nine-machine system," *IEEE Trans. Power Syst.,* vol. 5, no. 2, pp. 353-358, May 1990.

[60] J. C. R. Ferraz, N. Martins, and G. N. Taranto, "Simultaneous partial pole placement for power system oscillation damping control," in *IEEE PES Winter Meeting*, 2001.

[61] P. S. Rao and I. Sen, "Robust pole placement stabilizer design using linear matrix inequalities," *IEEE Trans. Power Syst.,* vol. 15, no. 1, pp. 313-319, Feb. 2000.

[62] B. Moore, "On the flexibility offered by state feedback in multivariable systems beyond closed loop eigenvalue assignment," *IEEE Trans. Autom.*

Control, vol. AC-21, pp. 689-692, Oct. 1976.

[63] G. Liu and R. Patton, *Eigenstructure assignment for control system design.* Chichester, U. K.: Wiley, 1998.

[64] J. Lu, H. D. Chiang, and J. S. Thorp, "Eigenstructure assignment by decentralized feedback control," *IEEE Trans. Autom. Control,* vol. 38, no. 4, pp. 587-593, Apr. 1993.

[65] P.-H. Huang and Y.-Y. Hsu, "Eigenstructure assignment in a longitudinal power system via excitation control," *IEEE Trans. Power Syst.,* vol. 5, no. 1, pp. 96-102, Feb. 1990.

[66] M. R. Khaldi, A. K. Sarkar, K. Y. Lee, and Y. M. Park, "The modal performance measure for parameter optimization of power system stabilizers," *IEEE Trans. Energy Conversion,* vol. 8, no. 4, pp. 660-666, Dec. 1993.

[67] J. B. Simo, I. Kamwa, G. Trudel, and S.-A. Tahan, "Validation of a new modal performance measure for flexible controllers design," *IEEE Trans. Power Syst.,* vol. 11, no. 2, pp. 819-826, May 1996.

[68] A. J. Urdaneta, B. Feijoo, N. J. Bacalao, L. Flores, and R. Diaz, "Tuning of power system stabilizers using optimization techniques," *IEEE Trans. Power Syst.,* vol. 6, no. 1, pp. 127-134, Feb. 1991.

[69] X. Lei, E. N. Lerch, and D. Povh, "Optimization and coordination of damping controls for improving system dynamic performance," *IEEE Trans. Power Syst.,* vol. 16, no. 3, pp. 473-480, Aug. 2001.

[70] I. Kamwa, G. Trudel, and L. Gerin-Lajoie, "Robust design and coordination of multiple damping controllers using nonlinear constrained optimization," *IEEE Trans. Power Syst.,* vol. 15, no. 3, pp. 1084-1092, Aug.

2000.

[71] J. Nocedal and S. J. Wright, *Numerical optimization*. New York: Springer, 2006.

[72] M. C. Joshi and K. M. Moudgalya, *Optimization: theory and practice*. Harrow: Alpha Science International Ltd., 2004.

[73] A. Qing, *Differential evolution: fundamentals and applications in electrical engineering*. Singapore: Wiley, 2009.

[74] A. Mendonca and J. A. P. Lopes, "Simultaneous tuning of power system stabilizers installed in DFIG-based wind generation," in *IEEE Power Tech*, 2007.

[75] I. A. Hiskens and M. A. Pai, "Trajectory sensitivity analysis of hybrid system," *IEEE Trans. Circuits Syst. Part I,* vol. 47, no. 2, pp. 204-220, Feb. 2000.

[76] T. V. Cutsem and C. Vournas, *Voltage stability of electric power systems*. Boston, Mass: Kluwer Academic Publishers, 1998.

[77] I. J. Perez-Arriaga, G. C. Verghese, and F. C. Schweppe, "Selective modal analysis with applications to electric power systems, part I: heuristic introduction," *IEEE Trans. Power App. Syst.,* vol. PAS-101, no. 9, pp. 3117-3125, Sep. 1982.

[78] A. Heniche and I. Kamwa, "Control loops selection to damp inter-area oscillations of electrical networks," *IEEE Trans. Power Syst.,* vol. 17, no. 2, pp. 378-384, May 2002.

[79] A. Heniche and I. Kamwa, "Assessment of two methods to select wide-area signals for power system damping control," *IEEE Trans. Power Syst.,* vol. 23, no.2, pp. 572-581, May 2008.

[80] F. L. Pagola, I. J. Perez-Arriaga, and G. C. Verghese, "On sensitivities, residues and participations: applications to oscillatory stability analysis and control," *IEEE Trans. Power Syst.,* vol. 4, no. 1, pp. 278-285, Feb. 1989.

[81] J. R. Leigh, *Control theory*. London: Institution of Electrical Engineers, 2004.

[82] M. J. Gibbard, "Co-ordinated design of multimachine power system stabilisers based on damping torque concepts," *IEE Proceedings, Part C,* vol. 135, no. 4, pp. 276-284, Jul. 1988.

[83] M. J. Gibbard, "Robust design of fixed-parameter power system stabilisers over a wide range of operating conditions," *IEEE Trans. Power Syst.,* vol. 6, no. 2, pp. 794-800, May 1991.

[84] P. Pourbeik, M. J. Gibbard, and D. J. Vowles, "Proof of the equivalence of residues and induced torque coefficients for use in the calculation of eigenvalue shifts," *IEEE Power Eng. Rev. ,* vol. 22, no. 1, pp. 58-60, Jan. 2002.

[85] P. Pourbeik and M. J. Gibbard, "Simultaneous coordination of power system stabilizers and facts device stabilizers in a multi-machine power system for enhancing dynamic performance," *IEEE Trans. Power Syst.,* vol. 13, no. 2, pp. 473-479, May 1998.

[86] M. G. Safonov and R. Y. Chiang, "A Schur method for balanced model reduction," *IEEE Trans. Autom. Control,* vol. AC-34, no. 7, pp. 729-733, Jul. 1989.

[87] K. Glover, "All optimal Hankel norm approximation of linear multivariable systems and their l infinite error bounds," *International journal of control,* vol. 39, no. 6, pp. 1115-1193, 1984.

[88] N. Martins, F. G. Silva, P. C. Pellanda, and A. de Castro, "Utilizing transfer function modal equivalents of low-order for the design of power oscillation damping controllers in large power systems," in *IEEE PES General Meeting*, 2005.

[89] F. D. Freitas, J. Rommes, and N. Martins, "Gramian-based reduction method applied to large sparse power system descriptor models," *IEEE Trans. Power Syst.,* vol. 23, no. 3, pp. 1258-1270, Aug. 2008.

[90] D. Chaniotis and M. A. Pai, "Model reduction in power systems using Krylov subspace methods," *IEEE Trans. Power Syst.,* vol. 20, no. 2, pp. 888-894, May 2005.

[91] N. Martins and P. E. M. Quintao, "Computing dominant poles of power system multivariable transfer functions," *IEEE Trans. Power Syst.,* vol. 18, no. 1, pp. 152-159, Feb. 2003.

[92] N. Martins, P. C. Pellanda, and J. Rommes, "Computation of transfer function dominant zeros with applications to oscillation damping control of large power systems," *IEEE Trans. Power Syst.,* vol. 22, no. 4, pp. 1657-1664, Nov. 2007.

[93] D. J. Trudnowski, J. R. Smith, and T. A. Short, "An application of Prony methods in PSS design for multimachine systems," *IEEE Trans. Power Syst.,* vol. 6, no. 1, pp. 118-126, Feb. 1991.

[94] J. R. Smith, J. F. Hauer, and D. J. Trudnowski, "Transfer function identification in power system applications," *IEEE Trans. Power Syst.,* vol. 8, no. 3, pp. 1282-1290, Aug. 1993.

[95] I. Kamwa, R. Grondin, J. Dickinson, and S. Fortin, "A minimal realization approach to reduced-order modeling and modal analysis for power system

response signals," *IEEE Trans. Power Syst.,* vol. 8, no. 3, pp. 1020-1029, Aug. 1993.

[96] J. J. Sanchez-Gasca and J. H. Chow, "Computation of power system low-order models from time domain simulations using a Hankel matrix," *IEEE Trans. Power Syst.,* vol. 12, no. 4, pp. 1461-1467, Nov. 1997.

[97] A. Hasanovic, A. Feliachi, A. Hasanovic, N. B. Bhatt, and A. G. DeGroff, "Practical robust PSS design through identification of low-order transfer function," *IEEE Trans. Power Syst.,* vol. 19, no. 3, pp. 1492-1500, Aug. 2004.

[98] D. Dotta, A. S. Silva, and I. C. Decker, "Wide-area measurements-based two-level control design considering signal transmission delay," *IEEE Trans. Power Syst.,* vol. 24, no. 1, pp. 208-216, Feb. 2009.

[99] L. J. Cai and I. Erlich, "Simultaneous coordinated tuning of PSS and FACTS damping controllers in large power systems," *IEEE Trans. Power Syst.,* vol. 20, no. 1, pp. 294-300, Feb. 2005.

[100] J. H. Chow, J. J. Sanchez-Gasca, R. Haoxing, and S. Wang, "Power system damping controller design using multiple input signals," *IEEE Control Syst. Mag. ,* vol. 20, no. 4, pp. 82-90, Aug. 2000.

[101] H. Wu, S. T. Konstantinos, and G. T. Heydt, "Evaluation of time delay effects to wide-area power system stabilizer design," *IEEE Trans. Power Syst.,* vol. 19, no. 4, pp. 1935-1941, Nov. 2004.

[102] I. Kamwa, R. Grondin, and Y. Hebert, "Wide-area measurement based stabilizing control of large power systems-a decentralized/hierarchical approach," *IEEE Trans. Power Syst.,* vol. 16, no. 1, pp. 136-153, Feb. 2001.

[103] H. Ni, G. T. Heydt, and L. Mili, "Power system stability agents using

robust wide-area control," *IEEE Trans. Power Syst.,* vol. 17, no. 4, pp. 1123-1131, Nov. 2002.

[104] R. Grondin, I. Kamwa, G. Trudel, J. Taborda, R. Lenstroem, L. Gerin-Lajoie, J. P. Gingras, M. Racine, and H. Baumberger, "The multi-band PSS: a flexible technology designed to meet opening markets," in *Proc. CIGRE,* France, 2000.

[105] R. V. de Oliveira, R. Kuiava, R. A. Ramos, and N. G. Bretas, "Automatic tuning method for the design of supplementary damping controllers for flexible alternating current transmission system devices," *IET Gener. Transm. Distrib.,* vol. 3, no. 10, pp. 919-929, 2009.

[106] B. Chaudhuri, S. Ray, and R. Majumder, "Robust low-order controller design for multi-modal power oscillation damping using flexible AC transmission system devices," *IET Gener. Transm. Distrib.,* vol. 3, no. 10, pp. 919-929, 2009.

[107] A. J. A. S. Costa, F. D. Freitas, and H. E. Pena, "Power system stabilizer design via structurally constrained optimal control," *Electr. Power Syst. Res.,* vol. 33, no. 1, pp. 33-40, Apr. 1995.

[108] S. Q. Yuan and D. Z. Fang, "Robust PSS parameters design using a trajectory sensitivity approach," *IEEE Trans. Power Syst.,* vol. 24, no. 2, pp. 1011-1018, May 2009.

[109] R. A. Jabr, B. C. Pal, and N. Martins, "A sequential conic programming approach for the coordinated and robust design of power system stabilizers," *IEEE Trans. Power Syst.,* vol. 25, no. 3, pp. 1627-1637, Aug. 2010.

[110] R. Majumder, B. Chaudhuri, H. El-Zobaidi, B. Pal, and I. Jaimoukha, "LMI

approach to normalised H infinite loop-shaping design of power system damping controllers," *IEE Proc.-Gener. Transm. Distrib.,* vol. 152, no. 6, pp. 952-960, Nov. 2005.

[111] M. Djukanovic, M. Khammash, and V. Vittal, "Sequential synthesis of structured sigular value based decentralized controllers in power systems," *IEEE Trans. Power Syst.,* vol. 14, no. 2, pp. 635-641, May 1999.

[112] S. Skogestad and I. Postlethwaite, *Multivariable feedback control: analysis and design.* Chichester England; Hoboken, NJ: John Wiley, 2005.

[113] R. A. Ramos, A. C. P. Martins, and N. G. Bretas, "An improved methodology for the design of power system damping controllers," *IEEE Trans. Power Syst.,* vol. 20, no. 4, pp. 1938-1945, Nov. 2005.

[114] A. C. Zolotas, B. Chaudhuri, I. M. Jaimoukha, and P. Korba, "A study on LQG/LTR control for damping inter-area oscillations in power systems," *IEEE Trans. Control Syst. Technol.,* vol. 15, no. 1, pp. 151-160, Jan. 2007.

[115] R. A. Ramos, L. F. C. Alberto, and N. G. Bretas, "A new methodology for the coordinated design of robust decentralized power system damping controllers," *IEEE Trans. Power Syst.,* vol. 19, no. 1, pp. 444-454, Feb. 2004.

[116] Z. Wang, C. Y. Chung, K. P. Wong, C. T. Tse, and K. W. Wang, "Robust power system stabilizer design under multioperating conditions using differential evoluation," *IET Gener. Transm. Distrib.,* vol. 2, no. 5, pp. 690-700, 2008.

[117] D. Z. Fang, S. Q. Yuan, Y. J. Wang, and T. S. Chung, "Coordinated parameter design of STATCOM stabilizer and PSS using MSSA algorithm," *IET Gener. Transm. Distrib.,* vol. 1, no. 4, pp. 670-678, 2007.

[118] A. J. A. S. Costa, F. D. Freitas, and A. S. e Silva, "Design of decentralized controllers for large power systems considering sparsity," *IEEE Trans. Power Syst.,* vol. 12, no. 1, pp. 144-152, Feb. 1997.

[119] J. J. Sanchez, V. Vittal, M. J. Gibbard, A. R. Messina, D. J. Vowles, S. Liu, and U. D. Annakkage, "Inclusion of higher order terms for small-signal (modal) analysis: committee report-task force on assessing the need to include high order terms for small-signal (modal) analysis," *IEEE Trans. Power Syst.,* vol. 20, no. 4, pp. 1886-1904, Nov. 2005.

[120] M. H. Haque, "Improvement of first swing stability limit by utilizing full benefit of shunt FACTS devices," *IEEE Trans. Power Syst.,* vol. 19, no. 4, pp. 1894-1902, Nov. 2004.

[121] C. W. Taylor, D. C. Erickson, K. E. Martins, R. E. Wilson, and V. Venkatasubramanian, "WACS-Wide-area stability and voltage control system: R&D and online demonstration," *Proc. IEEE,* vol. 93, no. 5, pp. 892-906, May 2005.

[122] J. W. Stahlhut, T. J. Browne, G. T. Heydt, and V. Vittal, "Latency viewed as a stochastic process and its impact on wide area power system control signals," *IEEE Trans. Power Syst.,* vol. 23, no. 1, pp. 84-91, Feb. 2008.

[123] G. J. W. Dudgeon, W. E. Leithead, A. Dysko, J. O'Reilly, and J. R. McDonald, "The effective role of AVR and PSS in power systems: frequency response analysis," *IEEE Trans. Power Syst.,* vol. 22, no. 4, pp. 1986-1994, Nov. 2007.

[124] M. Zarghami, M. L. Crow, J. Sarangapani, Y. Liu, and S. Atcitty, "A novel approach to interarea oscillation damping by unified power flow controllers utilizing ultracapacitors," *IEEE Trans. Power Syst.,* vol. 25, no. 1, pp. 404-

412, Feb. 2010.

[125] W. Yao, L. Jiang, Q. H. Wu, J. Y. Wen, and S. J. Cheng, "Delay-dependent stability analysis of the power system with a wide-area damping controller embedded," *IEEE Trans. Power Syst.,* vol. 26, no. 1, pp. 233-240, Feb. 2011.

[126] M. Chilali and P. Gahinet, "H infinite design with pole placement constraints: an LMI approach," *IEEE Trans. Autom. Control,* vol. 41, no. 3, pp. 499-506, Mar. 1996.

[127] B. C. Pal, "Robust damping of interarea oscillations with unified power flow controller," *IEE Proc.-Gener. Transm. Distrib.,* vol. 149, no. 6, pp. 733-738, 2002.

[128] Y. Zhang and A. Bose, "Design of wide-area damping controllers for interarea oscillations," *IEEE Trans. Power Syst.,* vol. 23, no. 3, pp. 1136-1143, Aug. 2008.

[129] T. T. Nguyen and R. Gianto, "Optimization-based control coordination of PSSs and FACTS devices for optimal oscillations damping in multimachine power system," *IET Gener. Transm. Distrib.,* vol. 1, no. 4, pp. 564-573, 2009.

[130] J. L. C. Zanetta and J. J. D. Cruz, "An incremental approach to the coordinated tuning of power system stabilizers using mathematical programming," *IEEE Trans. Power Syst.,* vol. 20, no. 2, pp. 895-902, May 2005.

[131] M. V. A. Nunes, J. A. P. Lopes, H. H. Zurn, U. H. Bezerra, and R. G. Almeida, "Influence of the variable-speed wind generators in transient stability margin of the conventional generators integrated in electrical

grids," *IEEE Trans. Energy Conversion,* vol. 19, no. 4, pp. 692-701, Dec. 2004.

[132] S. O. Faried, R. Billinton, and S. Aboreshaid, "Probabilistic evaluation of transient stability of a power system incorporating wind farms," *IET Gener. Transm. Distrib.,* vol. 4, no. 4, pp. 299-307, 2010.

[133] D. J. Trudnowski, A. Gentile, J. M. Khan, and E. M. Petritz, "Fixed-speed wind-generator and wind-park modeling for transient stability studies," *IEEE Trans. Power Syst.,* vol. 19, no. 4, pp. 1911-1917, Nov. 2004.

[134] N. R. Ullah, T. Thiringer, and D. Karlsson, "Voltage and transient stability support by wind farms complying with the E.ON netz grid code," *IEEE Trans. Power Syst.,* vol. 22, no. 4, pp. 1647-1656, Nov. 2007.

[135] J. Ekanayake and N. Jenkins, "Comparison of the response of doubly fed and fix-speed induction generator wind turbines to changes in network frequency," *IEEE Trans. Energy Conversion,* vol. 19, no. 4, pp. 800-802, Dec. 2004.

[136] E. Muljadi, C. P. Butterfield, B. Parsons, and A. Ellis, "Effect of variable speed wind turbine generator on stability of a weak grid," *IEEE Trans. Energy Conversion,* vol. 22, no. 1, pp. 29-36, Mar. 2007.

[137] J. J. Sanchez-Gasca, N. W. Miller, and W. W. Price, "A modal analysis of a two-area system with significant wind power penetration," in *IEEE Power Syst. Conf. Expo.*, 2004.

[138] J. G. Slootweg and W. L. Kling, "The impact of large scale wind power generation on power system oscillations," *Electr. Power Syst. Res.,* vol. 67, pp. 9-20, 2003.

[139] D. Vowles, C. Samarasinghe, M. Gibbard, and G. Ancell, "Effect of wind

generation on small-signal stability—a New Zealand example," in *IEEE PES General Meeting*, 2008.

[140] A. Mendonca and J. A. P. Lopes, "Impact of large scale wind power integration on small signal stability," in *Int. Conf. Future Power Systems*, 2005.

[141] D. Gautam, V. Vittal, and T. Harbour, "Impact of increased penetration of DFIG-based wind turbine generators on transient and small signal stability of power systems," *IEEE Trans. Power Syst.,* vol. 24, no. 3, pp. 1426-1434, Aug. 2009.

[142] G. Tsourakis, B. M. Nomikos, and C. D. Vournas, "Effect of wind parks with doubly fed asynchronous generators on small-signal stability," *Electr. Power Syst. Res.,* vol. 79, no. 1, pp. 190-200, Jan. 2009.

[143] P. Ledesma and C. Gallardo, "Contribution of variable-speed wind farms to damping of power system oscillations," in *IEEE Power Tech.*, 2007.

[144] G. Tsourakis, B. M. Nomikos, and C. D. Vournas, "Contribution of doubly fed wind generators to oscillation damping," *IEEE Trans. Energy Conversion,* vol. 24, no. 3, pp. 783-791, Sep. 2009.

[145] D. Gautam, L. Goel, R. Ayyanar, V. Vittal, and T. Harbour, "Control strategy to mitigate the impact of reduced inertia due to doubly fed induction generators on large power systems," *IEEE Trans. Power Syst.,* vol. 26, no. 1, pp. 214-224, Feb. 2011.

[146] P. Ledesma and J. Usaola, "Doubly fed induction generator model for transient stability analysis," *IEEE Trans. Energy Conversion,* vol. 20, no. 2, pp. 388-397, Jun. 2005.

[147] J. F. M. Padron and A. E. F. Lorenzo, "Calculating steady-state operating

conditions for doubly-fed induction generator wind turbines," *IEEE Trans. Power Syst.,* vol. 25, no. 2, pp. 922-928, May 2010.

[148] F. M. Hughes, O. Anaya-Lara, G. Ramtharan, N. Jenkins, and G. Strbac, "Influence of tower shadow and wind turbulence on the performance of power system stabilizers for DFIG-based wind farms," *IEEE Trans. Energy Conversion,* vol. 23, no. 2, pp. 519-528, Jun. 2008.

[149] L. Fan, Z. Miao, S. Yuvarajan, and J. Glower, "A comparison of slip control, FMA control and vector control in DFIG converter," in *Industrial Electronics*, 2008.

[150] A. Tapia, G. Tapia, J. X. Ostolaza, and J. R. Saenz, "Modelling and control of a wind turbine driven doubly fed induction generator," *IEEE Trans. Energy Conversion,* vol. 18, no. 2, pp. 194-204, Jun. 2003.

[151] W. Chen and Y. Hsu, "Controller design for an induction generator driven by a variable-speed wind turbine," *IEEE Trans. Energy Conversion,* vol. 21, no. 3, pp. 625-635, Sep. 2006.

[152] Y. Lei, A. Mullane, G. Lightbody, and R. Yacamini, "Modeling of the wind turbine with a doubly fed induction generator for grid integration studies," *IEEE Trans. Energy Conversion,* vol. 21, no. 1, pp. 257-264, Mar. 2006.

[153] Y. Sun, L. Wang, G. Li, and J. Lin, "A review on analysis and control of small signal stability of power systems with large scale integration of wind power," in *International Conference on Power System Technology*, 2010.

[154] Y. Mishra, S. Mishra, M. Tripathy, N. Senroy, and Z. Y. Dong, "Improving stability of a DFIG-based wind power system with tuned damping controller," *IEEE Trans. Energy Conversion,* vol. 24, no. 3, pp. 650-660,

Sep. 2009.

[155] Y. Mishra, S. Mishra, F. Li, Z. Y. Dong, and R. C. Bansal, "Small-signal stability analysis of a DFIG-based wind power system under different modes of operation," *IEEE Trans. Energy Conversion,* vol. 24, no. 4, pp. 972-982, Dec. 2009.

[156] A. Mendonca and J. A. P. Lopes, "Robust tuning of power system stabilizers to installed in wind energy conversion system," *IET Renew. Power Gener.,* vol. 3, no. 4, pp. 465-475, 2009.

[157] P. P. (convener), "Modeling and dynamic behavior of wind generation as it relates to power system control and dynamic performance," in *CIGRE,* France, 2007.

[158] P. Ledesma and J. Usaola, "Effect of neglecting stator transients in doubly fed induction generators models," *IEEE Trans. Energy Conversion,* vol. 19, no. 2, pp. 459-461, Jun. 2004.

[159] F. Mei and B. C. Pal, "Modelling and small-signal analysis of a grid connected doubly-fed induction generator," in *IEEE PES General Meeting,* 2005.

[160] J. B. Ekanayake, L. Holdsworth, X. Wu, and N. Jenkins, "Dynamic modeling of doubly fed induction generator wind turbines," *IEEE Trans. Power Syst.,* vol. 18, no. 2, pp. 803-809, May 2003.

[161] F. Mei and B. Pal, "Modal analysis of grid-connected doubly fed induction generators," *IEEE Trans. Energy Conversion,* vol. 22, no. 3, pp. 728-736, Sep. 2007.

[162] R. G. de Almeida, J. A. P. Lopes, and J. A. L. Barreiros, "Improving power system dynamic behavior through doubly fed induction machines

controlled by static converter using fuzzy control," *IEEE Trans. Power Syst.,* vol. 19, no. 4, pp. 1942-1950, Nov. 2004.

[163] S. K. Salman and A. L. J. Teo, "Windmill modeling consideration and factors influencing the stability of a grid-connected wind power-based embedded generator," *IEEE Trans. Power Syst.,* vol. 18, no. 2, pp. 793-802, May 2003.

[164] F. Wu, X.-P. Zhang, and P. Ju, "Small signal stability analysis and optimal control of a wind turbine with doubly fed induction generator," *IET Gener. Transm. Distrib.,* vol. 1, no. 5, pp. 751-760, 2007.

[165] J. P. A. Vieira, M. V. A. Nunes, U. H. Bezerra, and A. C. do Nascimento, "Design optimal controllers for doubly fed induction generators using a genetic algorithm," *IET Gener. Transm. Distrib.,* vol. 3, no. 5, pp. 472-484, 2009.

[166] K. J. Astrom and T. Hagglund, *PID Controllers: Theory, Design, and Tuning.* Research Triangle Park, NC: Instrument Society of America, 1995.

[167] K. Elkington, M. Ghandhari, and L. Soder, "Using power system stabilizers in doubly fed induction generators," in *Australasian Universities Power Engineering Conference*, 2008.